Effect of substitution at the transition metal site on the magnetic properties of rare earth ternary silicides

By

Rajeswari Roy Chowdhury

Enrolment No.: PHYS05201004006

Saha Institute of Nuclear Physics

Kolkata

A thesis submitted to the
Board of Studies in Physical Sciences
In partial fulfillment of requirements
For the Degree of

DOCTOR OF PHILOSOPHY

of

HOMI BHABHA NATIONAL INSTITUTE

August, 2016

Homi Bhabha National Institute

Recommendations of the Viva Voce Committee

As members of the Viva Voce Committee, we certify that we have read the dissertation prepared by Rajeswari Roy Chowdhury entitled "Effect of substitution at the transition metal site on the magnetic properties of rare earth ternary silicides" and recommend that it may be accepted as fulfilling the thesis requirement for the award of Degree of Doctor of Philosophy.

PRABHAT MANDAL P. Mandal **Date :** 17.2.2017

Chairman : **Prof. Prabhat Mandal**, SINP

Date : 17/03/2017

Guide & Convener : **Prof. Bilwadal Bandyopadhyay**, SINP

Date : 17/03/17

Examiner : **Dr. Rajeev Rawat**, UGC-DAE CSR, Indore

Date : 17/3/17

Member : **Prof. Indranil Das**, SINP

Gayathri N. **Date :** 17/3/17

Member : **Dr. Gayathri N. Banerjee**, VECC

Final approval and acceptance of this thesis is contingent upon the candidate's submission of the final copies of the thesis to HBNI.

I hereby certify that I have read this thesis prepared under my direction and recommend that it may be accepted as fulfilling the thesis requirement.

Date : 17/03/2017
Place : SINP, Kolkata

Guide

STATEMENT BY AUTHOR

This dissertation has been submitted in partial fulfillment of requirements for an advanced degree at Homi Bhabha National Institute (HBNI) and is deposited in the Library to be made available to borrowers under rules of the HBNI.

Brief quotations from this dissertation are allowable without special permission, provided that accurate acknowledgement of source is made. Requests for permission for extended quotation from or reproduction of this manuscript in whole or in part may be granted by the Competent Authority of HBNI when in his or her judgment the proposed use of the material is in the interests of scholarship. In all other instances, however, permission must be obtained from the author.

Rajeswari Roy Chowdhury

DECLARATION

I, hereby declare that the investigation presented in the thesis has been carried out by me. The work is original and has not been submitted earlier as a whole or in part for a degree / diploma at this or any other Institution / University.

Rajeswari Roy Chowdhury

“Life is not easy for any of us. But what of that? We must have perseverance and above all confidence in ourselves. We must believe that we are gifted for something and that this thing must be attained."

— Marie Curie

“Dream, Dream, Dream.. Dreams transform into thoughts and thoughts result in action."

— Dr. A. P. J. Abdul Kalam

List of Publications arising from the thesis

Journal

1. **"Evidence of ferromagnetism in vanadium substituted layered intermetallic compounds RE$(Co_{1-x}V_x)_2Si_2$ (RE =Pr and Nd; 0=x=0.35)"**,
   R. Roy Chowdhury, S. Dhara, and B. Bandyopadhyay,
   J. Magn. Magn. Mater. **401**, 998-1005 (2015).

2. **"Enhancement of magnetocaloric effect in intermetallic Nd$(Co_{1-x}V_x)_2Si_2$ (x = 0, 0.2, 0.35) compound"**,
   R. Roy Chowdhury, S. Dhara, and B. Bandyopadhyay
   (Accepted in AIP Advances in February 2017).

3. **"Large positive magnetoresistance in intermetallic compound $NdCo_2Si_2$"**,
   R. Roy Chowdhury, S. Dhara, I. Das, R. Rawat and B. Bandyopadhyay
   (communicated).

4. **"Comparative studies of magnetoresistance and magnetocaloric effect to understand the anomalous magnetoresistance in layered intermetallic $NdRu_2Si_2$"**,
   R. Roy Chowdhury, S. Dhara, and B. Bandyopadhyay
   (manuscript under preparation).

Conferences

5. **" Ferromagnetism in Nd$(Co_{1-x}V_x)_2Si_2$ ($0 \leq x \leq 0.5$)."**,
   Rajeswari Roy Chowdhury, Susmita Dhara, Bilwadal Bandyopadhyay,
   Proc. Int. Conf. of Magnetic Materials and
   Applications (MagMA-2013), Phys. Procedia. **54**, 113-117 (2014).

6. **"Crossover From Antiferro-To-Ferromagnetism On Substitution Of Co By V In RE$(Co_{1-x}V_x)_2Si_2$ (0≤x≤0.35). "**,
   Rajeswari Roy Chowdhury, Susmita Dhara, Bilwadal Bandyopadhyay,
   59^{th} DAE Symp. on Solid State Physics, AIP Conf. Proc. **1665**, 130040 (2015).

7. **"Effect of Vanadium Substitution of Cobalt in $NdCo_2Si_2$"**,
   Rajeswari Roy Chowdhury, Susmita Dhara, Bilwadal Bandyopadhyay,
   Acta Physica Polonica A. Proc. **128(4)**, 530 (2015)
   13^{th} Int. Symp. on Physics of Materials (ISPMA13).

Other Publications

1. **"Synthesis, characterization and magnetic properties of Co_xCu_{1-x} ($x \sim 0.01 - 0.3$) granular alloys"**,
   S. Dhara, R. Roy Chowdhury, S. Lahiri, P. Ray and B. Bandyopadhyay,
   J. Magn. Magn. Mater. **374**, 647-654 (2015).

2. **"Strong memory effect at room temperature in nanostructured granular alloy $Co_{0.3}Cu_{0.7}$"**,
   S. Dhara, R. Roy Chowdhury, and B. Bandyopadhyay,
   RSC. Adv. **5**, 95695-95702 (2015).

3. **"Observation of resistivity minimum in low temperature in nanostructured granular alloys Co_xCu_{1-x} ($x \sim 0.17 - 0.76$)"**,
   S. Dhara, R. Roy Chowdhury, and B. Bandyopadhyay,
   Phys. Rev. B **93**, 214413 (2016).

4. **"Magnetization study of Co_xCu_{1-x} nanoparticles"**,
   Susmita Dhara, Rajeswari Roy Chowdhury, Bilwadal Bandyopadhyay,
   Proc. Int. Conf. of Magnetic Materials and
   Applications (MagMA-2013), Phys. Procedia. **54**, 38-44 (2014).

5. **"Kondo effect in Co_xCu_{1-x} granular alloys prepared by chemical reduction method"**,

   Susmita Dhara, Rajeswari Roy Chowdhury, Bilwadal Bandyopadhyay,

   59^{th} DAE Symp. on Solid State Physics, AIP Conf. Proc. **1665**, 130056 (2015).

6. **"Evidence of formation of Co_xCu_{1-x} nanoparticles with core-shell structure"**,

   Susmita Dhara, Rajeswari Roy Chowdhury, Bilwadal Bandyopadhyay,

   Acta Physica Polonica A, Proc. **128(4)**, 533 (2015)

   13^{th} Int. Symp. on Physics of Materials (ISPMA13).

DEDICATIONS

Dedicated to my family, my teachers and my friends

ACKNOWLEDGMENTS

"We can only be said to be alive in those moments when our hearts are conscious of our treasures." $\sim$ Thornton Wilder

This thesis is a complication of tireless effort and countless hours of work which would not have been possible without the help and support of so many wonderful people who have guided me in this entire curriculum. My dream would never have been possible without all of these people from whom I wish to express sincere gratitude from the bottom of my heart.

First of all, I feel pleasure to express my gratitude to Prof. Bilwadal Bandyopadhyay, my thesis supervisor, for his kind guidance and encouragement. It has been a wonderful experience to work with him. He is an excellent physicist and an admirable teacher and above all a nice person. He is a person with great composure and I would definitely like to inculcate this quality of him. Thank you sir, for sharing your wealth of knowledge, wisdom and experience which has been tremendously helpful for me. I will always be indebted to you for all the fruitful discussions which has helped me to enrich myself as a research fellow and it has been an honor to be able to work with you.

I am thankful to DAE, Govt. of India for providing me the fellowship by awarding Junior Research Fellow. I am grateful to the director of SINP for providing me the opportunity to work in the Experimental Condensed Matter Physics Division, and for hostel accommodation.

I convey my sincere gratitude to all my teachers from University of Calcutta from where I received my MSc. (physics) degree. I would like to thank Prof. Biswajit Ray for his one remark that changed my life "you are meant to be an experimentalist, nothing

else" which drove me to dedicate myself to this field. I am grateful to all my teachers of Asutosh College where I pursued my graduate studies. I would like to acknowledge Prof. Phalguni Mukherjee of same college for his belief in my abilities. I am thankful to all the teachers of Bidya Bharati Girls' High School who have always treated me as their own daughter and showered me with love and care. Thanks for your blessings. I would specially thank my English teacher Sukanya aunty for her inspiration throughout my life and inculcating self-belief. They have been the strongest pillars of my life. I would like to acknowledge Somnath sir, my mathematics teacher. I am thankful to Nabendu-da for developing my interest in physics. For a girl who was devoted to English literature from her very childhood, turning it to physics was because of you and of course the physics division of Bethune college. It changed the course of my life.

Many thanks to Susmita, my lab mate for her continuous support in my research work. Thanks for being a wonderful friend. It was a wonderful journey that we travelled together. I will miss all our runaways from lab for shopping and movies. I wish her best of luck for all the future endeavors.

I would like to express my gratitude to seniors of my lab Mayukh da and Manasi di. Working with them has been a great experience. Thanks to Mr. Dhrubojyoti Seth, scientific assistant of our NMR group, for his technical assistance during experiments. Many thanks to Anis da, Dhrubo da, Arun da, Arindam da, Tapan Pyne da and Jishnu sir from workshop for their tremendous support to carry out crucial experimental work and designing equipments.

I am really thankful to Mr. Kalipada Das for all the stimulating discussions that we had. I have always been inspired by his devotion towards his research work. I have learnt a lot from you. Thanks for being a great senior.

I would like to specially thank Mr. Samik Duttagupta. You have been a great senior, a great motivator and above all a wonderful friend. You are an inspiration to me. I am indebted for all those brain storming discussion sessions we used to have and as you always

say, this will continue throughout our scientific career.

I am thankful to Nazir-da, although we had very less interactions but you guys are all who have taught me what dedication and a true experimentalist means. I am fortunate to come across seniors like Rima di, Papridi and Sudipta di. They have been more like elder sisters, than seniors. Thanks to my juniors Shovan, Suvayan, Sanjib, Mili and Binita.

My sincere thanks to all my professors of Experimental Condensed Matter Physics Division, Prof. R. Ranganathan, Prof. Chandan Mazumdar, Prof. Indranil Das, Prof. Prabhat Mondal, Prof. Asok Poddar, Prof. Amitabha Ghoshray, Prof. Kajal Ghoshray and Prof. Biswajit Karmakar for their support during my stay in SINP. I should express my best thanks to all the members of Experimental Condensed Matter Physics Division of SINP for their help.

My sincere thanks to Prof. Rajeev Rawat of UGC-DAE Consortium for Scientific Research, Indore for allowing me to perform the transport property measurements in his lab. I am also thankful to Sachin sir, Pallab da, Vikram, Saroj and especially Pampi for their cooperation during my stay in Indore. It was a nice experience to work with Prof. Rawat especially I could learn a lot from his thesis work.

Thanks to Mala, Moumita, Abhik, Atanu, Bijoy, Amit, Kamakshya, Tapas, Aminul and all my post M. Sc friends for their great friendship which I will cherish throughout my life. I treasure every minute I have spent with them. I will miss our movie sessions and pandal hopping during the pujas.

I am thankful to my landlady Uma di for allowing me to stay in her house. It was a nice experience to stay with you and your family in Keshtopur.

I am also thankful to the canteen staff of both hostel and institute for providing us wonderful lunch and dinner. I am thankful to the security section and library staff for their cooperation. I feel very lucky to receive immense love and support from all SINPians!!

A special thanks to my family. Words will fall short to express my gratitude to my loving parents. They have always taught me to dream big yet stay grounded. I owe my

values to them. I would take this opportunity to thank my brother and sister in law. I would like to pay tribute to my late paternal and maternal grand fathers, my aunt and uncles. Credit goes to my big family that this thesis will fall short to name each of them, so a big big thanks to my grand parents, all my aunties, uncles, brothers, sisters, sister in laws, niece, nephew... in one word EVERYONE!!. I am thankful for all your prayers.

Last but not the least, my heartiest thanks goes to all my friends for providing me such a wonderful and cheerful community, for their encouragements and mental support to overcome my personal and professional wears and tears. Once again, space will fall short if I try to count and name all of them as the list travels worldwide, but a big thanks to all. I would like to specially name and acknowledge some of them. Thanks Utpal for your support. Thanks for standing beside me through thick and thin. Thanks SDG once again for being there for me. Thank you Arunima, Sayani, Sreoshi, Anirban, Debanjan, Indranil and our crazy gang.

Let me thank once again all the people for their support and I would remain grateful to all of them.

CONTENTS

SYNOPSIS

During last few decades, the intermetallic compounds containing rare earth elements have been a subject of intensive studies because of their intriguing physical properties, which have both fundamental and practical significance. The electronic configuration of rare earth atoms can be described in terms of the following configuration [Xe]$4f^n5d^16s^2$ (n = 0 to 14 as one goes from La to Lu). In most of the rare earth intermetallic compounds the rare earth ion remains in trivalent state and the $5d^16s^2$ electrons form the conduction band. Magnetism in rare earth elements arises due to the unfilled $4f$ orbital of rare earth ions. The $4f$ electron couple together according to Russel-Saunders coupling (LS coupling) and Hund's rules. The magnetic moment of the free trivalent rare earth ions is given as $g_J\sqrt{J(J+1)}\mu_B$, where g_J is the Lande factor, J is the total angular momentum and μ_B is the Bohr magneton. In the absence of crystal electric field effects the effective magnetic moment obtained from the temperature dependence of susceptibility in the paramagnetic region will be equal to this value. In case of rare earth intermetallic compounds the localized moments interacts indirectly through conduction electrons and it is known as (Ruderman-Kittel- Kasuya- Yosida) RKKY exchange interaction.

The electronic and magnetic properties of the intermetallic compounds of the type RET_2X_2 (RE = rare earths or actinides, T = transition metals, and X = Si or Ge) have been a subject of intensive studies over the years. These compounds crystallize in the body centered tetragonal $ThCr_2Si_2$ type structure with space group D_{4h}^{17}-I4/mmm. The RE, T, and X atoms occupy the $2(a)$, $4(d)$, and $4(e)$ positions respectively. The structure consists of an arrangement of atoms in layers perpendicular to c-axis with the sequence $RE-X-T-X-RE$. Magnetic properties of $RECo_2Si_2$ compounds have been extensively studied. Both $PrCo_2Si_2$ and $NdCo_2Si_2$ are antiferromagnetic compounds. Neutron diffraction studies on single crystal of $PrCo_2Si_2$ shows magnetic moments occuring only on rare-earth ions in a square-wave structure with propagation vectors (0,0,l), (0,0,0.074) and (0,0,0.223) appear in

the sequence of $T \leq 9$ K (T_1), 9 K $\leq T \leq 17$ K (T_2) and 17 K $\leq T \leq 30$ K (T_N), respectively. $NdCo_2Si_2$ also have a similar magnetic structure in which the propagation vectors (0,0,l), (0,0,0.07) and (0,0,0.21) appear in the sequence of $T \leq 15$ K (T_1), 15 K $\leq T \leq 24$ K (T_2) and 24 K $\leq T \leq 32$ K (T_N), respectively. Therefore, at lowest temperatures, both compounds exhibit a collinear antiferromagnetic (AFM) ordering of alternate up and down moments along c-axis. However, it is important to note that in planes perpendicular to c-axis, the moments are ferromagnetically aligned. The temperatures 30 K and 32 K are denoted as the AFM ordering temperatures, T_N, for $PrCo_2Si_2$ and $NdCo_2Si_2$, respectively. $CeCo_2Si_2$ shows weak paramagnetism characteristic of Ce ion valency fluctuation.

RET_2X_2 compounds have a tendency of magnetic instability arising out of an interplay of on-site and inter-site magnetic fluctuations. Significant modifications in their magnetic properties have been obtained by the use of externally applied pressure or substitution at either *RE* or T sites. In more recent works, rhodium in $YbRh_2Si_2$ was isoelectronically substituted by cobalt, resulting in a positive chemical pressure, and ferromagnetism was obtained in $Yb(Rh_{1-x}Co_x)_2Si_2$ for x = 0.27 below T_c = 1.30 K. So far, all the substitutions involved combinations of only those *RE* and T elements that are known to form RET_2X_2 compounds of $ThCr_2Si_2$ type structure. In this work, we have studied modifications in the magnetic properties of $RECo_2Si_2$ (*RE* = Pr,Nd) compounds upon substitution of cobalt with vanadium which is not reported to be among the elements forming $ThCr_2Si_2$ type pure compounds.

Polycrystalline samples of $RE(Co_{1-x}V_x)_2Si_2$ (*RE* = Ce, Pr, Nd; $0 \leq x \leq 0.35$ for Pr, Nd and $0 \leq x \leq 0.50$ for Ce) were prepared by arc melting high-purity elements in purified argon atmosphere. For better homogeneity, the ingots were remelted six times resulting in the end a weight loss of less than 1 %. The samples were subsequently annealed at 900° C for 7 days. To determine the crystal structure and the lattice parameters of the prepared compounds, powder x-ray diffraction (XRD) studies at room temperature were performed with a Rigaku TTRAX-III x-ray diffractometer. The obtained XRD patterns are analyzed

by the Rietveld refinement using Fullprof program to determine the lattice parameters and the number of phases present in the sample as shown in Figure 1(a). The XRD studies showed the samples to be single phase for low doping of vanadium. However, for Vanadium doping, $x > 0.35$, there were lines due to un-reacted elemental Ce, Pr, Nd and Si that constituted $\sim 3\%$ of XRD peak intensities. No extra lines due to V were obtained, and also no minority phase could be detected. From the Scanning electron microscope (SEM) images (Figure 1(c)) as observed by us, it can be inferred that the prepared sample consists of well connected grains of regular shape. Energy dispersive x-ray spectroscopy (EDS) analysis shows the relative atomic percentages of vanadium substitution matching with the desired values within the error limit. It can be concluded that the samples have formed in a single phase, with well connected structure and negligible secondary or impurity phases. For the parent compounds, the lattice parameters agree quite well with the published data. Vanadium has a molar volume larger than that of cobalt. In substituted compounds, with increase in V, the lattice parameter a shows small increase, but c increases markedly as can be seen in Figure 1(b). The change in the lattice parameters as a function of V concentration is a strong indication of Co being replaced by V.

Magnetic measurements in the temperature range 4-300 K were carried out using SQUID-vsm magnetometer of Quantum Design. For the parent compound, *i.e.*, $PrCo_2Si_2$ ($x = 0$) and $Pr(Co_{0.95}V_{0.05})_2Si_2$, χ_M have small values The three reported transitions in the parent compound have been obtained as different peaks in χ_M versus temperature at positions T_1 = 9 K, T_2 = 17 K and T_N = 32 K. Above 32 K, χ_M follows Curie-Weiss (CW) behavior. For V substituted samples, with increase in V content, χ_M increases more and more rapidly as temperature is decreased below 60 K. For x values of 0.05 and 0.10, an AFM transition is observed as a broad peak in χ_M at around 26 K which is followed by a minimum at 11 K. For $x \geq 0.15$, χ_M does not show the peak. Instead, it reaches a broad plateau at ~ 30 K, and then it tends to increase further as temperature goes below ~ 12 K. The latter behavior is clearly observed in the sample with $x \geq 0.30$. In high temperature

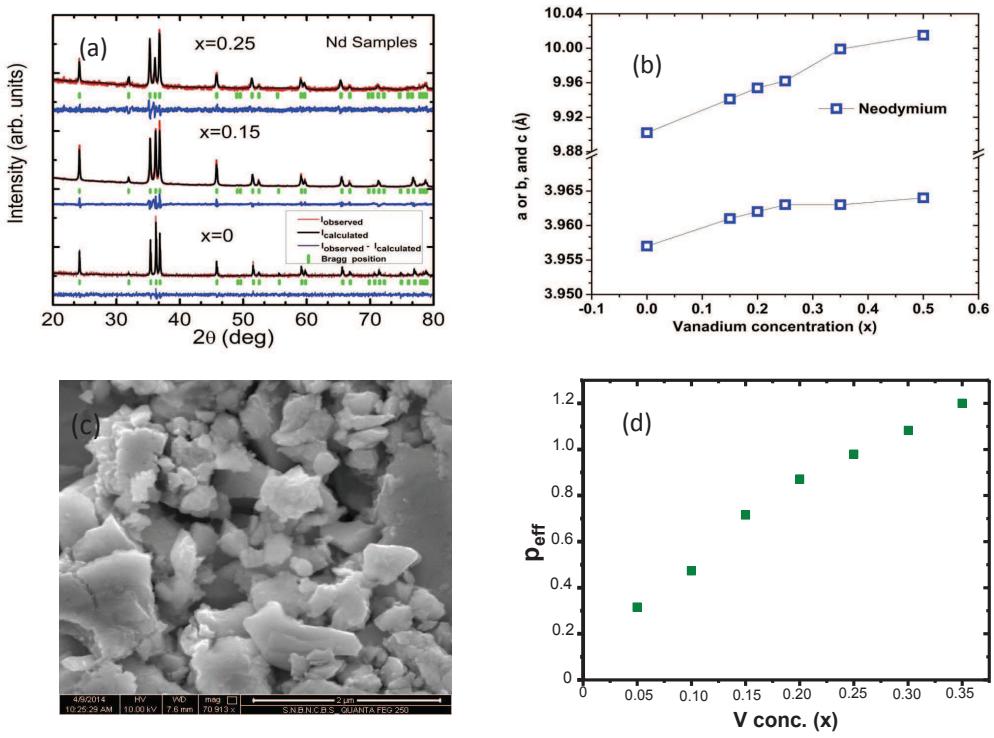

Figure 1: (a) Powder x-ray diffraction patterns of $Nd(Co_{1-x}V_x)_2Si_2$ at 300 K with Rietveld fitting, (b) Lattice parameters (a, b and c) in $Nd(Co_{1-x}V_x)_2Si_2$ (0$\leq$ x $\leq$ 0.35.), (c) FESEM images of $Nd(Co_{1-x}V_x)_2Si_2$; $x = 0.05$ and (d) Change in effective no. of Bohr magneton (p_{eff}) with vanadium concentration(x)in $Ce(Co_{1-x}V_x)_2Si_2$ ($0 \leq x \leq 0.35$).

side, $50 \leq T \leq 300$ K, χ_M in samples with $x \geq 0.15$ follow ferrimagnetic behavior which is given by,

$$\chi_M = \chi_0 + [(T-\theta)/C + \xi/(T-\theta_1)]^{-1}, \quad (1)$$

where, θ_1 and ξ are proportional to $\eta_i\eta_j C(\eta_i - \eta_j)$ and $\eta_i\eta_j C$ (η_i and η_j are the fractional occupancies of the two magnetic sublattice sites in ferrimagnetism, C being the Curie constant), respectively. The magnetic ordering temperature (θ_1) corresponds to the point where the hyperbola of equation 1 crosses the temperature axis. Table 1 shows the values of various parameters in equation 1 as obtained from the simulation of the data of temperature dependence of inverse molar susceptibility. For the parent compound (x = 0), C yields an effective magnetic moment, p_{eff}, of 3.86 Bohr magneton per formula unit (μ_B/f.u.), which is close to the theoretical p_{eff} of Pr^{3+}. For the V substituted samples, p_{eff} is reduced, and

Table 1: Paramagnetic Curie constant(θ), effective number of Bohr magnetons (p_{eff}), constant (ξ), magnetic ordering temperature (θ_1), and saturation magnetization (M_S) obtained from the fitting of magnetization data, $1/\chi_M$ vs. temperature and M vs. H at 4 K, with equations 1 and 2, respectively, in $Pr(Co_{1-x}V_x)_2Si_2$ ($0 \leq x \leq 0.35$)

x	θ (K)	p_{eff}	ξ mol.K/emu	θ_1 (K)	M_S (μ_B/f.u.)
0	-66(2)	3.86(1)	–	–	–
0.15	-90(2)	3.41(1)	-600(5)	45(2)	0.080(2)
0.20	-60(2)	3.46(1)	-600(5)	45(2)	0.139(2)
0.25	-50(2)	3.29(1)	-600(5)	45(2)	0.152(2)
0.30	-22(2)	3.35(1)	-600(5)	42(2)	0.220(2)
0.35	-20(2)	3.43(1)	-600(5)	40(2)	0.245(2)

the ferrimagnetic ordering temperature (θ_1) is in the range 40-45 K, which is much higher than T_N of the parent compound. Study of magnetic field (H) dependence of magnetization (M) shows that below $\sim$ 30 K, M in $Pr(Co_{1-x}V_x)_2Si_2$ for x $\geq$ 0.15 have a tendency of saturation at $H \geq 2$ T, and they exhibit hysteresis loops. For the parent compound (x = 0), M versus H plot is linear and shows step-like increase in magnetization near 2 and 5 T. For samples of $x \geq 0.15$, magnetization increases with increasing V content, and their M versus H data have been compared with the following equation,

$$M(H) = \chi_1 H + M_S \tan^{-1} \chi_2 H, \tag{2}$$

The first term in the equation 2 is linear in magnetic field and represents the paramagnetic contribution to the magnetization. It remains significantly large in all samples with χ_1 being in the range 0.5-1.0 x 10^{-3} emu/mol. The second term represents magnetic field dependence of magnetization in a ferromagnetic material giving saturation of magnetization at high field. Table 1 lists the saturation magnetization, M_S, in terms of Bohr magneton per formula unit (μ_B/f.u.).

Vanadium substitution in $NdCo_2Si_2$ results in a similar effect as that in $PrCo_2Si_2$. The temperature dependence of χ_M in $NdCo_2Si_2$ and $Nd(Co_{1-x}V_x)_2Si_2$ ($0.15 \leq x \leq 0.35$) at 0.5

T in between 4-250 K is shown in Figure 2(a). $NdCo_2Si_2$ shows the three transitions at T_1 = 13 K, T_2 = 24 K and T_N = 34 K, and above 34 K,χ_M follows CW behavior. In V containing samples, deviation from CW behavior is observed below 60 K. Below this temperature, χ_M increases markedly with decrease in temperature and increase in vanadium concentration x.In higher V containing samples, as temperature decreases, χ_M goes on increasing, though not monotonously. There are plateaus in magnetization near 28 K and again below about 8 K. Figure 2(b) shows temperature dependence of $1/\chi_M$ and its fit to equation 1 for all the samples. The fitting parameters are given in Table 2. The high temperature magnetization behavior is almost paramagnetic, and the C values very nearly correspond to free Nd^{3+} ions. The ferrimagnetic ordering temperature (θ_1) is in the range 38-41 K, higher than T_N of the parent compound. Paramagnetic Curie temperature, θ increases markedly with increase in V content and tends to become positive.

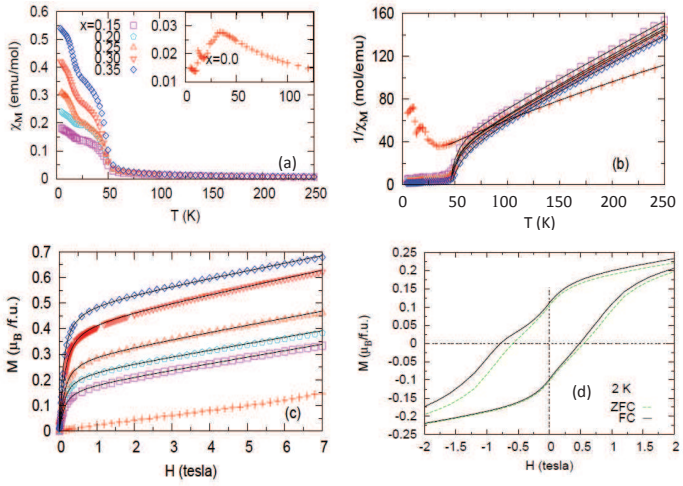

Figure 2: Plots of magnetic measurements in $Nd(Co_{1-x}V_x)_2Si_2$ ($0 \leq x \leq 0.35$), (a) temperature dependence of molar susceptibility χ_M, inset shows data for the parent compound, (b) temperature dependence of $1/\chi_M$ and the fitting with equation 1 as line plots, and, (c) magnetic field (H) dependence of Magnetization (M) at 4 K and the fitting with equation 2 as line plots and (d) Hysteresis loops at 2 K in zero-field cooled (ZFC) and field cooled (FC) conditions in $Nd(Co_{0.85}V_{0.15})_2Si_2$.

Figure 2(c) shows the plots of M versus H at 4 K and 0-7 T for all the $Nd(Co_{1-x}V_x)_2Si_2$ (x = 0, 0.15, 0.20, 0.25, 0.30 and 0.35) samples and their fitting with equation 2. For V

Table 2: Similar parameters as in Table 1 obtained from the fitting of magnetization data, $1/\chi_M$ vs. temperature and M vs. H at 4 K, with equations 1 and 2, respectively, in $Nd(Co_{1-x}V_x)_2Si_2$ ($0 \leq x \leq 0.35$)

x	θ (K)	p_{eff}	ξ mol.K/emu	θ_1 (K)	M_S (μ_B/f.u.)
0	-37(2)	4.00(1)	–	–	–
0.15	-40(2)	3.88(1)	-220(5)	41(2)	0.108(2)
0.20	-28(2)	3.89(1)	-220(5)	41(2)	0.148(2)
0.25	-27(2)	3.85(1)	-220(5)	40(2)	0.180(2)
0.30	-22(2)	3.87(1)	-220(5)	40(2)	0.265(2)
0.35	-7(2)	3.61(1)	-300(5)	38(2)	0.310(2)

containing samples, the plots clearly show the effect of saturation of magnetization at a field of about 2 T, though the slope of the plots beyond 2 T remains almost same as that of the M versus H plot of the parent compound. Although these samples behave as ferromagnets, there remain a paramagnetic component which is as strong as that would arise from $4f$ moments in the parent compound. This observation and also the fact that M_S is much smaller than p_{eff}, clearly indicate that $4f$ moments may not be responsible for the observed ferromagnetic-like behavior in V substituted samples. The magnetic hysteresis of V doped samples were studied in zero-field cooled (ZFC) and field cooled (FC)condition in the range $2 \leq T \leq 30$ K. In the ZFC condition, the hysteresis loop in between $-7 \leq H \leq 7$ T was found to be symmetric about the zero on the field axis. In the FC condition, the hysteresis loop was asymmetric and both the ascending and descending curves of $M-H$ loop were shifted from their ZFC positions in the direction of low magnetic field. The average of the shifts measured on both sides of the H-axis is defined as the exchange bias field (H_{EB}). An appreciable coercive field (H_C)is obtained in all the V doped samples(Figure 3(a)).Though there are variations in H_C from sample to sample, it does not vary with the vanadium content. Above $\sim$ 30 K, H_C values are very small. H_{EB} values are small in between 30-10 K, but increases sharply below this temperature(Figure 3(b)) and reaches $\sim$ 16 % of H_C at 2 K.The logarithm of H_C when plotted against temperature shows two well-defined linear

segments below and above $\sim$ 10 K, indicating that the ferromagnetic phase below $\sim$ 10 K is different from the ferromagnetic phase above this temperature.

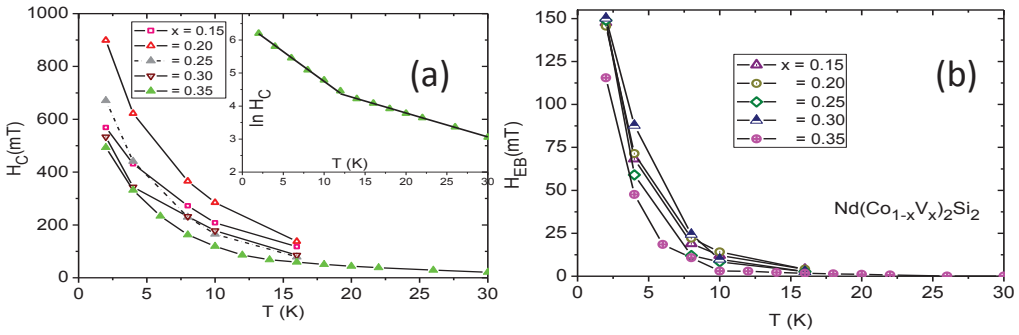

Figure 3: (a) Temperature dependence of coercive field (H_C)in $Nd(Co_{1-x}V_x)_2Si_2$ (x = 0.15, 0.20, 0.25, 0.30 and 0.35). Inset shows the plot of lnH_C vs. temperature having two linear segments, (b)temperature dependence of exchange bias field (H_{EB}) for the same samples.

The specific heat, $C_P(T)$, at zero external magnetic field were measured for the parent compounds and some of the vanadium substituted compounds and also for isostructural $LaCo_2Si_2$ from 2-300 K. Figure 4(a),(b) shows the data for the temperature range $2 \leq T \leq$ 80 K. In parent compounds, the T_N and T_2 transitions are clearly indicated by λ-like peaks at the respective temperatures. At the lowest temperature T_1 transition (commensurate-incommensurate), there is a barely detectable hump. All the V doped samples show two prominent peaks. The higher temperature peaks are at 52 K and 46 K for Pr and Nd samples respectively. The lower temperature peaks, at 23 K for V doped Pr compounds and at 27 K for V doped Nd compounds, are at a slightly lower position compared to that of the onset of ferromagnetism indicated in magnetic studies. From experimental data of $C_P(T)$, the magnetic specific heat $C_m(T)$ was separated out by subtracting the lattice contributions, which was obtained from the data of nonmagnetic $LaCo_2Si_2$. Hence, the magnetic entropies, S_m, have been calculated by integrating $(C_m/T)dT$, and are also shown in Figure 4. It has been observed that S_m levels off at $\sim$ 120 K in Pr compounds, and at $\sim$ 100 K in Nd compounds giving an idea of their overall crystal field splitting energies.As for the parent compounds, $PrCo_2Si_2$ attains only 46% of the theoretical S_m expected for

Pr^{3+} ions, whereas, for $NdCo_2Si_2$, S_m is 94% of the theoretically expected value for Nd^{3+} ions. Such a large difference in experimental S_m could be found also in $PrCo_2Ge_2$ and $NdCo_2Ge_2$. In $Pr(Co_{1-x}V_x)_2Si_2$, S_m increases consistently with V doping which is possibly an indication of an overall increase in the number of magnetic ions that are involved in the magnetic ordering. In Nd compounds in which crystal field seems to have a comparatively small effect, S_m at the ordering temperature of 27 K reach values close to $Rln3$ indicating that the ordering moment comes from a pseudo-triplet ground state.

Temperature (T) dependence of resistivity (ρ) measured as ρ_T/ρ_{300}, were obtained at zero magnetic field and in the magnetic field of 9 T. The various transitions are clearly indicated specially in zero-field resistivity behavior. In both the parent compounds, the AFM transition at $T_N \sim 30$ K is reflected as a rapid change in the slope of ρ_T/ρ_{300} near that temperature both in zero field and in 9 T magnetic field. An overall positive magnetoresistance is observed below T_N. In V doped samples, a similar change in the slope of ρ_T/ρ_{300} appear near 50 K for Pr samples and 45 K for Nd samples. In contrast to the parent samples, a negative magnetoresistance is obtained below these temperatures and down to $\sim$ 10 K. Interestingly, below $\sim$ 9 K, there is a sharp drop in zero field resistivity in all V doped samples, indicating occurrence of another magnetic transition. On application of a magnetic field of 9 T, the drop in resistivity occurs at a lower temperature. Consequently, a positive magnetoresistance is obtained in all V doped samples in between 2-9 K.

Effect of vanadium substitution in the magnetocaloric properties of $Nd(Co_{1-x}V_x)_2Si_2$ (x = 0, 0.20 and 0.35) have been investigated. Our experimental results reveal that the antiferromagnetic transition is gradually suppressed due to the vanadium doping in Co-site and results in a drastic modification of the ground state of the doped compound. In addition to that, predominant ferromagnetism appears for the $Nd(Co_{0.65}V_{0.35})_2Si_2$ compound. The modification of the ground state due to the vanadium substitution in the parent $NdCo_2Si_2$ compound is directly reflected in the magnetocaloric properties. Astonishingly we have

observed conventional large magnetocaloric effect for x = 0.35 doping instead of the inverse magnetocaloric responses of the parent compound. Our study indicates a route for the enhancement of magnetocaloric effect in such intermetallic compounds.

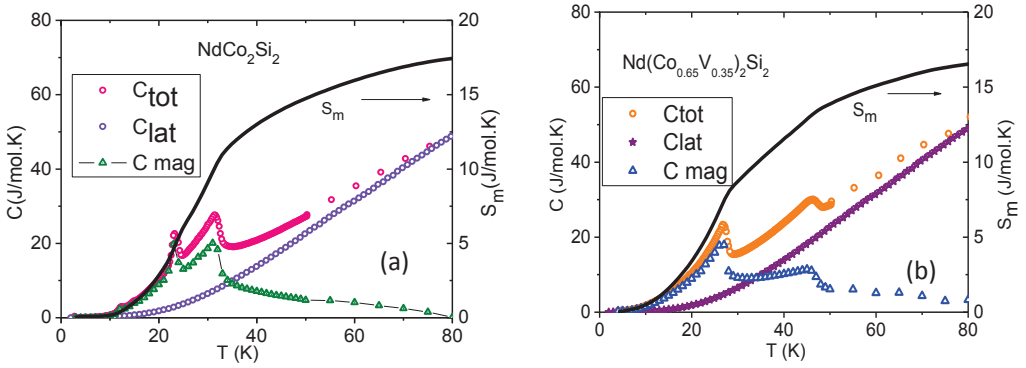

Figure 4: Heat capacity (C_P, left y-axis)and calculated magnetic entropy (S_m, right y-axis) as continuous lines in (a) $NdCo_2Si_2$ and (b) $Nd(Co_{0.65}V_{0.35})_2Si_2$.

In the work reported here, the XRD results have shown that partial substitution of Co by V in $PrCo_2Si_2$ and $NdCo_2Si_2$ results in lattice expansion which is more pronounced along c axis than in ab plane. These compounds have a layered structure with one type of atom in each layer, and in V substituted compounds, the atoms are stacked in a sequence Pr(Nd)-Si-Co/V-Si-Pr(Nd). Presumably, there should be a dominant antiferromagnetic interaction involving only Pr(Nd) moments along c axis, as in parent compounds. However, the magnetic, specific heat and resistivity measurements indicate a magnetic transition, which, in spite of the lattice expansion, takes place at a temperature of 40-45 K, much higher than the Neel temperature ($\sim$ 30 K) of the parent compounds. This clearly indicates a possibility of occurrence of magnetism in the intervening Co/V layers facilitating the interaction between successive Pr(Nd) layers. Indeed, the analysis of the data indicates ferrimagnetism, and hence, the presence of more than one type of magnetic ions. The increased value of exponent in the temperature dependence of resistivity just below the ferrimagnetic transitions and the increased values of S_m also indicate the participation of more magnetic ions in the magnetic ordering of V doped samples compared to that in

parent compounds.In parent compounds, the rare-earth ions are already in 3^+ state.The magnetization of substituted samples at low temperatures has a strong paramagnetic component (χ_1 in equation 2) and a rather small value of saturation magnetization. These are strong indications that rare-earth $4f$ moments contribute only to paramagnetism even at low temperatures, and that the ferrimagnetic behavior at high temperatures and weak ferromagnetism at low temperatures arise from partial localization of $3d$ electrons. There is no localized moment on Co atoms in parent compounds. Either the Co-$3d$ levels are completely filled up by p-electrons from Si atoms, or there is $3d$ band which is close to the Fermi level and therefore completely filled. Substitution of cobalt by vanadium which has fewer $3d$ electrons than cobalt, should affect the $3d$ electron character in these compounds. Moreover, a negative chemical pressure resulting from lattice expansion may also lead to the localization of the $3d$ electrons. However, even though there is electron localization, vanadium substitution actually lowers the value of C (Tables 1 and 2), which might be a result of lattice distortion and an increased effect of crystalline electric field. The change of sign of magnetoresistance from being positive in parent compounds to being negative upon vanadium substitution is a definite indication of a change in the magnetic interactions. The peak in specific heat at $\sim$ 30 K coincides with the onset of saturation of magnetization at a comparatively small magnetic field of $\sim$ 2 T and appearance of a coercive field which has a temperature dependence that of a ferromagnetic material. There also appears a small exchange bias field at these temperatures. These are indications that V doped samples undergo a ferromagnetic ordering coexisting with antiferromagnetism, which might be assumed to be a consequence of the existence of both AFM and FM interactions. If we assume that the ferromagnetic behavior is due to the magnetism of only vanadium, then at 4 K the saturation magnetic moments (Tables 1 and 2) are $0.31\mu_B \pm 0.05$ per V atom in Pr samples and $0.40\mu_B \pm 0.04$ per V atom in Nd samples. These values are comparable to the magnetic moments appearing on vanadium when it is present in dilute quantities in alloys and thin films. At low temperatures, the localized $3d$ moments on Co and/or V might order

ferromagnetically in *ab* plane, similar to the ordering of Mn ions in isostructural $PrMn_2Ge_2$ and $NdMn_2Ge_2$. The transition at $\sim$ 8 K leads also to a positive magnetoresistance below this temperature. The magnetoresistance has a maximum value of $\sim 8\%$ at 4 K and 9 T. Isostructural ferromagnetic compound $LaMn_2Ge_2$ has shown a positive magnetoresistance. In addition to positive magnetoresistance, the V substituted compounds have also yielded a significant exchange bias field which might be due to the existence of $3d$ and $4f$ magnetic moments in different atomic layers. The present study therefore strengthens the notion of natural multilayers attributed to these compounds. Further studies using microscopic techniques, such as, inelastic neutron scattering and nuclear magnetic resonance would be helpful to identify the local moments and magnetic structures of the substituted compounds. On the other hand, there are many other rare-earth ternary silicides of $ThCr_2Si_2$ or related structure types $TbFeSi_2$ and CeFeSi, and it would be interesting to perform similar studies on those compounds.

Detailed study on the magnetic, magneto-transport and magnetocaloric properties of antiferromagnetic intermetallic compound $NdCo_2Si_2$ (T_N = 32 K) has been carried out. Magnetoresistance (MR) measurements reveal large positive MR values of about $\sim$ 123% at $\sim$ 5 K in the presence of 8 T field. Figure 5(a) shows the field dependence of magnetoresistance in the parent compound. Positive magnetoresistance of such large magnitude has not been reported earlier in magnetically ordered polycrystalline compound of the $RECo_2Si_2$ series. It may be associated with the magnetic ordering of the lattice as its value is reduced in the paramagnetic temperature regime. In addition to this it is worth mentioning that the signature of the field induced pseudo energy gaps on the fermi surface was observed. In such layer structure compound the appearance of the energy gap is taken into consideration to explain such an unconventional magnetoresistive behavior at low temperature. Vanadium doping in the antiferromagnetic parent compound $NdCo_2Si_2$ brings out drastic modifications in the magneto-transport properties. The doped compound $Nd(Co_{0.65}V_{0.35})_2Si_2$ is observed to be ferromagnetic from magnetization studies. This

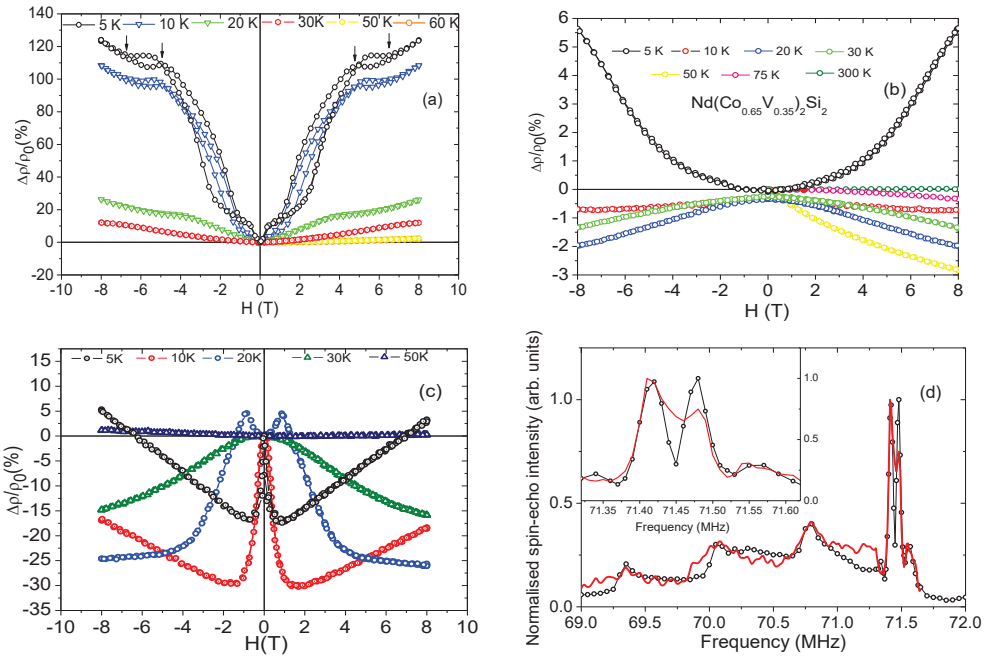

Figure 5: Figure indicates (a) Field dependence of magnetoresistance (MR) at different temperatures in $NdCo_2Si_2$, (b) Field dependence of magnetoresistance (MR) at different temperatures in $Nd(Co_{0.65}V_{0.35})_2Si_2$, (c)Field dependence of magnetoresistance (MR) at different temperatures in $NdRu_2Si_2$ and (d) Typical ^{59}Co NMR spectra at 100 K and 7 T in random polycrystalline powder of $CeCo_2Si_2$. Inset shows the central transition.

behaviour is also reflected in the magneto-transport studies. We observed a negative MR in the entire ferromagnetic regime of the compound. However, below about 10 K an anomaly has been observed in the MR data. Magnetoresistance is observed to be positive for the doped compound even when it is in its ferromagnetic regime as shown in Figure 5(b).

Magnetic, electronic transport and magneto-caloric properties of the ternary intermetallic compound $NdRu_2Si_2$ have been investigated in detail. Previous investigations on this ternary compound focused on the investigation of the magnetic and the transport properties of this compound near the antiferromagnetic transition while, not much attention has been given to the low temperature complex magnetic phase of this compound. These naturally occurring layered compounds exhibit a wide range of complex magnetic phases and thus in this article we report on the low temperature magnetic phase of $NdRu_2Si_2$ by comparison of the magnetic, electronic transport and magneto-caloric properties. We

have shown that an applied magnetic field greatly modifies the magneto-resistance (MR) properties of the compound at low T ($T < 10$ K) from the usual negative MR to an unusual positive MR (Figure 5(c)). In addition, an interesting anomaly between the MR and the magneto-caloric properties in this compound at $T < 10$ K with the application of high magnetic field of H > 5 T is also observed. Magneto-caloric investigations at this field and temperature range indicates that the compound is predominantly ferromagnetic while MR results indicates the presence of additional interactions which leads to positive MR in the ferromagnetic phase. Negative MR near T_N shows a modest value of 33% under an applied field of 8 T while lowering of T results in a reversal of MR up to 5%. The results have been explained by considering the appearance of field induced pseudo gaps in the Fermi surface of the compound $NdRu_2Si_2$. Our study indicates that detailed investigations of magnetic, electronic and magneto-caloric properties are important for ternary intermetallic compounds to unravel the complex magnetic and transport properties of these compounds.

Vanadium substitution in the cobalt site in parent compound $CeCo_2Si_2$ has been studied. The parent compound is a weak paramagnet. The magnetic susceptibility of $Ce(Co_{1-x}V_x)_2Si_2$ increases with increase in V content. Figure 1(d) shows p_{eff}, the effective number of Bohr magneton per formula unit, increases almost linearly with increase in vanadium content and reaches a value of 1.21 when vanadium concentration x is 0.35, *i.e.*, 35 % of cobalt is replaced by vanadium. NMR spectra for the parent compound $CeCo_2Si_2$ has been shown in Figure 5(d). The NMR spectra of the doped compounds are increasingly broadened and shifted to higher frequency. The broadening of the spectra also results in the disappearance of the quadrupolar satellites in the spectra of $Ce(Co_{0.85}V_{0.15})_2Si_2$ and $Ce(Co_{0.75}V_{0.25})_2Si_2$. The NMR results therefore indicate that in $RECo_2Si_2$ compounds, partial substitution of Co by V modifies the crystalline electric field which could also affect the magnetic properties of these compounds. Furthermore, the NMR study in this series of compounds also strengthens our claim of single phase nature of the doped compounds. The observed NMR signal is a signature of the intrinsic properties of the samples. Therefore,

the present study in this chapter confirms the purity of the doped compounds and indicates the magnetic properties observed in the doped samples are purely intrinsic and not due to formation of any unidentified binary phases of the constituent elements.

The thesis is composed of six chapters and these are as follows,

Chapter 1. Introduction

In this chapter the preliminary words of magnetism and magnetism in rare earth compounds, scientific interest, motivation and scope of work in $RECo_2Si_2$ (RE = rare earth) rare earth ternary silicide has been discussed. A brief introduction of some basic theories that have been used in the analysis of our work has also been mentioned.

Chapter 2. Experimental Techniques

The sample preparation procedures are thoroughly described in this chapter. To characterize and measure the physical properties of the prepared sample some commercial instruments were used. The working principle of those instruments are discussed in this chapter briefly.

Chapter 3. Study of Magnetic and magnetocaloric properties of vanadium substituted layered intermetallic compounds $RE(Co_{1-x}V_x)_2Si_2$ (RE = Pr and Nd; 0 $\leq x \leq$ 0.35

Efforts have been made to investigate the changes in the magnetic properties of intermetallic compounds $PrCo_2Si_2$ and $NdCo_2Si_2$ upon vanadium substitution of the cobalt site. The studies involved both temperature and field dependence of magnetization. Exchange bias, heat capacity, transport property studies are also performed for the samples. Magnetocaloric effect has been used as a tool to throw some insight into the magnetic ordering of some of the compounds.

Chapter 4. Transport property study of NdT_2Si_2 (T = Co, $Co_{0.65}V_{0.35}$, Ru) intermetallic compounds

In this chapter we address the basic physics behind the transport properties of some of the samples mentioned in Chapter 3. Effect of vanadium substitution in the transport properties in parent as well as the doped sample has been studied. Magneto-transport and magnetocaloric properties of isostructural compound $NdRu_2Si_2$ have also been presented.

Chapter 5. Study of vanadium substitution at cobalt site in $CeCo_2Si_2$

In this chapter, we have investigated the changes in magnetic properties in $CeCo_2Si_2$ compound as a result of substitution of cobalt with another non-magnetic transition element vanadium. A brief analysis of the NMR spectra of the parent as well as the doped compounds have been presented.

Chapter 6. Summary and future scope of work

In this chapter we address the basic physics behind the comparative study of magnetic, magneto-transport and magnetocaloric properties of the samples and present the key point of our thesis work in the summary section. This chapter also deals with the future aspects of the thesis.

LIST OF FIGURES

LIST OF TABLES

CHAPTER 1

Introduction

The discovery of the "attractive" or "magnetic" ore Loadstone, which was later used for navigation in compass marked the advent of one fascinating subject called magnetism. Apart from navigation, pointer made of loadstone was also used for geomancy, being a technique for aligning buildings in order to be in harmony with the forces of nature. Since then, magnetism and magnetic phenomena have been among the important aspects of human civilization. Today our understanding of magnetism is related to the concept of spin which arises from relativistic description of an electron in an external electromagnetic field and becomes manifest in the Dirac equation. Magnetism is closely related to applications throughout the industrial era. A lot of today's useful devices would be unthinkable without the forefront research in magnetism. Nowadays, magnets and magnetic materials are omnipresent in read heads in hard disks, computer memory disks, identity cards, speakers, refrigerator door seals, cars and toys etc. The scientific development of the subject of magnetism has come through various landmark discoveries beginning with the remarkable conclusion by William Gilbert in 1600 that earth behaves as a giant magnet. That an electric current produces a magnetic field was established through the works of Hans Christian Ørsted, André-Marie Ampère, Carl Friedrich Gauss, Jean-Baptiste Biot, and Félix Savart

in early 19th century. Then in 1831, Michael Faraday found that a time-varying magnetic flux through a loop of wire induced a voltage. Finally, James Clerk Maxwell synthesized and expanded these insights into what is now known as Maxwell's equations that constitute the foundation of classical electrodynamics.

However, it is the magnetism in condensed matter systems which is still of great interest today. Macroscopic systems exhibit magnetic properties which are fundamentally different from those of atoms and molecules, despite the fact that they are composed of the same basic constituents. This arises because magnetism is a collective phenomenon, involving the mutual cooperation of enormous numbers of particles, and is in this sense similar to superconductivity, superfluidity and even to the phenomenon of the solid state itself. The interest in answering fundamental questions runs in parallel with the technological drive to find new materials for use as permanent magnets, sensors, or in recording applications.

A deeper insight into the origin of magnetism has become possible by the quantum mechanical concept of atomic magnetic moment resulting from orbital and spin angular momentum of unpaired electrons. We begin with a discussion on magnetism and the classification of various materials based on their magnetic properties.

1.0.1 Magnetic Materials

The magnetic induction (**B**) is the response of a material to the applied magnetic field (**H**). The relationship between **B** and **H** depends on the material. The magnetization (**M**) is defined as the magnetic moment per unit volume such that

$$\mathbf{B} = \mu_0(\mathbf{H} + \mathbf{M}) \tag{1.1}$$

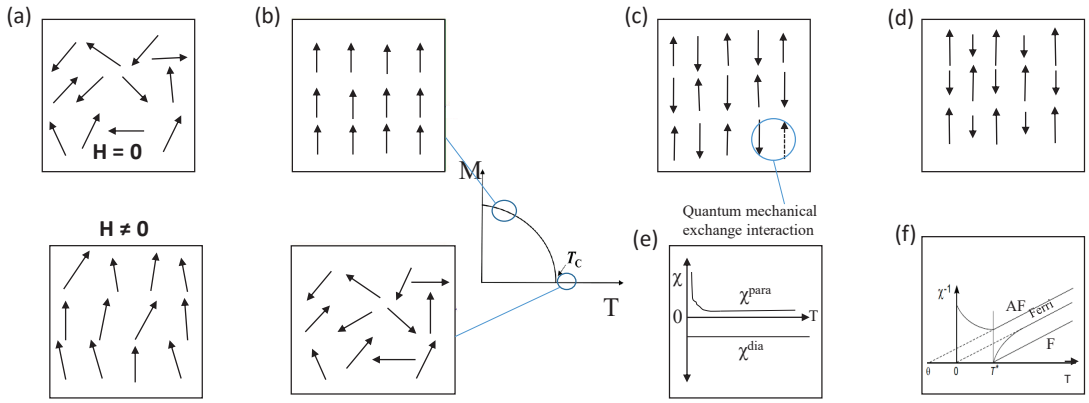

Figure 1.1: Schematic representation of magnetic spin structure; (a) paramagnetic spin moments in absence and presence of external magnetic field, (b) ferromagnetic spin moments below and above T_C, (c) antiferromagnetic spin moments, (d) ferrimagnetic spin moments, (e) temperature dependence (T) of the magnetic susceptibility (χ) in the case of diamagnetism and paramagnetism, (f) temperature dependence of inverse magnetic susceptibility (χ^{-1}) in the case of ferromagnetism (F), antiferromagnetism (AF), and ferrimagnetism (Ferri) with T^* being the critical temperature and θ the paramagnetic Curie temperature.

where, μ_0 is the permeability of free space. Apart from these, susceptibility (χ) which indicates the response of a material to a magnetic field and the permeability (μ), are defined from the relations

$$\mathbf{M} = \chi(\mathbf{H}) \tag{1.2}$$

and

$$\mathbf{B} = \mu(\mathbf{H}) \tag{1.3}$$

A material's magnetic property can be understood from the **M** or **B** versus **H** curves, called the magnetization curves. Based on the behaviour of the materials for an applied magnetic field H, susceptibility χ and spin structure of the material, materials can be

classified as:

- Diamagnetic
- Paramagnetic
- Ferromagnetic
- Antiferromagnetic
- Ferrimagnetic

1.0.2 Diamagnetism

Diamagnetic substances are composed of atoms that have all the orbitals filled and hence the net magnetic moment is zero in the absence of an applied field. However, when exposed to a magnetic field, atomic or molecular magnetic dipoles are induced which gets oriented antiparallel to the field due to Lenz's law. Thus a negative magnetization is produced, and hence the susceptibility is negative ($\chi < 0$) as shown in Figure 1.1(e).

$$\chi^{dia} = Const. < 0 \tag{1.4}$$

Some examples of diamagnetic materials are nearly all organic substances, metals like Hg, superconductors below the critical temperature. For an ideal diamagnet, χ^{dia} is -1. Usually substances have weak diamagnetic response which gets suppressed in presence of other forms of magnetism.

1.0.3 Paramagnetism

Paramagnetic materials have a net magnetic moment due to the presence of unpaired electrons in the outermost orbitals. The atoms or molecules of the substance have net orbital or spin magnetic moments that tend to be randomly orientated due to thermal fluctuations when there is no magnetic field (shown in Figure 1.1(a)). When a magnetic field is applied, there is a partial alignment of the atomic magnetic moments in the direction of the field. However, the individual magnetic moments do not interact and the net magnetic moment is zero when the field is removed. This results in a net positive magnetization and positive susceptibility as shown in Figure 1.1(e). Paramagnetism occurs in all atoms and molecules with unpaired electrons, *e.g.*, free atoms, free radicals, and compounds of transition metals containing ions with unfilled electron shells. There are magnetic moments associated with the spins of the conducting electrons in a metal, and in presence of a magnetic field, the imbalance in the numbers of parallel and antiparallel spins results in weak and almost temperature independent paramagnetism. The magnetic susceptibility (χ) of paramagnetic materials is characterized by,

$$\chi^{para} = Const. > 0 \tag{1.5}$$

1.0.4 Ferromagnetism

Ferromagnetic materials exhibit parallel alignment of moments as shown in Figure 1.1(b), which results in a spontaneous magnetization at room temperature, even in the absence of a magnetic field. The inverse susceptibility curve for a ferromagnet is provided in Figure 1.1(f). The transition elements Fe, Ni, Co and many of their alloys are typical examples of ferromagnetic (FM) materials. Adjacent moments are aligned parallel due to positive exchange coupling between moments in FM materials. Moreover, FM materials

retain the magnetization even after the applied field is removed, and this behavior is known as 'remanence'. Below a characteristic temperature known as the Curie temperature T_C, the material from the point of view of magnetism is subdivided into 'domains'. The magnetic moments enclosed in these domains exhibit a nearly parallel orientation even in absence of an external magnetic field, *i.e.*, each domain of the material has a spontaneous magnetization. The magnetic moments can again be localized (*e.g.*, Gd, EuO) or itinerant(*e.g.*, Fe, Co, Ni). Depending upon the temperature a ferromagnetic material can be in one of the three states. First condition is when,

$$T > T_C \tag{1.6}$$

The magnetic moments exhibit a random orientation like in paramagnetism. The susceptibility is given by,

$$\chi = \frac{C}{T - T_C} \tag{1.7}$$

which is the Curie-Weiss law. The constant C is called the Curie constant. The second condition is when,

$$0 < T < T_C \tag{1.8}$$

The magnetic moments exhibit a preferential orientation. The susceptibility exhibits a significantly more complicated functionality of different parameters compared to dia− and paramagnetism.

$$\chi^{Ferro} = \chi^{Ferro}(T, H, History) \tag{1.9}$$

The third state is when,

$$T = 0 \tag{1.10}$$

1.0.5 Antiferromagnetism

If, in a magnetic structure, the moments of two nearby sub-lattices are exactly equal but opposite, the net moment of the material is zero. This type of magnetic ordering is called antiferromagnetism (AFM), shown in Figure 1.1(c). In some materials, the atomic magnetic moments exhibit very strong interactions, which are produced by electronic exchange forces that have quantum mechanical origin. This exchange force results in the parallel or antiparallel alignment of atomic moments. In some materials, exchange interactions favour antiparallel alignment of atomic magnetic moments. Materials are magnetically ordered but have zero remnant magnetization. In antiferromagnets, the exchange force between the neighbouring moments is antiparallel, unlike in ferromagnets, in which exchange force is parallel. Above a certain temperature, called the Néel temperature, thermal energy overcomes the exchange energy and randomizes the moments. The exchange coupling constant depends on the ratio of inter-atomic distance to the atomic diameter. We observe that, for smaller values of this ratio, the exchange constant is negative for AFM materials like Cr and Mn indicating an antiparallel coupling of moments. A typical inverse susceptibility with temperature of a antiferromagnetic material is shown in the Figure 1.1(f).

1.0.6 Ferrimagnetism

In 1948, Neel proposed the existence of a third type of cooperative magnetic phenomena of which Mn_2Sb was a special case and worked out a simple yet detailed theory of such phenomena. This third type to which Neel gave the name ferrimagnetism

may be considered as a generalization of ferromagnetism and antiferromagnetism. In a ferrimagnetic material the substructures into which the magnetic structure may be divided are not identical because the complete magnetic structure contains more than one kind of magnetic atom, or more than one kind of crystallographic site or both. The point is that certain interactions which would be equal if the substructures were identical are no longer same. This asymmetry is responsible for the special properties of ferrimagnetic materials. To make it simpler, more complex forms of magnetic ordering as shown in Figure 1.1(d) can occur in ferrimagnets where, the magnetic moments of two nearby sublattices are opposite but unequal, unlike in AFM. This results in a net magnetic moment at room temperature. Even though ferrimagnetism exhibits similar characteristics as ferromagnetism, the ferrimagnetic materials are not good conductors like FM materials. A typical inverse susceptibility with temperature of a ferrimagnetic material is shown in the Figure 1.1(f).

1.1 Magnetic interactions

In this section we want to discuss about the different magnetic interactions which are responsible for magnetic ordering in different bulk materials.

1.1.1 Direct exchange

Direct exchange operates between moments, which are close enough to have sufficient overlap of their wavefunctions. It gives a strong but short range coupling which decreases rapidly as the ions are separated. An initial simple way of understanding direct exchange is to look at two atoms with one electron each. When the atoms are very close together the Coulomb interaction is minimal when the electrons spend most of their time

in between the nuclei. Since the electrons are then required to be at the same place in space at the same time, Pauli's exclusion principle requires that they possess opposite spins. According to Bethe and Slater the electrons spend most of their time in between neighboring atoms when the interatomic distance is small. This gives rise to antiparallel alignment and therefore negative exchange (antiferromagnetism), Figure 1.2(a). If the atoms are far apart the electrons spend their time away from each other in order to minimize the electron-electron repulsion. This gives rise to parallel alignment or positive exchange (ferromagnetism), Figure 1.2(a).

The direct inter-atomic exchange j can be positive or negative depending on the balance between the Coulomb and kinetic energies. The Bethe-Slater curve represents the magnitude of direct exchange as a function of interatomic distance. Cobalt is situated near the peak of this curve, while chromium and manganese are on the side of negative exchange. Iron, with its sign depending on the crystal structure is probably around the zero-crossing point of the curve, Figure 1.2(a).

1.1.2 Indirect exchange

- Superexchange interaction

  This type of indirect exchange interaction is usually observed in ionic solids. The exchange interaction between non-neighbouring ions is mediated by means of a non-magnetic ion which is located in between. The distance between the magnetic ions is too large for a direct exchange to occur. We take as an example the coupling between the moments on a pair of metal cations separated by a diatomic anion as illustrated in Figure 1.2(b). The ferric ion has a half filled $3d$ shell and so has a spherically symmetric charge distribution (S state ion). The triply charged rare-earth (RE) ion is not symmetric and has a strong spin-orbit coupling; its charge distribution

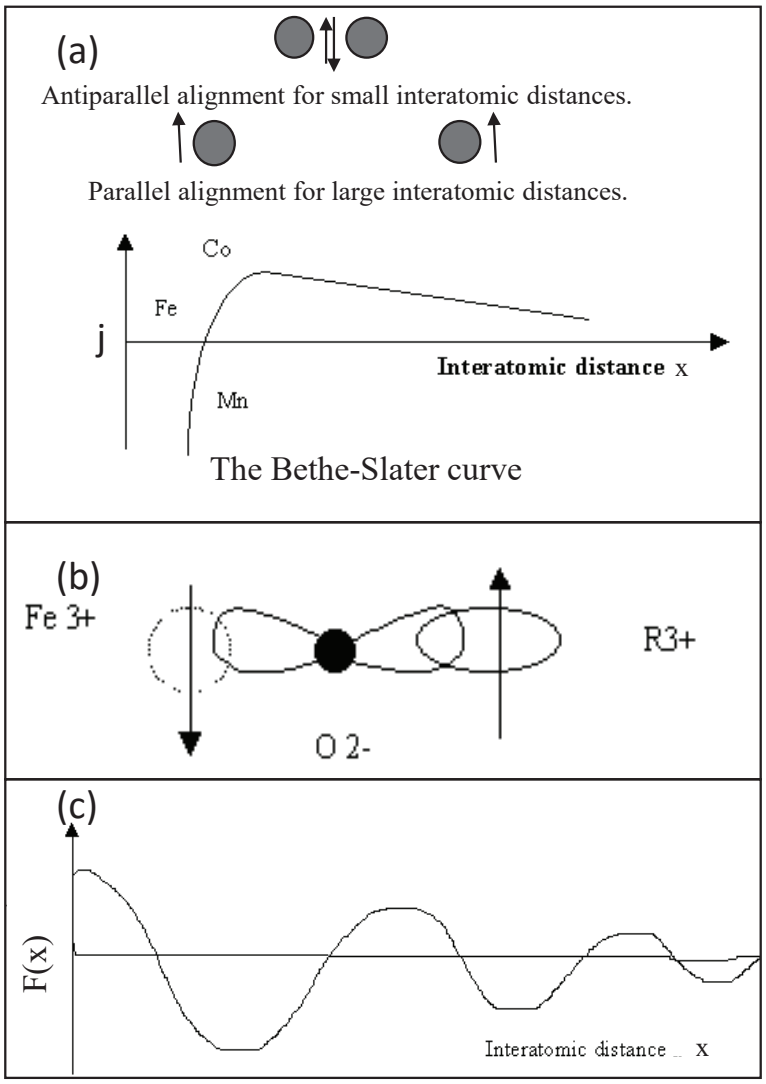

Figure 1.2: Figure (a) represents the pictorial diagram of direct exchange interaction and the Bethe - slater curve, (b) Superexchange in ferric-rare earth interaction in a garnet, and, (c) graphical representation of the function F(x). Positive values represent the ferromagnetic where as negative ones result in an antiferromagnetic arrangement.

is coupled to its moment. The ion's moments are coupled via superexchange, so turning the Fe moment alters the overlap of the *RE* cation in the molecule. This changes the magnitude of both the Coulomb and exchange interactions between the cations, leading to a coupling, which depends on the moment's orientation.

- RKKY interaction

Indirect exchange couples moments over relatively large distances. It is the dominant exchange interaction in metals, where there is little or no direct overlap between neighboring electrons. It therefore acts through an intermediary, which in metals are the conduction electrons (itinerant electrons). This type of exchange is better known as the *RKKY* interaction named after Ruderman, Kittel, Kasuya and Yoshida. The coupling is characterized by the distance dependent exchange coefficient J_{RKKY}:

$$J_{RKKY} \propto F(2k_F r) \tag{1.11}$$

with

$$F(x) = \frac{sinx - xcosx}{x^4} \tag{1.12}$$

where, k_F is the Fermi vector, and r is the separation between two interacting ions. The *RKKY* exchange coefficient J_{RKKY} oscillates from positive to negative as the separation of the ion changes and has the damped oscillatory nature shown in Figure 1.2(c). Therefore depending on the separation between a pair of ions their magnetic coupling can be ferromagnetic or antiferromagnetic. A magnetic ion induces a spin polarization in the conduction electrons in its neighborhood. This spin polarization in the itinerant electrons is felt by the moments of other magnetic ions within the range leading to an indirect coupling. In rare-earth metals, whose magnetic electrons in the $4f$ shell are shielded by the $5s$ and $5p$ electrons, direct exchange is rare and indirect exchange via the conduction electrons gives rise to magnetic order in these materials.

- Double exchange interaction

  In some oxides the magnetic ions exhibit mixed valencies which results in a ferromagnetic arrangement. Magnetite (Fe_3O_4)which includes both Fe^{2+} and Fe^{3+} ions is such a compound.

1.2 Intermetallic compounds

Intermetallics is the short designation for the intermetallic phases and compounds which result from the combination of various metals. It forms a tremendously numerous and manifold class of materials. According to a simple definition [1, 2], intermetallics are compounds of metals whose crystal structures are different from those of the constituent metals, and thus intermetallic phases and ordered alloys are included. During past several decades, intermetallics have been of enormous, and still increasing, interest in materials science and technology with respect to applications as well as fundamental physics. The rare earth intermetallics exhibit a number of interesting features. The rare earths are prolific compound formers, entering into chemical union with metals of almost every group in the periodic table. The numerous compounds show great range and diversity in respect to their structures and stoichiometries. They display a number of esoteric characteristics, *viz*., magnetic ordering producing in some cases rather exotic magnetic structures, a wide range of crystal field effects, unusual transport properties, such as resistance minima, large magnetoresistance, superconductivity, etc. In addition, the rare earth intermetallics afford the investigator the opportunity of studying a series of closely related isostructural compounds which differ only in the nature of the rare earth constituent.

Only a limited number studies of the magnetic properties of rare earth intermetallics predated the decade of the sixties. However, the present era of intensive investigation of these materials began with the work of Nesbitt et al. in 1959 and that of Hubbard et al. and Nassau et al. in 1960, on systems involving the rare earths in chemical union with a $3d$-transition metal [3]. All these seminal studies paved the way for extensive investigation of the fundamental properties of these and other rare earth intermetallics compounds.

1.2.1 Magnetism in rare-earth (*RE*) intermetallic compounds

The electronic configuration of rare earth atoms can be described in terms of folowing configuration

[Xe]$4f^n5d^16s^2$ (n = 1,2, ..., 14)

In most of the rare earth intermetallic compounds the rare earth ion remains in the trivalent state and the $5d^16s^2$ electrons form the conduction band. However the elements Ce, Eu and Yb often exhibit a valency other than 3^+. This is because depending upon the chemical environment, any one of completely filled, half filled or empty $4f$ orbitals can be energetically preferred. Magnetism in rare earth elements arises due to the unfilled $4f$ orbital of rare earth ions. The $4f$ electrons couple together according to Russel Saunders coupling and Hund's rule. The magnetic moment of the free trivalent rare earth ions is given as $g_J\sqrt{J(J+1)}\mu_B$ where g_J is the Lande g-factor, J is the total angular momentum and μ_B is the Bohr magneton. In the absence of crystal electric field effects the effective magnetic moment obtained from the temperature dependence of susceptibility in the paramagnetic region will be equal to this value. Some of the important magnetic properties of the rare earth ions are listed in the Table 1.1.

As mentioned before, in case of rare earth intermetallic compounds the localized moments interacts indirectly through conduction electrons via the *RKKY* interaction. Localized magnetic moment polarizes conduction spin near its vicinity. At a given lattice site, the actual spin polarization (**P**) of conduction electron consists of contributions from every lattice site. The polarized electron cloud in turn decides the orientation of the localized magnetic moment at a lattice site. The expression for the paramagnetic Curie

Table 1.1: Table showing magnetic properties of free rare earth ions. Here S, L, J, g_J, Q_{zz} denotes the total spin, total angular momentum, total momentum, Lande factor and quadrupolar moment of rare earth ion respectively. The factor $g_J\sqrt{J(J+1)}$ is the magnetic moment of the free rare earth ion.

Rare earth ion	$4f$ configuration	Ground term	S	L	J	g_J	$g_J\sqrt{J(J+1)}$	de Gennes factor G	Q_{zz}
La^{3+}, Ce^{4+},Y^{3+}	$4f^0$	$^1S_0$	0	0	0	-	0	0	-
Ce^{3+}	$4f^1$	$^2F_{5/2}$	1/2	3	5/2	6/7	2.54	0.011	-0.286
Pr^{3+}	$4f^2$	$^3H_4$	1	5	4	4/5	3.58	0.051	-0.294
Nd^{3+}	$4f^3$	$^4I_{9/2}$	3/2	6	9/2	8/11	3.62	0.116	-0.116
Pm^{3+}	$4f^4$	$^5I_4$	2	6	4	3/5	2.68	0.217	+0.108
Sm^{3+}	$4f^5$	$^6H_{5/2}$	5/2	5	5/2	2/7	0.84	0.283	+0.206
Eu^{3+}, Sm^{2+}	$4f^6$	$^7F_0$	3	3	0	0	0	0	0
Gd^{3+}, Eu^{2+}	$4f^7$	$^8S_{7/2}$	7/2	0	7/2	2	7.94	1	0
Tb^{3+}	$4f^8$	$^7F_6$	3	3	6	3/2	9.72	0.667	-0.333
Dy^{3+}	$4f^9$	$^6H_{15/2}$	5/2	5	15/2	4/3	10.63	0.450	-0.333
Ho^{3+}	$4f^10$	$^5I_8$	2	6	8	5/4	10.60	0.386	-0.133
Er^{3+}	$4f^11$	$^4I_{15/2}$	3/2	6	15/2	6/5	9.59	0.162	+0.133
Tm^{3+}	$4f^12$	$^3H_6$	1	5	6	7/6	7.57	0.074	+0.333
Yb^{3+} Tm^{2+}	$4f^13$	$^2F_{7/2}$	1/2	3	7/2	8/7	4.54	0.020	+0.333
Lu^{3+}, Yb^{2+}	$4f^14$	$^1S_0$	0	0	0	-	0	0	-

temperature θ_p in the molecular field model [4]considering $RKKY$ interaction is given by,

$$\theta_p = -\frac{3\pi n^2 J_{RKKY}(0)^2}{k_B E_F}(g_J-1)^2 J(J+1)\sum_i F(2k_F R_i|) \tag{1.13}$$

where, the factor $(g_J-1)^2$J(J+1) is known as de Gennes factor. It has been generally assumed that J_{RKKY} is a constant for a given isostructural rare earth series. Thus for an isostructural rare earth series the ordering temperatures are expected to scale with the de Gennes factor and is known as the de Gennes scaling of magnetic ordering temperature.

However, anomalously high magnetic ordering temperatures have been observed in various lighter rare earth compounds. It results due to the deviations from the following simplifying assumptions. In *RKKY* interaction the conduction electrons are treated as free electrons and the Fermi surface is spherically symmetric. Also the exchange integral J_{RKKY} is considered to remain constant across a rare earth series. In case of light rare earths the exchange integral can be different due to the partial delocalization of $4f$ orbital compared to the heavy ones. It was shown by Zhang and Levy [5] that the hybridization effect between $4f$ and conduction band will greatly influence the *RKKY* interaction. It is especially valid when the $4f$ orbitals are not well localized. It was shown by them that *RKKY* interaction in such cases will decay as $1/r^2$ or $1/r$ in particular directions and give rise to enhanced ordering temperature, instead of normal $1/r^3$ decay.

The *RKKY* model does not take into account the effect of crystalline electric field on *RE* ions. The intermetallic compounds can be considered as a lattice of charge immersed in a sea of conduction electrons. The $4f$ electrons residing on a given *RE* ion experience electron field produced by the screened charge of the surrounding ions. The effect of the non-uniform electric field leads to the removal of $(2J+1)$ fold degeneracy of the orbital momentum of rare earth ion. Since the spatial extent of the $4f$ wave function is small, the crystal field splitting is small compared to the spin orbit interaction. The total angular momentum can, therefore be taken as a good quantum number and the effect of the crystal field can be regarded as a small perturbation on the $(2J+1)$ fold degenerate ground multiplet. The presence of crystal field effect in *RE* intermetallic compounds can result in reduction of the bulk magnetic moment, although the magnitude of the actual moment may be close to the free ion value. The influence of crystalline electric field effect on the magnetic ordering temperature was considered by Noakes and Shenoy [6] by adding a *CEF* term in the exchange Hamiltonian. Using such Hamilton they were successful in explaining the enhancement of the magnetic ordering temperature in $RERh_4B_4$ (*RE* = Gd - Tm). Crystal field effect can also influence the transport and thermodynamic behavior of

RE compounds in some cases [6].

1.2.2 Quadrupolar interaction in Rare-Earth(RE) Intermetallic Compounds

In the case of *RE* elements for which total orbital momentum L is non-zero, the $4f$ distribution is not spherically symmetric. The dominant factor of this anisotropic charge distribution is the $4f$-electric quadrupolar moment. For symmetry the quadrupole moment is given by $Q_{zz} = \langle 3{J_z}^2 - J(J+1)\rangle$, the value of which for different rare earth elements is exhibited in Table 1.2. The single quadrupole can interact with *CEF* and can get oriented slowly with lowering temperature along favourable crystallographic axis [7, 8]. In rare earth intermetallic compounds the quadrupoles interact with each other and the coupling between the two quadrupoles is mediated by the conduction electrons [9]. This quadrupole pair interaction can dominate the magnetoelastic coupling and drive a quadrupolar ordering in the paramagnetic state. According to the sign of quadrupolar interaction ferro or antiferro ordering can take place. The quadrupole ordering in some of the compounds is listed in Table 1.2. Due to the quadrupolar interaction, the magnetic transition can be of first order in nature [9]. When the quadrupole gets oriented either by the single ion quadrupole lattice interaction by the *CEF* or due to quadrupole-quadrupole pair interaction lattice distortion may occur [9]. Such lattice distortions are observed for the ferroquadrupolar ordering as shown in Table 1.2.

The localized magnetic moment of *RE* ion is axially bound with the anisotropic charge distribution of $4f$ orbital. With the application of an external magnetic field in the paramagnetic state the partial alignment of magnetic moments can force the electric quadrupoles to orient in a particular direction. This can give rise to lattice distortion in the presence of magnetic field as observed in the magnetostriction data of $Y_xRE_{1-x}Cu_2Si_2$ [8].

Table 1.2: Table showing some of the compounds with ferroquadrupolar (FQ) or antiferoquadrupolar (AFQ) ordering. The values in the column of lattice distortion exhibits the structural distortions observed near quadrupolar ordering temperature. The ferromagnetic ordering temperature is denoted by T_C whereas T_N indicates the antiferomagnetic ordering temperature.

Compound	Type of quadrupolar ordering	Ordering temperature	Lattice distortion	Magnetic ordering	Ref
DyB_2C_2	AFQ	24.7 K	–	T_C = 16.4 K	[10]
$TmAg_2$	FQ	5.0 K	Tetra - ortho	–	[11]
CeAg	FQ	15.85 K	Cubic-Tetra	T_C = 5.5 K	[9]
HoB_2C_2	AFQ	5.0 K	–	T_N = 5.8 K	[12]
TmZn	FQ	8.55 K	Cubic-Tetra	T_C = 8.12 K	[9]
$PrPb_3$	AFQ	0.35 K	–	–	[9]

1.3 Scientific background and motivation

In the last few decades much attention has been paid to the understanding of the intermetallic compounds containing rare earth elements because of their intriguing physical properties, which have both fundamental and practical significance. Investigations of lanthanide intermetallics started about four decades ago when lanthanide elements were separated. Neutron diffraction experiments for pure elements indicate complex magnetic structures [13]. Those experimental data led to the development of theoretical models of magnetic interactions in lanthanide metals [14, 15]. Systematic investigations of binary and ternary lanthanide compounds have been performed. These investigations provided lots of new results that were interesting for the fundamental aspects of magnetism, such as crystalline electric field, exchange interactions, magnetoelastic and quadrupolar coupling, etc. The impact for starting fundamental research on $5f$ electron materials was doubtlessly the determination of the ferromagnetic properties of UH_3 and UD_3 and the detection of the superconducting state in UBe_{12} [16]. Special attention has been given to ternary compounds. For example, ternary compounds based on transition metals show physical

properties different from binary compounds. The synthesis performed using the Pauli paramagnetic compounds CoTi and CoSn results in the strongly ferromagnetic compound Co_2TiSn, with T_C close to room temperature [17]. In the course of investigating the physical properties of binary and ternary lanthanide and uranium phases, a number of new effects have been either discovered or confirmed. Effects such as mixed valence, Kondo lattice spin fluctuations, heavy fermions, and the coexistence of magnetism and superconductivity were found to depend on the electronic structure of lanthanide and uranium ions, in particular they are strongly related to the position of the $4f$ or $5f$ electron levels with respect to the Fermi energy. Rare earth intermetallics play an important role in a large part of current research that concerns new magnetostrictive and permanent magnetic materials, spin glass, and random anisotropy systems.

One of the many 'families' of intermetallic systems, which turned out to be particularly interesting, consists of compounds exhibiting the tetragonal $BaAl_4$ type of structure and its modifications. A large number of these type of compounds have been synthesized up to now and their properties have been investigated. Their general chemical formula is RET_2X_2, where *RE* is a rare earth, T is a transition metal ($3d, 4d, or 5d$) and X stands for silicon or germanium. These compounds are stable over a large temperature range and they appear in a strict stoichiometric ratio of 1:2:2. The crystal structure of these class of compounds is of tetragonal symmetry with large c/a ratio equal to about 2.5 in all cases, so one may expect a large anisotropy of physical properties. These compounds crystallize in either of two allotropic modifications of the tetragonal $BaAl_4$ type structure [18]; a body-centered tetragonal structure (space group I4/mmm, $ThCr_2Si_2$ type) [19] or a primitive tetragonal structure (space group P4/nmm, $CaBe_2Ge_2$ type) [20]. The unit cell of $ThCr_2Si_2$ type is displayed in Figure 1.3. The atomic framework of this structure can be displayed as a monatomic sequence perpendicular to the *c*-axis;

- for the $ThCr_2Si_2$ type structure : *RE* –X –T –X –*RE* –X –T –X –*RE*

The atoms are distributed as follows :

RE(Th) in 2*a* site : $0,0,0$;

T(Cr) in 4*d* site : $0,\frac{1}{2},\frac{1}{4};\frac{1}{2},0,\frac{1}{4}$;

X(Si) in 4*e* site : $0,0,z;0,0,\bar{z}$; + body centering translation.

This type of crystal structure consists of tetrahedra of X atoms with a T atom embedded inside. The X–X distances are usually close to the sum of covalent radii of X atoms, just as the T–X contacts. Strong chemical interactions are expected within the layers composed of tetrahedra which in turn consists of four X atoms. The bond lengths are dependent on the magnitude of the z parameter and the c/a ratio (where a, b, c are the lattice constants). In the case of a regular tetrahedron:

$z = \frac{1}{4} + \frac{1}{2\sqrt{2}}\frac{a}{c} = \frac{3}{8}$ if $c/a = 2\sqrt{2}$.

Therefore, the crystal structure of $ThCr_2Si_2$ type is characterized by two key parameters, *viz.*, the free parameter z and the c/a ratio. The values of these parameters for rare earth compounds change with the kind of transition metal involved [21]. The z values are found to be ~ 0.375. For compounds containing Ru and Os, this z parameter is found to be smaller than 0.375. The a/c values are in the range from 0.366 to 0.424. This indicates that the tetrahedra deviate from the regular shape. The shortest distance between two X atoms belonging to two adjacent layers of 4X tetrahedra is $(1-2z)c$. It implies that strong X-X interaction exists. The layers form a sandwich framework with *RE* atoms in between. Each *RE* atom coordinates 8X atoms and 8T atoms at the corners of a cube at a distance smaller than corresponding sum of the ionic radii but larger than the sum of covalent radii. The distortion of the *RE* ˇ 8X cube is also dependent on the z parameter.

The atomic framework for the $CaBe_2Ge_2$ structure can be alternatively displayed as a monatomic sequence perpendicular to the c-axis: *RE* –T –X –T –*RE* –X –T –X –*RE*

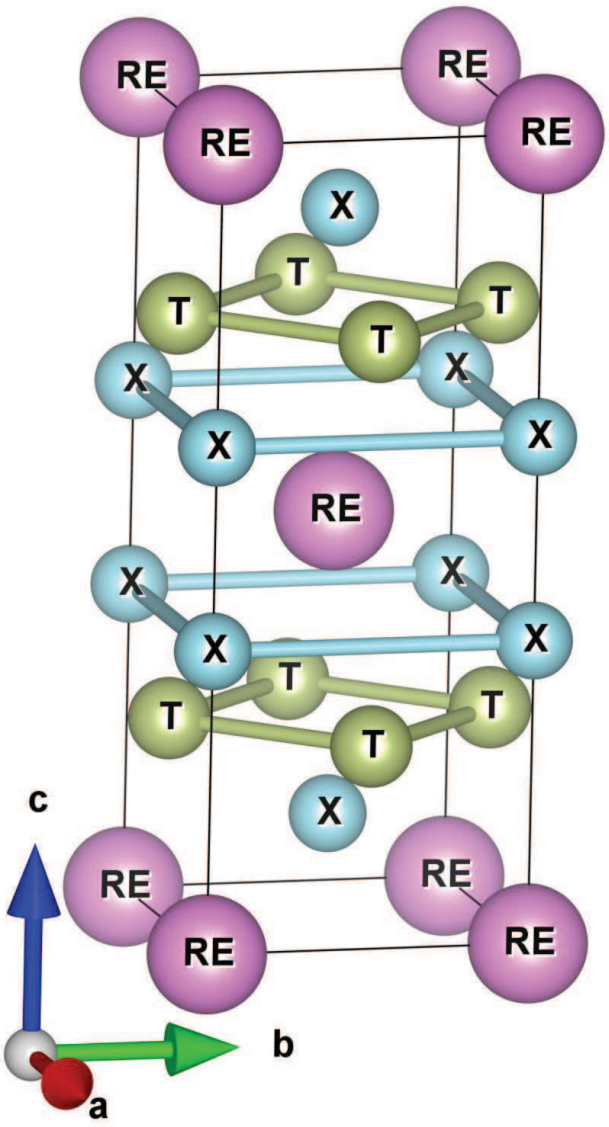

Figure 1.3: Crystal structure of RET_2X_2 compounds of $ThCr_2Si_2$ type

Both of these structures can be considered as consisting of three dimensional framework with short bond distances, where the rare earth atoms occupy the largest open spaces. The layered character of the crystal structure of these compounds is strongly reflected in their magnetic properties.

The intermetallic compounds of the ternary rare earth silicide/germanide series have attracted many researchers through decades for their intriguing crystal structure, complex magnetic structures and above all interesting magnetic properties. They were synthesized

for the first time by Rieger and Parthe [22] and Rossi et al. [23]. Temperature dependence of magnetic susceptibility of few $RECr_2X_2$ compounds, *viz.*, $GdCr_2Si_2$, $DyCr_2Ge_2$ have been reported around 1980s [24, 25, 26]. Mössbauer effect measurement performed by Nowik et al. at low temperature yielded the hyperfine fields for these compounds. In the past years magnetic properties of $REMn_2X_2$ compounds were studied extensively by both magnetometric and neutron diffraction methods. Magnetometric measurements by Szytula et al. [27] indicate that $REMn_2X_2$ compounds exhibit two critical magnetic ordering temperatures. The results of investigations indicate that the T component in this RET_2X_2 compounds carry no magnetic moment in most compounds, except for those with Mn. In $REMn_2X_2$ compounds Mn moments order at high temperature, while the rare earth moments usually order antiferromagnetically or ferromagnetically at low temperature. Magnetic properties of $REMn_2X_2$ compounds along with their magnetic structure has been presented in references [28, 29, 30, 31]. $REFe_2Si_2$ and $REFe_2Ge_2$ have also been widely studied. First results of magnetometric and Mössbauer effect experiments suggested that $REFe_2Si_2$ and $REFe_2Ge_2$ compounds are weak ferromagnets below temperature of ~ 700 K [32]. Felner et al. reported that $NdFe_2Si_2$ and $NdFe_2Ge_2$ order antiferromagnetically with Neel temperature of 13 K and 11 K respectively [33], while other $REFe_2Ge_2$ compounds (*RE* = La, Ce, Pr, Sm and Dy) did not order down to 4.2 K. Malik et al. investigated the magnetic properties of $REFe_2Ge_2$ (*RE* = Pr, Gd, Tb and Er) [34]. $ErFe_2Ge_2$ was found to be paramagnetic down to 4.2 K, while the remaining ones ordered antiferromagnetically. Magnetometric and neutron diffraction studies have been carried out in other RET_2X_2 compounds, where T = Ni, Cu, Pd, Pt [35, 36, 37, 38, 39, 40, 41, 42, 43, 44, 45].

The RET_2X_2 compounds with T = Co and X = Si have been studied by researchers because of their exciting properties. These properties are found to vary depending on the rare earth element [36, 46, 47]. The $RECo_2Si_2$ compounds with *RE* = La, Ce, Lu and Y are Pauli paramagnets, *i.e.*, their magnetic susceptibilities are independent of temperature. Compounds of this series with *RE* = Sm, Er and Tm are found to obey Curie-Weiss law

down to about 4.2 K and show a lack of ordering of the magnetic moments above that temperature. The temperature dependence of the magnetic susceptibility for the $RECo_2Si_2$ (*RE* = Pr, Nd, Gd - Er) and $RECo_2Ge_2$ (*RE* = Pr, Nd, Eu - Ho) compounds exhibit characteristic maxima connected with their respective Neel temperatures between 6 and 46 K. Magnetic measurements (1.6 to 600 K) for fields up to 1 T showed enhanced Pauli paramagnetism with spin fluctuation temperature around 150 K with Co and Ni as T element [48]. It was revealed from the magnetic and resistivity measurements on single crystal of $CeCo_2Si_2$ that the physical properties are well characterized as a valence fluctuating system and there was no evidence of superconductivity down to about 0.3 K [49]. Cerium compounds, *viz.*, $CeFe_2Si_2$, $CeCo_2Si_2$, $CeNi_2Si_2$ were shown to be Kondo lattice [50]. Neutron diffraction study on $PrCo_2Si_2$ and $NdCo_2Si_2$ carried out at liquid helium temperature indicates the magnetic moments to be localized on *RE* ion situated at $(0,0,0)$ and $(\frac{1}{2},\frac{1}{2},\frac{1}{2})$ sites and are pointing along the tetragonal *c*-axis. This type of magnetic ordering can be visualized as a + - + - sequence of FM sheets piled up along the *c*-axis [51]. Neel points were determined from the temperature dependence of magnetic peak heights. Other magnetic and neutron diffraction experiments on a single crystal of $NdCo_2Si_2$ yielded interesting results. Square-wave structures with propagation vectors **K** = (0,0,0.928) and (0,0,0.785) appear for 15 K$\leq$ T $\leq$ 24 K and $24K \leq T \leq 32$ K (T_N) respectively. A simple collinear AFM phase was observed to be stable in the temperature range between 0-15 K [52]. Various other properties of $NdCo_2Si_2$ compound *viz.*, effect of high magnetic field on the magnetic transitions, molecular field calculations of the phase transitions and effect of pressure on magnetic structure have been studied [53, 54, 55].

Magnetic phases in $PrCo_2Si_2$ have been studied by measurements of magnetization, neutron diffraction and electrical resistivity. For $T < 9$ K, the magnetic structure with a propagation vector $\mathbf{K} = (0,0,1)[2\pi/c]$ is stable [56]. High field magnetization and neutron diffraction on single crystal of $PrCo_2Si_2$ have been studied [57, 58]. Metamagnetic transitions with four steps are observable in the *c*-axis magnetization process up to 300

kOe. The $PrCo_2Si_2$ compound has a high-order commensurate structure with a propagation vector Q_3 = (0, 0, 0.777) for $T_N \sim$ 30 K $\geq$ T$\geq$ 17 K and a structure with Q_2 =(0, 0, 0.926) for 17 K $\geq$T$\geq$ 9 K, and undergoes a transition between the high-order commensurate structure and a commensurate structure with Q_z= (0, 0,1) at 9 K. The magnetic moments are parallel or antiparallel to the *c*-axis and perpendicular to the ferromagnetic *c*-planes for all the ordered structures. The magnetization at 4.2 K proceeds by a four-step metamagnetic process. The magnetic transitions and the magnetization process have been studied by introducing a wave-like molecular field H_m(i)= $\sum_q \lambda(q)\langle J_q\rangle \cos(\pi qi + \phi_q)$. Results of the numerical calculations made with the Ising spin chain are presented. The wavenumber-dependent molecular field coefficient $\lambda(q)$ has a maximum at $q = Q_3$ and is large positive for $1 \geq q \geq Q_3$ and is negative for $0.4 \geq q \geq 0$. The appearance of the magnetic transitions is shown by calculating the free energy [59]. Thermodynamic study of the magnetic transitions in this compound has been carried out by Takeda et al. [60]. In the magnetically commensurate phases in the anisotropic compound $PrCo_2Si_2$, the contribution from the paramagnetic ions to the entropy was detected to be about $K_B ln2$ from the heat capacity and the adiabatic magnetization experiment. The possibility of the phase-slipping of the sinusoidal exchange field has been suggested to be driven by the variation of temperature in zero field. These results suggest that the $PrCo_2Si_2$ and $NdCo_2Si_2$ intermetallic compounds are of great interest from the point of both macroscopic and microscopic studies.

The research on $RERu_2Si_2$ started around 1970-80's due to the realization that these intermetallic compounds exhibit several interesting magnetic and electron transport properties. Magnetic investigations over a large range of T indicated these compounds show van-Vleck paramagnetic type behavior typical of RE^{3+} ions for $T > 300$ K while complicated magnetic properties at low temperatures [61]. Further studies on the isostructural family ($RERh_2Ge_2$) revealed that conduction electrons play an important role for the determination of magnetic properties of compounds [62]. Neutron diffraction studies also indicated that the magnetic properties of these class of compounds are complex and multiple magnetic

structures have been observed with transitions from one structure to another with the lowering of temperature [63]. This resulted in exhaustive investigations of the magnetism in these class of compounds both in polycrystalline and single crystalline forms [64]. One of the important compound of this series is $NdRu_2Si_2$ which exhibits several complicated magnetic structures [64, 65]. Magnetic investigations using neutron diffraction techniques revealed antiferromagnetic ordering of the Nd moments at $T_N = 23$ K, with incommensurate propagation vector $\mathbf{K} = (0.13, 0.13, 0)$. With the decrease of temperature a third harmonic of $\mathbf{K}$ was observed which indicates a squaring of the primary structure below 16 K. At about 9 K magnetic ordering changes from antiferromagnetic to coexisting ferromagnetic and antiferromagnetic ones with domination of the ferromagnetic phase. Along with the magnetic properties of this compound, there was also an increased interest on the electronic transport properties [66, 67, 68]. These results suggested that $RERu_2Si_2$ exhibits interesting low temperature magnetic phases with the existence of correlation between electronic and magnetic properties.

1.4 Scope of work

In recent years much attention has been paid to the understanding of rare earth based intermetallic materials for their varied magnetic and transport properties. Apart from the interesting magnetic properties (as discussed in earlier section), these compounds are known to exhibit anomalous and intriguing transport and magneto-transport properties which are even subjected to modifications upon substitution in either of the rare earth or the transition metal sites.*e.g.* [69, 70, 71, 72, 73, 74].

It is to be noted, that, so far, all the substitutions involved combinations of only those rare earth and transition metal elements that are reported to form RET_2X_2 compounds of $ThCr_2Si_2$ type structure. The present thesis describes the modifications in the magnetic

properties of $RECo_2Si_2$ (RE = Ce, Pr, Nd) compounds upon substitution of cobalt with vanadium which is not known to be among the elements forming ThCr_2Si_2 type pure compounds. In the first portion of the work reported here non magnetic Co has been replaced partially by another non-magnetic element vanadium. V substitution causes lattice expansion which can be thought of as a negative pressure acting on the system. With this motivation, we have carried out a systematic study of the temperature and vanadium concentration dependent evolution of the magnetization and electrical resistivity of the $RECo_2Si_2$ systems.

In this thesis we investigated the following rare earth intermetallic compounds. The studies are carried out systematically in the following sequences:

(i) Effect of V substitution in the Co site in $RE(Co_{1-x}V_x)_2Si_2$ ($0 \leq x \leq 0.35$) (RE = Pr, Nd) have been studied. The sequence of study for this part of the thesis goes as : synthesis of $RE(Co_{1-x}V_x)_2Si_2$ compounds by arc melting method. X-ray diffraction measurement was carried out to check the single phase nature of the samples. To characterize the samples FESEM of some of the doped samples were carried out. Magnetization measurements, heat capacity and resistivity measurements have been performed. It has been realized that the field of magnetocaloric effect (MCE) has both technological and fundamental interest. Magnetocaloric studies can give more insight about magnetic ordering of a system. We have utilized this to probe the changes in the magnetization properties in the doped compounds. The magnetic behavior of the $RECo_2Si_2$ (RE = Pr and Nd) compounds upon being doped with vanadium is reported for the first time.

(ii) The RET_2X_2 compounds exhibit interesting transport and magneto-transport properties. In view of this we carried out the magneto-transport study in one of the $RECo_2Si_2$ compounds where RE is Nd yielding interesting results. Our magneto-transport study was further extended to see the effect of vanadium doping in the transport properties in $Nd(Co_{1-x}V_x)_2Si_2$ (x = 0.35). The results of the magneto-transport study in the V

doped compound, $Nd(Co_{0.65}V_{0.35})_2Si_2$, drove us to study the magneto-transport property of an isostructural compound $NdRu_2Si_2$. Comparative studies of magnetoresistance and magnetocaloric effect has been carried out in order to distinguish between the different contributions to the magneto-transport property in this compound.

(iii) Lastly, attempts have been made to understand the effect of V substitution in the Co site in $CeCo_2Si_2$ using magnetization and Nuclear magnetic resonance (NMR).

1.5 Some basic theories

1.5.1 Exchange bias

The exchange bias effect is an old phenomenon which was discovered in 1956 by Meiklejohn and Bean. They observed a shift of the magnetic hysteresis loop along the field axis at low temperature when Co/CoO core-shell nanoparticles were cooled in a static magnetic field [75, 76]. Exchange bias effect is the shift of the magnetic hysteresis loop resulting from the pinning effect at the interface between soft and hard magnetic substances. One of the most interesting interfaces for studying the exchange bias effect is interface between a ferromagnetic (FM) and an antiferromagnetic (AFM) material. Spin arrangement in a FM/AFM layer at the temperature $T_N < T < T_C$ and at the temperature $T < T_N$ is shown in the Figure 1.4(a) and (b). An example of a simple hysteresis loop at the temperature $T_N < T < T_C$ and such a shifted hysteresis loop at the temperature $T < T_N$ of a material with a FM/AFM layer are sketched in Figure 1.4(c) and (d). The center of the hysteresis loop is shifted from zero applied magnetic field by an amount H_{EB}, the exchange bias field. There are three different fields used to characterize the bias; the left and right coercive fields, H_{c1} and H_{c2}, and the bias field H_{EB}. In a FM/AFM system, a shifted hysteresis loop can be experimentally obtained below T_N of the AFM material in

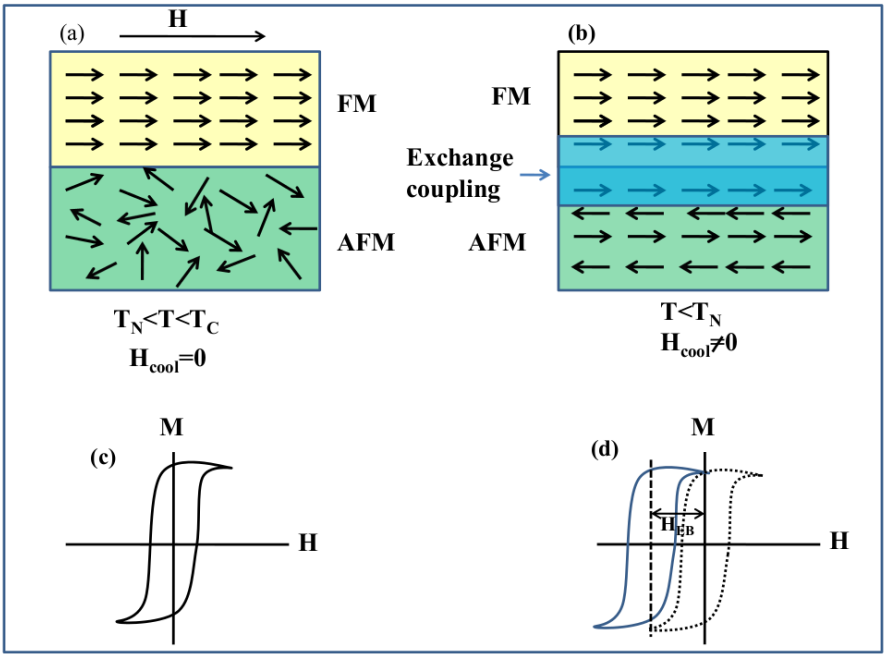

Figure 1.4: Figure represents (a) Spin arrangments in a FM/AFM layer at the temperature $T_N < T < T_C$; (b) Spin arrangments in a FM/AFM layer at the temperature $T < T_N$; (c) hysteresis loop of a material with FM/AFM layer at the temperature $T_N < T < T_C$; (d) a shifted hysteresis loop of a material with FM/AFM layer at the temperature $T < T_N$.

the following protocol. First, the hysteresis curve is drawn in the zero field cooled (ZFC) condition. After that a magnetic field is applied at a temperature higher than T_N in order to saturate the ferromagnetic material. The second step is to cool the sample below T_N in the presence of the same magnetic field. Then again hysteresis curve is drawn in this field cooled (FC) condition. The hysteresis loop in FC condition is shifted compared with the loop in ZFC condition. This shift is due to the strong anisotropy and a weak exchange energy coupling between the FM and AFM material.

The macroscopic observation of the hysteresis loop shift due to unidirectional anisotropy of a FM/AFM bilayer can be qualitatively understood by analyzing the microscopic magnetic structure of their common interface. The critical temperature of FM and AFM layer should satisfy the condition $T_C > T_N$, where T_C is the Curie temperature of the FM layer and T_N is the Neel temperature of the AFM layer. At a temperature

$T_N < T < T_C$, the FM spins align along the direction of the applied field, whereas the AFM spins remain randomly oriented in a paramagnetic state. The hysteresis curve of the ferromagnetic material is centered around zero. Next, a high magnetic field is applied which is higher than the saturation field of ferromagnetic layer and then, without changing the applied field, the temperature is being decreased to a finite value lower then T_N (field cooling procedure). After field cooling the system, due to the exchange interaction at the interface, the first monolayer of the AFM layer will align ferromagnetically (or antiferromagetically) to the FM spins. The next monolayer of the antiferromagnet will have to align antiparallel to the previous layer as to complete the AFM order, and so on. Note that the AFM interface spins are uncompensated, leading to a finite net magnetization of this monolayer. It is assumed that both the ferromagnetic and the antiferromagnetic are in a single domain state and that they will remain single domains during the re-magnetization process. When reversing the field, the FM spins will try to rotate in-plane to the opposite direction. Being coupled to the AFM, which is considered to be rigid, it takes a stronger force and therefore a stronger external field is needed to overcome this coupling and to rotate the ferromagnetic spins. As a result, the first coercive field is higher than the previous one at $T > T_N$, when the FM/AFM interaction was not yet active. On the way back from negative saturation to positive one, the FM spins will need a smaller external force in order to rotate back to the original direction. A torque is acting on the FM spins for all angles except the stable direction which is along the field cooling direction (unidirectional anisotropy). As a result, the magnetization curve is shifted to negative values of the applied field.

1.5.2 Specific heat: Debye theory

Specific heat is the amount of heat required to change the temperature of one unit of mass of a substance by one degree. By heat capacity, it is often referred that heat capacity at constant volume, which is more fundamental than the heat capacity at constant

pressure. Any theory used to calculate lattice vibration heat capacities of crystalline solids must explain two things:

1. Near room temperature, the heat capacity of most solids is around 3 K per atom (the molar heat capacity for a solid consisting of n-atom molecules is $\sim 3nR$). This is the well-known Dulong and Petit law.

2. At low temperatures, C_v decreases, becoming zero at $T = 0$. Heat capacities have a temperature dependence of the form $\alpha T^3 + \gamma T$, where the T^3 term arises from lattice vibrations, and the linear term from conduction electrons.

Classical mechanics would predict $C_v = 3R$ at all temperatures, in violation of both experiment and the third law of thermodynamics. The Debye model was developed by Peter Debye in 1912. He estimated the phonon contribution to the heat capacity in solids. The Debye model treats the vibration of the lattice as phonons in a box, in contrast to Einstein model, which treats the solid as non-interacting harmonic oscillators. The Debye model predicts the low temperature dependence of heat capacity T^3 that confirms the experimental results. Moreover, it covers the high temperature limits like the Einstein model. Debye improved on Einstein's theory by treating the coupled vibrations of the solid in terms of 3N normal modes of vibration of the whole system, each with its own frequency. The lattice vibrations are therefore equivalent to 3N independent harmonic oscillators with these normal mode frequencies. For low frequency vibrations, defined as those for which the wavelength is much greater than the atomic spacing, $\lambda >> a$, the crystal may be treated as a homogeneous elastic medium. The normal modes are the frequencies of the standing waves that are possible in the medium.

Debye derived an expression for the number of modes with frequency between ν and $\nu + d\nu$ in such a medium. As outlined above, this expression applies only to low frequency vibrations in a crystal. Debye used the approximation that it applied to all frequencies,

and introduced a maximum frequency ν_D (the Debye frequency) such that there were 3N modes in total, *i.e.*, $\int_0^{\nu_D} g(\nu)d\nu$ = 3N. The Debye frequency corresponds to $\lambda = 2a$, when neighboring atoms vibrate in antiphase with each other. With this approximation in place, Debye integrated over all of the frequencies to find the internal energy of the crystal, and then calculated the heat capacity using $C_v = (\partial U/\partial T)v$. The resulting expression is given below.

$$C_v = 3NK\left(\frac{3}{{x_D}^3}\int_0^{x_D}\frac{x^4e^x dx}{(e^x-1)^2}\right) \tag{1.14}$$

where x = $\frac{h_\nu}{KT}$, and x_D = $\frac{\theta_D}{T}$.

where θ_D is the Debye temperature.

1.5.3 Resistivity behaviour of rare earth intermetallic compounds

According to the Matthiessen's rule the electrical resistivity (ρ) of rare earth intermetallic compounds, can be represented as

$$\rho(T) = \rho_0 + \rho_{ph}(T) + \rho_{mag}(T) \tag{1.15}$$

where ρ_0 is the residual resistivity, ρ_{ph} and ρ_{mag} are the phonon and magnetic contributions to the resistivity. The residual resistivity is temperature independent. It arises due to the elastic scattering of the conduction electrons from vacancies, dislocations and impurities in the system etc. In most of the rare earth compounds it is difficult to obtain reliable values for residual resistivity because the rare earth intermetallic compounds are quite brittle. The phonon resistivity (ρ_{ph}) arises from the electron-phonon interaction and is given by Bloch-

Gruneisen law[77]

$$\rho_{ph} = 4A\left(\frac{T}{\theta_D}\right)^5 \int_0^{\theta_D/T} \frac{x^5 dx}{(1-e^{-}x)(e^x-1)} \tag{1.16}$$

where, the constant A includes the electron-phonon coupling constant, the atomic mass of different types of atoms and a characteristic temperature θ_D for the phonons. At low temperature, the resistivity due to electron-phonon interaction is proportional to T^5 and is also proportional to T at high temperatures. The magnetic contribution to resistivity (ρ_{mag}) arises from the disorder in the arrangement of magnetic moments. In the paramagnetic region magnetic contribution to resistivity is generally known as spin disorder resistivity (ρ_{spd}) and it is given by the following relation [78, 79]

$$\rho_{spd} = \left(\frac{3\pi N m^*}{2\hbar e^2 E_F}\right)|J_{RKKY}|^2(g_J-1)^2 J(J+1) \tag{1.17}$$

This relation has been derived considering the assumption of free electron with an effective mass m^* and in the absence of crystal field effects. Equation 1.16 exhibits in the paramagnetic region, the magnetic contribution to resistivity is proportional to the de Gennes factor and temperature independent. However, in the presence of crystal field effect spin disorder resistivity shows temperature dependence [80]. Below magnetic ordering temperature, the magnetic contribution to resistivity decreases. This decrease in spin disorder is reflected in the temperature dependence of the total resistivity of the system. This can be used to identify the magnetic transition temperatures of a compound. The other effect of magnetic ordering is that the conduction electron experiences the periodicity of the ordered magnetic lattice via the $s-f$ interaction. In case of ferromagnets, $s-f$ interaction give rise to **k** independent exchange splitting of the spin up and spin down bands. When the magnetic periodicity does not coincide with the lattice periodicity in case of antiferromagnets, an extra set of energy gaps may appear at the magnetic

superzone boundaries. Magnetic superzone gap can influence the Fermi surface below antiferomagnetic ordering and resistivity can increase with lowering of temperature.

1.5.4 Magnetoresistance behaviour of rare earth intermetallic compounds

Magneto-transport in rare earth intermetallic compounds is complicated. In the presence of magnetic field conduction electron experiences a Lorentz force. The magnetoresistance due to Lorentz force is small except at very low temperatures and in case of high purity samples. They should also have very low resistivity. It gives a positive H^2 to the magnetoresistance at low fields and magnetoresistance saturates at high fields and low temperatures [81]. In polycrystalline samples in some cases magnetoresistance has been observed to increase linearly with an increase of magnetic field. The linear H dependence results from the averaging over the separate crystallites, for some of which it is H^2, whereas for others it tends to saturate [81]. For samples containing localized moments in the paramagnetic state the application of magnetic field suppresses the spin fluctuations. This results in a negative magnetoresistance. Due to this effect the magnetoresistance was shown to give -H^2 [82, 83] well above magnetic ordering temperature. For a ferromagnetic material due to the suppression of spin fluctuation by externally applied magnetic field the magnetoresistance is negative and shows a linear dependence in H [82, 83]. According to spin fluctuation theory of Ueda [84, 85] the magnetoresistance is negative and proportional to H and H^2 for weak and nearly ferromagnetic metals respectively, while for a strong magnetic field it is proportional to $H^{-1/3}$. In the case of antiferromagnets with the application of magnetic field along the sublattice magnetization, spin fluctuation of the parallel sublattice decreases, whereas for the antiparallel one it increases. Yamada et al. showed that the combination of these two effects produces a positive magnetoresistance proportional to H^2 [83]. When the Zeeman energy due to the applied field overcomes

the anisotropy energy, the magnetic structure displays a spin flop transition. In this configuration magnetoresistance is small until a ferromagnetic configuration is achieved and magnetoresistance becomes negative. In the presence of superzone gap effect in an antiferromagnet, the situation can be complicated due to the modification of the gap with the application of magnetic field. If the magnetic structure changes with application of magnetic field then the superzone energy gap in the conduction band gets modified resulting in a change in the magnetoresistance.

1.5.5 Magnetocaloric effect

Magnetocaloric effect (MCE) is an area of great research interest. The study of MCE in rare earth intermetallics is of particular interest, because of their immense potential as magnetic cooling materials which serve as the basis for refrigeration from near room temperature to less than 1 K [86, 87]. Apart from its technological importance MCE can also yield basic information about magnetic interactions. The MCE was first discovered by Warburg about 120 years ago when he observed heat evolution in iron under the effect of a varying magnetic field [88].

- Relation between magnetization and MCE

  The relation between magnetization and MCE can be derived from the thermodynamic equations. From Maxwell's relation

$$\left(\frac{\partial S(T,H)}{\partial H}\right)_T = \left(\frac{\partial M(T,H)}{\partial T}\right)_H \tag{1.18}$$

  where S_M denotes the entropy and M the magnetization of a system at a temperature T and magnetic field H. The isothermal change in entropy (ΔS_M) with magnetic field

change from H_1 to H_2 is given by the relation,

$$\Delta S_M = \int_{H_1}^{H_2} \left(\frac{\partial M(T,H)}{\partial T} \right)_H dH \tag{1.19}$$

The adiabatic change in temperature (ΔT_{ad}) with the change in magnetic field can be calculated as following. Let us consider the total entropy of the system S_M(T,H) . Its total differential can be written as,

$$dS = \left(\frac{\partial S}{\partial T} \right)_H dT + \left(\frac{\partial S}{\partial H} \right)_T dH \tag{1.20}$$

Under adiabatic condition the total entropy of the system remains constant. Therefore under adiabatic condition equation 1.20 gives

$$dT = -\left(\frac{T}{C(T,H)} \right)_H \left(\frac{\partial M(T,H)}{\partial T} \right)_H dH \tag{1.21}$$

where C is the heat capacity of the system. In deriving this equation, the equation 1.18 was used along with the following relation,

$$\left(\frac{C}{T} \right)_H = \left(\frac{\partial S}{\partial T} \right)_H \tag{1.22}$$

The adiabatic change in temperature can be obtained as

$$\Delta T_{ad}(T,\Delta H) = -\int_{H_1}^{H_2} \left(\frac{T}{C(T,H)} \right)_H \left(\frac{\partial M(T,H)}{\partial T} \right)_H dH \tag{1.23}$$

Therefore from equation 1.19 and 1.23 it is evident that ΔS_M and ΔT_{ad} are proportional to the temperature derivative of magnetization and change in magnetic field. Maximum value of ΔS_M is expected in the vicinity of a magnetic transition as the temperature derivative of magnetization is largest at that temperature.

- Magnetocaloric effect and magnetic transition

The magnetocaloric effect can give valuable information about the nature of magnetic ordering. On application of external magnetic field the magnetic moments of the paramagnetic (PM) or ferromagnetic (FM) materials have the tendency to align along the direction of the magnetic field. As a result, in the presence of external magnetic field under adiabatic conditions an increase of temperature occurs to compensate the decrease of magnetic entropy, which is known as magnetocaloric effect (MCE) [89]. In contrast to the effect in PM or FM materials, in some magnetic materials (e.g. antiferromagnetic, ferrimagnetic materials) on application of external magnetic field the configurational entropy of spin structure increases. As a result, application of external magnetic field adiabatically, cools down (ΔS_M negative) the material due to the decrease of lattice entropy, which is known as inverse magnetocaloric effect (IMCE) [90]. From equation 1.19 and 1.23 it is evident that the MCE is proportional to the rate of change of magnetization, which is maximum around the magnetic transition temperature. This is because around the magnetic ordering temperature the application of a magnetic field under isothermal condition produces a larger change in magnetization than at higher or lower temperatures. Thus the magnitude of MCE is maximum near the magnetic transition. Above the transition temperature magnetic moments are oriented randomly. With increasing temperature the thermal effect of this randomness increases. As a result the external magnetic field will produce paramagnetic response and the MCE decreases with increase of temperature. At temperatures much lower than the transition temperature magnetization can not change significantly, as the external magnetic field will have same effect compared to strong exchange interaction. Thus the magnetocaloric effect for ferromagnetic systems shows a positive caret like shape whereas for an antiferromagnetic system it exhibits a negative caret like shape with minima around the magnetic ordering temperature [91]. Actually MCE reflects the transformation,

taking place in spin configuration of magnetic materials [89]. For example, we can get valuable information about magnetic materials like the nature of magnetic ordering [92, 93], metamagnetic transitions [94] etc.

- Indirect measurement technique: Magnetization measurement

  It is possible to measure MCE directly or to calculate indirectly from the measured magnetization and/or heat capacity data, both as a function of temperature and magnetic field. In the indirect method, magnetic field induced isothermal entropy change ΔS_M is calculated from the field dependence of magnetization at constant temperature using the equation 1.19. For the calculation of MCE from magnetization measurements care should be taken to measure the actual sample temperature accurately, because as in equation 1.19, ΔS_M is a function of the derivative of magnetization with respect to temperature. So, any small error in the measurement can lead to a large error. The adiabatic temperature can be calculated using equation 1.23 from the data of field dependence of magnetization and heat capacity data.

1.5.6 Some basics on nuclear magnetic resonance(NMR)

Nuclear Magnetic Resonance (NMR) technique is a powerful tool in condensed matter physics probing the static and dynamical properties in the atomic level. The static part, *i.e.*, the time averaged information is obtained by measuring the frequency of the NMR line. The dynamic part, which is originated due to the presence of rapid fluctuations of the local magnetic field and electric field gradient (EFG), broadens the resonance line and governs the various relaxation rates. In this thesis we are only concerned with the NMR line/spectra and not with the relaxation mechanisms. Both the time averaged and fluctuating parts of the local magnetic fields and EFG seen by the nucleus result from the effect of coupling of the nucleus to the lattice (in other words, the environment of the

nucleus) called hyperfine interaction. The hyperfine interactions is divided into two parts, namely magnetic interaction and quadrupolar interaction. The magnetic part involves a magnetic coupling of the nucleus with the magnetic field originating either from the orbital motion of the electrons and/or from the magnetic moment associated with the electron spin. The quadrupolar part involves an electrostatic coupling of the nucleus with the EFG originating from charges distributed around the nucleus.

- Magnetic Interaction

  In case of magnetic hyperfine interaction the electrons of an ion or atom have a resultant electronic magnetic moment, the magnetic moment interacts with the nuclear magnetic moment resulting in the magnetic hyperfine interaction. The total magnetic interaction is given by the Hamiltonian

$$H_M = -\gamma_n \hbar \mathbf{I}.(\mathbf{H}_0 + \mathbf{H}_M) \tag{1.24}$$

  The important contribution to the magnetic field $\mathbf{H}_M$ are the following: (a) Fermi contact term, (b) dipolar contribution and (c) orbital contribution.

  (a) Fermi contact term : The *s* electrons possess a non vanishing probability inside the nuclear volume and therefore can interact directly with the nuclear moment. So a magnetic field is produced at the nuclear site due to the *s* electrons. The shift caused due to this interaction is called the Knight shift.

  (b) Dipolar contribution : As an effect of the dipolar electron-nuclear coupling, the position of the nuclear resonance is shifted from its diamagnetic value. The dipolar field produces an anisotropic shift in the line position in case the local magnetic environment around the nucleus does not have cubic symmetry.

  (c) Orbital contribution : The third contribution, represents the interaction of the nuclear spin with the orbital motion of the electrons. In some transition metals this

term becomes important. In case of non-ferromagnetic metals, paramagnetism has been considered to be due to the spin of unpaired electrons. The contribution of the orbital magnetic moment to the paramagnetism is neglected for the reason that they are quenched by the crystal field. But Kubo and Obata had pointed out that in case of a metal with non-*s* bands, the orbital magnetic moment contributes to the paramagnetic susceptibility through the second order perturbation. This contribution of orbital paramagnetism is the analog in metals of the van Vleck temperature independent paramagnetism.

- Quadrupolar interaction

  Nuclei with spin I greater than 1/2 possess an electric quadrupole moment, having its origin in a non-spherically symmetric nuclear charge distribution. The nuclear electric quadrupole moment interact with the gradient of any electric field existing at the nucleus, no appreciable gradient can be produced by direct external means. Thus a significant gradient is always the result of internal fields. This internal field is produced by the electric charges rather close to the nucleus.

  The electric quadrupole interactions in NMR can be divided into (1) high field case, and, (2) low field case depending on the relative strength of the nuclear quadrupole interaction and the Zeeman interaction.

  In the high field case, the nuclear electric quadrupole interaction energy is assumed small compared to the interaction energy of the nuclear magnetic moment with the external magnetic field. Quadrupolar effects can be treated as a perturbation over the magnetic interaction. This can split the resonance line into several components. The number of such components can provide information about the nuclear spin whereas the separation in frequency between the components yields the nuclear quadrupole moment when the electrostatic field gradient at the nuclear position can be calculated. In addition to that of producing a fine structure of the resonance line, the quadrupole

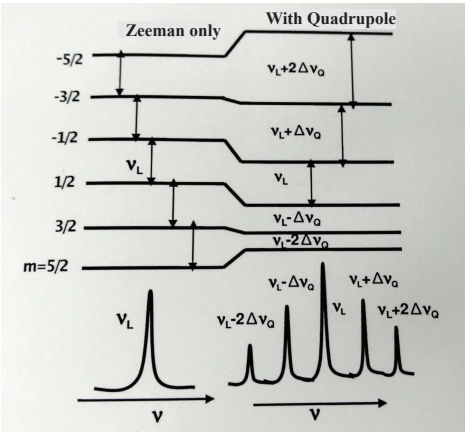

Figure 1.5: Schematic representation of the effect of the quadrupolar interaction on the NMR line shape over the Zeeman interaction for nuclear spin I = 5/2

interactions may led to a broadening or apparent loss of intensity of the resonance line.

On the other hand, in the low field case the nuclear quadrupole interaction is so large that it becomes responsible for almost the entire dependence of the energy of a nucleus on its spin orientation. NMR experiments in zero or very small external magnetic field then becomes possible. The schematic representation of the effect of the quadrupolar interaction on the NMR line shape over the Zeeman interaction for nuclear spin I = 5/2 is shown in Figure 1.5.

Measurement of the NMR shift

The NMR shift is measured by noting the resonance frequency of the central frequency of the central line from the reference position. Thus the NMR shift is

$$K(T) = \frac{(\nu(T) - \nu_{ref})}{\nu_{ref}} \tag{1.25}$$

The reference position is the resonance frequency (ν_{ref}) of standard diamagnetic sample. The experimentally measured NMR shift is actually the isotropic component of

the calculated shift, when the central line is symmetric. If the central resonance line is broad and asymmetric then it is better to calculate isotropic NMR shift from the theoretical fitting of the resonance line.

NMR Hamiltonian and NMR spectra: Transferred Hyperfine effects

In the first part of this section we have mentioned that the magnetic hyperfine field is the result of three contributions viz. the dipolar field from electron spins outside the nucleus volume, the orbital field associated with a not fully quenched orbital moment, and the Fermi contact field which originates from the spin polarisation of all electrons (essentially *s* shells) within the volume of the nucleus. For a pure metal this consideration is sufficient to understand the Knight shift. However, for the intermetallic compound, such as the metallic systems containing magnetic ions the hyperfine field is also modified. In that case the magnetic hyperfine field is modified due to the conduction electron polarisation. It is composed of a contribution of the conduction electron polarisation caused by the localised spin moment present at the atomic site under consideration, plus a contribution arising from conduction electron polarisation due to the polarising influence of magnetic moment present at the surrounding sites in the lattice. This later term is called the transferred hyperfine field. If we take into account all contributions, then we would get the transferred hyperfine effects.

In a metallic system containing magnetic ions, such as rare earths or transition metals for example, $CeNi_2Al_5$, the Hamiltonian for a nucleus with spin greater than 1/2 is written as,

$$\mathscr{H} = \mathscr{H}_Z + \mathscr{H}_{hf} + \mathscr{H}_Q + \mathscr{H}_N \tag{1.26}$$

where $\mathscr{H}_Z$ is the Zeeman interaction of the nucleus with an external magnetic field, $\mathscr{H}_{hf}$ is the hyperfine interaction, $\mathscr{H}_Q$ is the quadrupole interaction, and $\mathscr{H}_N$ is the nuclear

spin-spin interaction. Assuming that the principal axes of the electric field gradient (EFG) tensor and magnetic shift tensor are coincident, the resonance frequency ν of a given transition (m $\leftrightarrow$ m-1) is given by,

$$\nu(m \leftrightarrow m-1) = \nu_0 + \nu^{(2)}_{quad} + \nu_{ani} \tag{1.27}$$

with $\nu_0 = (1 + K_{iso})\nu_{ref}$, where ν_{ref} is the Larmor frequency of the nucleus in case of diamagnetic reference compound. K_{iso} is the isotropic part of the Knight shift.

$\nu^{(2)}_{quad}$ is due to second-order quadrupole effect and is given by

$$\begin{aligned}\nu^{(2)}_{quad} = -\Big(\frac{1}{32}\frac{\nu_Q^2}{\nu_0}\Big)(1-\cos^2\theta)\Bigg[&\big[102m(m-1)-18I(I+1)+39\big]\cos^2\theta(1+\frac{2}{3}\eta\cos 2\phi)\\ &-\big[6m(m-1)-2I(I+1)+3\big](1-\frac{2}{3}\eta\cos 2\phi)\Bigg]\\ +\frac{\eta^2}{72}\frac{\nu_Q^2}{\nu_0}\Bigg[&24m(m-1)-4I(I+1)+9-\big[30m(m-1)-6I(I+1)+12\big]\cos^2\theta\\ &-\big[\frac{51}{2}m(m-1)-\frac{9}{2}I(I+1)+\frac{39}{4}\big]\cos^2 2\phi(\cos^2\theta-1)^2\Bigg]\end{aligned} \tag{1.28}$$

and ν_{ani} is due to the anisotropic Knight shift and assuming that the principal axes of the EFG tensor (XYZ) coincide with those of the crystallites (a,b,c) it is given by,

$$\nu_{ani} = \frac{K_1\nu_{ref}}{2}(3\cos^2\theta - 1) + K_2\nu_{ref}\sin^2\theta\cos 2\phi \tag{1.29}$$

where, K_1 = K_{an}(c) and K_2 = K_{an}(b)-K_{an}(a).

CHAPTER 2

Experimental Techniques

Experimental works carried out related to this thesis has been described in this chapter. This chapter also includes the details about the procedure to make the polycrystalline RET_2Si_2 compounds by arc melting. To characterize our prepared samples we have utilized some commercial instruments. The RIGAKU-TTRAX III x-ray diffractometer was employed to perform the x-ray diffraction study. For further characterization, Field Emission Scanning Electron Transmission (FESEM) have also been used. To measure the magnetic properties and heat capacity, we have used magnetic properties measurement system (SQUID-VSM) and physical properties measurement system, both of Quantum Design. The experimental details of the transport and NMR measurements are discussed in the subsections.

2.1 Sample preparation technique

Arc melting method

The polycrystalline intermetallic compounds studied in this thesis were prepared by arc melting of constituent elements of purity $> 99.9\%$ in argon gas atmosphere. The ingots were turned over and remelted several times to ensure better homogeneity of the samples which resulted in a loss of less than 1%. The samples which need heat treatment were wrapped in titanium foil and sealed in evacuated quartz tubes. In order to obtain phase homogeneity, the samples were annealed at 900° C for one week and then slowly cooled. For $NdRu_2Si_2$, the sample after annealing was quenched in liquid nitrogen. Figure 2.1 shows an arc melting setup where the samples have been prepared.

2.2 Sample characterization techniques

2.2.1 X –ray diffraction (XRD)

The x-ray diffraction (XRD) measurements of all prepared samples in bulk polycrystalline form were carried out with a RIGAKU TTRAX-III diffractometer in Bragg-Brentano (BB) geometry using Cu-Kα radiation. In this arrangement, the x-ray beam incident upon the specimen at a particular angle is diffracted according to Bragg's law, as it is reflected from the various planes of the crystal lattice. The whole diffraction patterns of the compounds are collected by varying the incidence angle θ and the corresponding detector angle 2θ. The block diagram of the x-ray diffraction and the Bragg's law of diffraction is given in Figure 2.2. Here, the reflected beam was captured by a sensitive scintillation counter or a solid state detector. Each peak in the XRD patterns (2θ versus

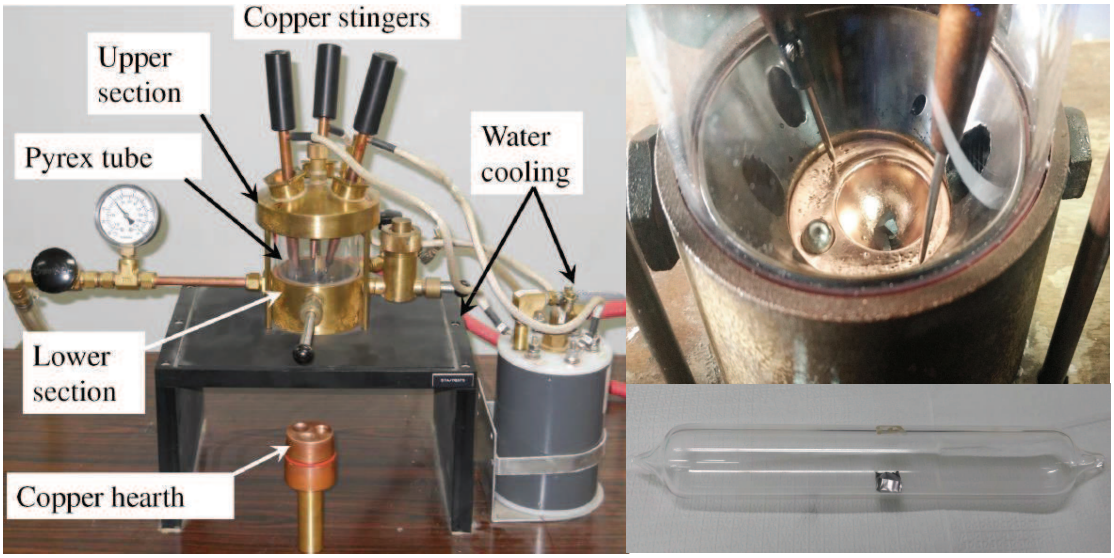

Figure 2.1: Image of an arc melting setup. The above image in the right hand side shows the copper hearth with the elements and titanium ball. The lower one shows an evacuated quartz tube with sample wrapped in titanium foil ready for annealing process.

intensity plot) corresponds to the response of individual crystallographic planes of the material. The structures were analyzed by standard profile fitting as well as full fitting method using FULLPROF 2009 program. The lattice parameters (a, b, c) were determined by Rietveld analysis.

2.2.2 Scanning electron microscopy

An energy dispersive x-ray spectroscope attached to a scanning electron microscope (FESEM, FEI INSPECT F50) has been used to determine the concentrations of the elements present in the sample. The scanning electron microscope (SEM), which is closely related to the electron probe, is designed primarily for producing electron images, but can also be used for element mapping, and even point-by-point analysis, if an x-ray spectrometer is added. A solid sample when bombarded with electrons of sufficient energy emits x-rays characteristic of constituent elements of the sample. Qualitative analysis involves the identification of the

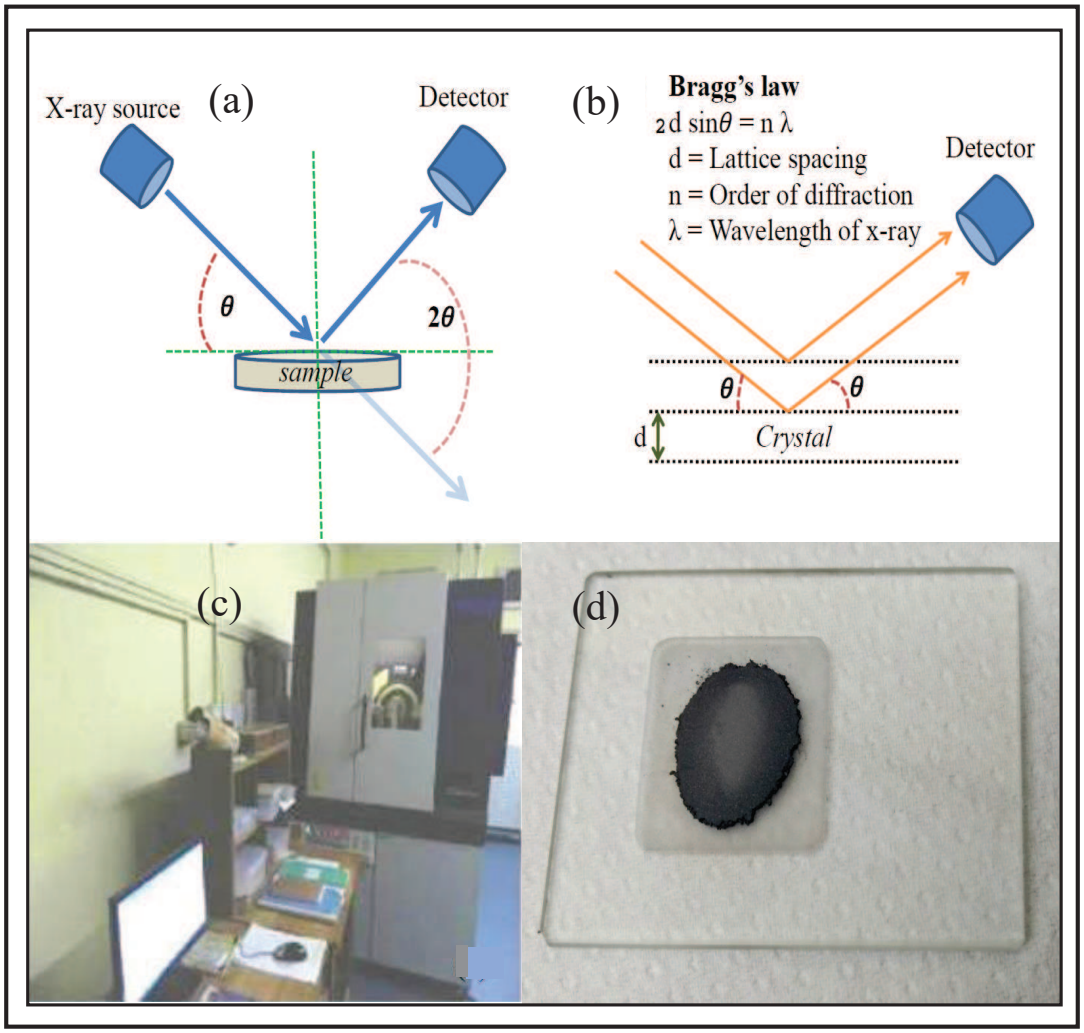

Figure 2.2: Figure represents (a) schematic diagram of a x-ray diffractometer, (b) Bragg diffraction diagram, (c) RIGAKU TTRAX-III diffractometer, (d) image of a sample holder with powder sample.

lines in the emitted spectrum. Quantitative analysis (determination of the concentrations of the elements present) entails measuring line intensities for each element in the sample and for the same elements in calibration standards of known composition. The three principal components of a basic EDS system are (1) the x-ray analyzer and detector, (2) a pulse processor that measures the voltage pulses corresponding to the x-ray energies, and, (3) a computer. The x-ray that is produced by and characteristic of elements present in the sample generates a current on entering the detector and it is then converted into a voltage

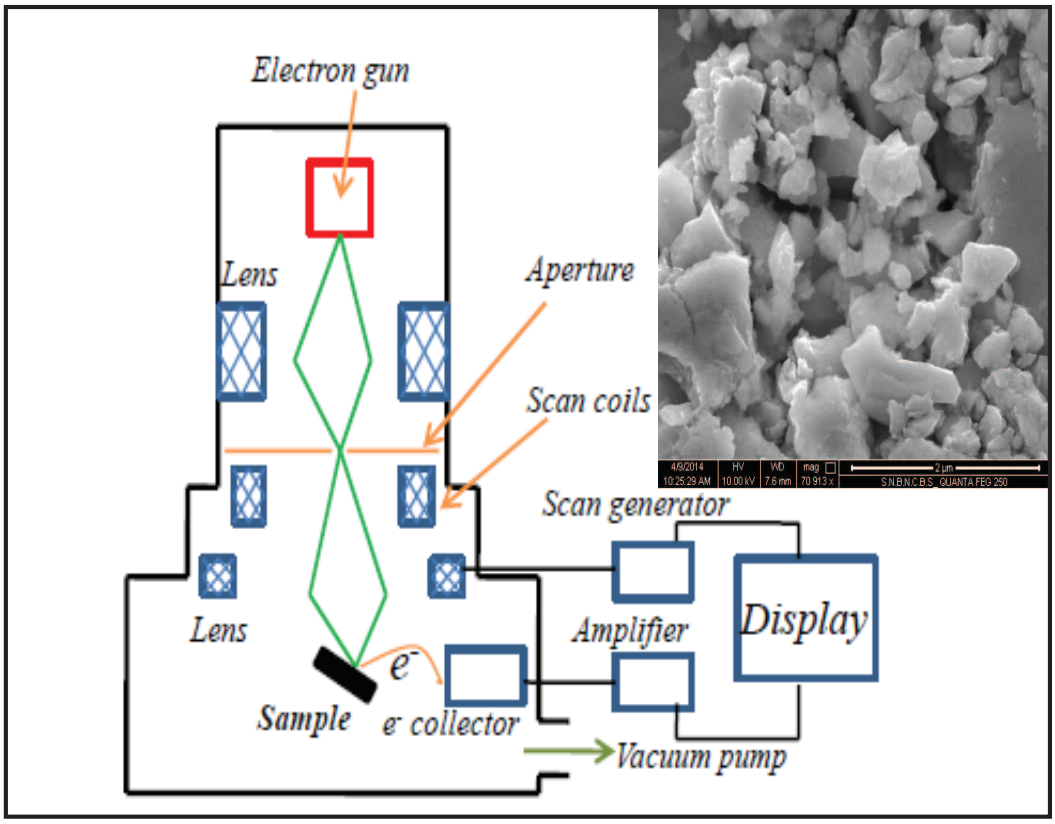

Figure 2.3: Schematic diagram of Scanning Electron Microscope(SEM). Inset shows the FESEM image of our sample.

pulse proportional to the energy of the x-ray. A computer measures the voltage pulses over a period of time, and plots them as a histogram which shows intensities at different x-ray energies that is compared with the similarly obtained histogram for the calibration standard. Figure 2.3 shows the schematic diagram of scanning electron microscope and the inset shows SEM image of one of the samples.

2.3 Measurement techniques

2.3.1 Magnetization measurements by VSM-SQUID (Quantum Design)

All the magnetic measurements related to this thesis were carried out using a 'magnetic properties measurement system', MPMS SQUID-VSM (Superconducting Quantum Interference Device Vibrating Sample Magnetometer) of Quantum Design.

The SQUID, which picks up changes in magnetic field, is the most sensitive detector for measuring extremely small magnetic fields. Only inherent quantum effects set its limits. It has become by far the most widely used small-scale superconducting device. The essential parts of a SQUID are superconducting magnet, superconducting detection coil, a SQUID connected to the detection coil and superconducting magnetic shield surrounding the SQUID. Generally during the measurements in static magnetic field the superconducting magnet is operated in persistent mode. In a short portion of superconducting magnet's wire a small heater is attached which acts as a persistent current switch. Superconducting detection coil is nothing but a piece of a superconducting wire which is configured as a second-order gradiometer. This detection coil is subjected in the region of uniform magnetic field, produced by the superconducting magnet and is connected with the SQUID. SQUID is consisting of a superconducting loop which is interrupted by one or more Josephson junction. During the charging of the magnet, heater should be on such that the adjoining portion of the superconducting wire becomes normal resistive. Due to the normal resistive state of the adjacent portion of the switch, the superconducting loop is electrically opened up. An external current source is connected to each side of the switch to pass the current through the superconducting wires in the magnet for producing the external magnetic field. The block diagram of a SQUID magnetometer is shown in

Figure 2.4(a). A picture of superconducting quantum interference device vibrating sample magnetometer (SQUID-VSM) of Quantum Design is shown in the Figure 2.4(b). Figure 2.4(c) show the sample loaded in the sample holder of SQUID-VSM. Figure 2.4(d) shows the data of one of the samples as measured in SQUID. In the closed superconducting current path there are one or two Josephson junctions. A dc SQUID consists of two Josephson junctions formed into a superconducting ring. Applying current to the SQUID (biasing it) sends Cooper pairs of electrons tunneling through the junctions. A magnetic field applied to the ring, alters the flow. Specifically, it changes the quantum-mechanical phase difference across each of the two junctions. These phase changes, in turn, affect the critical current of the SQUID. A progressive increase or decrease in the magnetic field causes the critical current to oscillate between a maximum value and a minimum one. The maximum occurs when the flux administered to the SQUID equals an integral number of flux quanta through the ring, the minimum value corresponds to a half-integer number of quanta. The period of these oscillations is the flux quantum. In practice, we do not measure the current but voltage across the SQUID, which swings back and forth under a steadily changing magnetic field. This quantum interference effect provides us with a digital magnetometer. Each digit represents one flux quantum. The SQUID in essence is a flux-to-voltage transducer, converting a tiny change in magnetic flux into a voltage. This effect closely resembles the double-slit experiment in optics; when coherent light passes through two parallel slits, the emerging beams "interfere" with each other to produce a series of light and dark fringes. In a superconductor a single wave function describes all the Cooper pairs. The wave functions at the two Josephson junctions interfere with each other to produce the current and voltage swings. In practice, we can detect changes that are smaller than the flux quantum. A tiny flux signal produces a corresponding voltage swing across the SQUID, which conventional electronics can measure. To take advantage of the extraordinary sensitivity of the SQUID, the devices are almost always coupled to an input circuit. For magnetometers, this circuit enhances the SQUID's sensitivity. With a flux transformer, a SQUID can reach femtotesla

(10^{15} T) resolution. One femtotesla corresponds to one part in 10^{11} of the earth's magnetic field. In a SQUID magnetometer, the sample is mounted in a straw through another straw segment such that the sample must not slip or rattle when the straw is shaken and attached to one end of a sample rod which is inserted into the dewar. The another end is attached to a servo-motor-controlled platform which is used to move the sample through the detection coils which are placed at the center of the magnet. Regarding the data collection procedure it should be mentioned that it cannot detect directly the magnetic moment of the specimen as described earlier. To estimate the magnetic moment the sample is allowed to vibrate through the superconducting detection coils, placed at the center of the magnet. The detection coil consists of a superconducting pick-up coil with four windings. Two center windings are in the same sense which basically add the pick-up signal whereas the rearer two are in counter sense with respect to the central windings. As a result of the movement of the sample, the change of the magnetic flux produces an alternating voltage in the pick-up coil which is proportional to the magnetic moment of the sample. In addition to that in a sensitive SQUID the sensor itself is shielded properly from the fluctuation of the ambient magnetic field of the laboratory and the magnetic field produced by the superconducting magnet.

2.3.2 Heat capacity measurement using physical property measurement system (Quantum Design)

The heat capacity measurement of some compounds related to this thesis were carried out by utilizing the commercial instrument 'physical properties measurement system'(PPMS), of Quantum Design. It measures the heat capacity at constant pressure.

$$C_p = (\frac{dQ}{dT})p \tag{2.1}$$

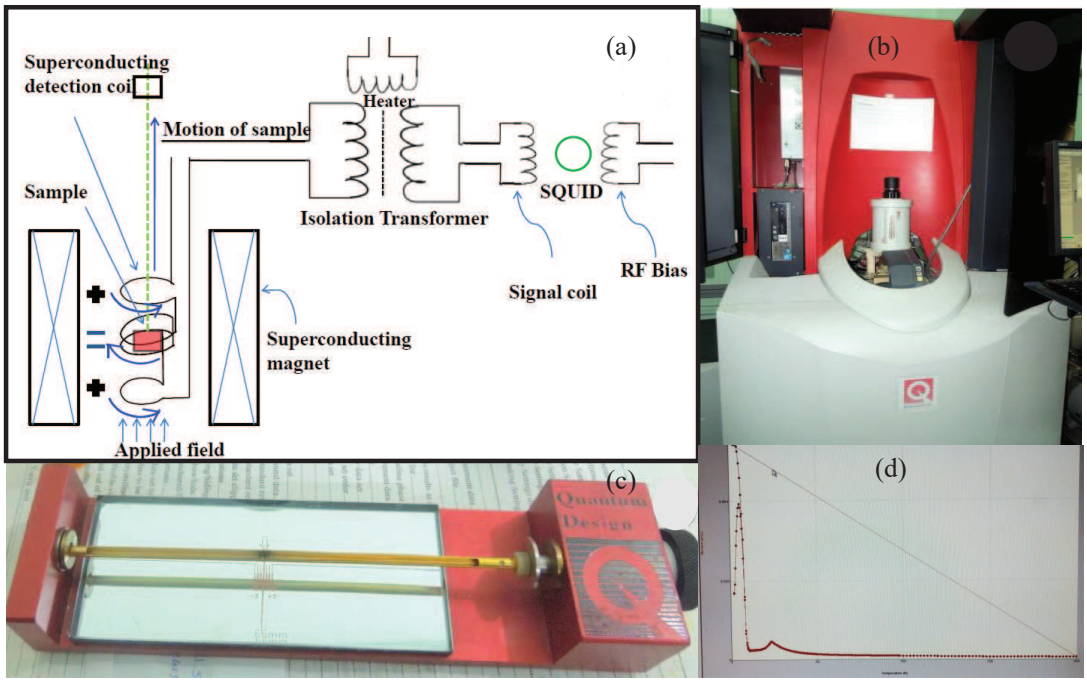

Figure 2.4: Figure represents (a) schematic diagram of SQUID-VSM magnetometer, (b) Image of superconducting quantum interference device (SQUID) magnetometer (Quantum Design), (c) sample holder of SQUID-VSM with sample placed in the holder, (d) shows the data of one of the samples as measured in SQUID.

A schematic diagram of the attachment of heat capacity measurement system is given in Figure 2.5. In this measurement protocol a known amount of the heat is supplied by a constant power for a fixed time and then the heating period is followed by a cooling period of the same duration. For supplying the heat energy and to note the temperature change, a platform heater and platform thermometer are attached to the bottom side of the sample platform. A small flat piece of sample is mounted on the platform by using the apiezon grease to make a good thermal contact to the platform. Generally the measurement of heat capacity is performed in high vacuum option mode in PPMS. In PPMS heat capacity option the relaxation technique is used to calculate the heat capacity. After each measurement cycle (which consists of heating and cooling period) the entire temperature response data is fitted by the model which includes the thermal relaxation of the sample platform to the bath temperature and the relaxation between the sample platform and the sample itself (in case

of poor contact). Generally two models are used to derive the heat capacity of a sample. The 'Simple model' and the 'Two-Tau Model'.

- Simple model

  When the sample and the platform are in good thermal contact with each other, this model is applied to estimate the total heat capacity (heat capacity of the sample and the platform). The temperature T of the platform as a function of time t obey the equation

$$C_{total}\frac{dT}{dt} = -K_w(T - T_b) + P(t) \tag{2.2}$$

  Where C_{total} is the total heat capacity of the sample and the platform; K_w is the thermal conductance of the supporting wires; T_b is the temperature of the thermal bath and $P(t)$ is the power applied by the heater (it is equal to P_0 during heating and zero during cooling cycle). The solution of the equation 2.2 is an exponential function with characteristic time constant equal to C_{total}/K_w

- Two-Tau Model

  However when the thermal contact between the sample and the platform is poor, there exists another sophisticated model, the two-tau model to measure the heat capacity. In this model the temperature difference between the platform and the sample is taken into account. The mathematical equations to derive the heat capacity in this model can be expressed as

$$C_{platform}\frac{dT_p}{dt} = P(t) - K_w[T_p(t) - T_b] + K_g[T_s(t) - T_p(t)] \tag{2.3}$$

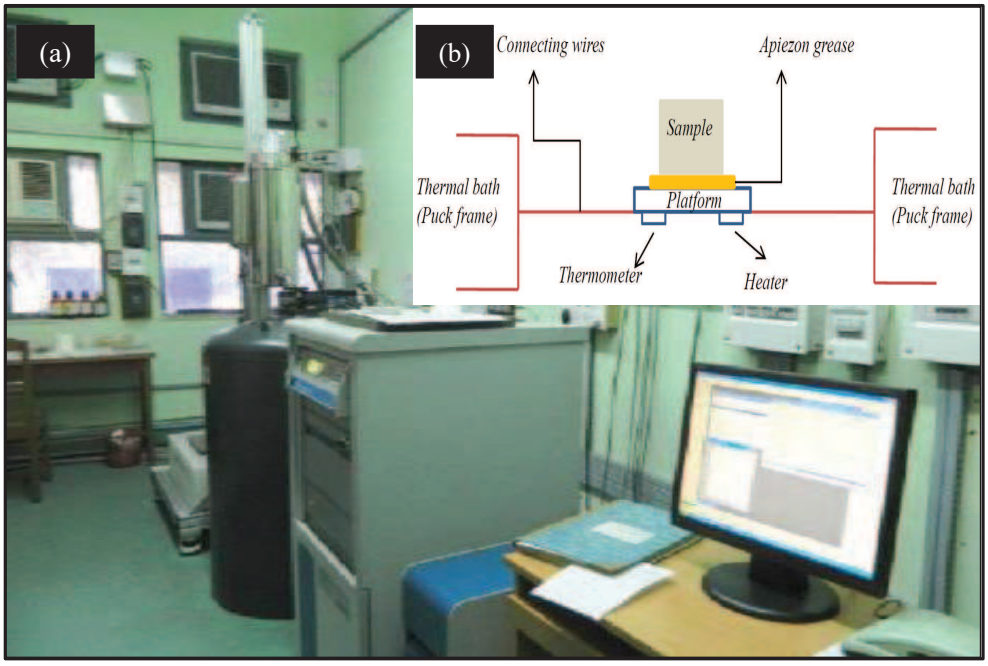

Figure 2.5: Figure represents (a) Physical property measurement system (PPMS) (Quntum Design) set up, (b) Thermal Connections to sample and sample platform in PPMS Heat Capacity Option.

$$C_{sample}\frac{dT_s}{dt} = -K_g[T_s(t) - T_p(t)] \tag{2.4}$$

Here $C_{platform}$ and C_{sample} are the heat capacities of the platform and the sample respectively. K_g is the thermal conductance of the grease. $T_p(t)$ and $T_s(t)$ represents the temperature of the platform and the sample respectively.

In our present work the transitions are weakly first order and as they occur well below the room temperature and therefore the experiment will require narrow heat pulses (typically 2 % of T)so that the underestimation of heat capacity will be small. For better estimation of heat capacity very close data points were taken using long stabilization time at each temperature.

2.3.3 Electric transport and magneto-transport measurement

The transport property measurements presented in this thesis have been carried out at UGC-DAE CSR, Indore. A home-built instrument working in the temperature range 1.5 - 300 K and magnetic fields 0 - 9 T was utilized to carry out the electrical transport measurements in four probe geometry. In this geometry, four contact points were formed on the sample in a line. Outer two contacts are used to send current through the sample and inner two contacts are used to measure the voltage.The schematic diagram of the insert has been given in Figure 2.6. An oxygen free highly pure copper (OFHC) block (marked by B in Figure 2.6) was used to make the square sample holder that had capacity of holding sixteen samples for simultaneous measurements. The samples were mounted using GE varnish ensuring proper electrical isolation and good thermal contact. To make the electrical connections for four probe configuration, PCB stripes were used. The temperature of the sample space was precisely measured by a calibrated cernox temperature sensor mounted on the copper block. For uniform heating of the sample holder, a pair wise twisted manganine wire was wounded around both ends of the sample holder. A meter long SS tube was connected with the sample holder (A in Figure 2.6) and some copper baffles were brazed (C in Figure 2.6) which acted as radiation shields. Different types of the copper wires were used for the electrical connections from sample holder to the room temperature end of the insert (D in Figure 2.6).

Various electronic instruments were connected with the set-up during the experiment. A temperature controller (Lakeshore 340) was utilized to measure and stabilize temperature of the sample holder. A switching System (Keithley, Model7002) was used for selecting different samples. A nanovolt scanner card along with a general purpose scanner card were utilized for switching between the voltage leads and current leads of different samples respectively. Current was sent through the current leads from a source meter (Keithley,

Model2400 source-meter) and corresponding voltage drop was recorded by a nanovoltmeter (Keithley, model 182). The insert was placed inside the magnetic system after mounting the samples and making electrical connections. After stabilization of the specified temperature, a particular sample is selected by scanner. A pre-determined amount of current is allowed to send through the current leads of that sample and corresponding voltage across the voltage leads is recorded by the nanovoltmeter. In order to nullify the thermo-emf effect, the current is reversed and the voltage is measured again. The same process is repeated several times to improve the accuracy. After finishing measurement on one sample, scanner card selects the next one. Once the measurement of all the samples are completed the temperature controller sets next pre-determined temperature. The data is plotted as resistance versus temperature and can be monitored in real time on the computer screen. The resistivity (ρ) is determined from the measured resistance (R) from the following relation

$$\rho = R\frac{A}{l} \tag{2.5}$$

where A is the cross sectional area and l is the length of the sample, *i.e.*, distance between the voltage leads. It should be mentioned that there is some degree of ambiguity as to the appropriate cross sectional area, as the value will depend on the precise path of the current through the sample. It has been assumed that the current flows uniformly throughout the width of the sample. The resistivity values thus obtained should be treated as an upper bound, as the area the current travels through may be restricted.

2.3.4 Nuclear magnetic resonance(NMR) spectrometer

The essential components of NMR spectrometer are: (1) a magnet for Zeeman splitting of the nuclear spin energy levels, (2) a radio frequency (RF) source to tune the resonance frequency of the nuclei, (3) a switch or gate for turning the RF irradiation on and

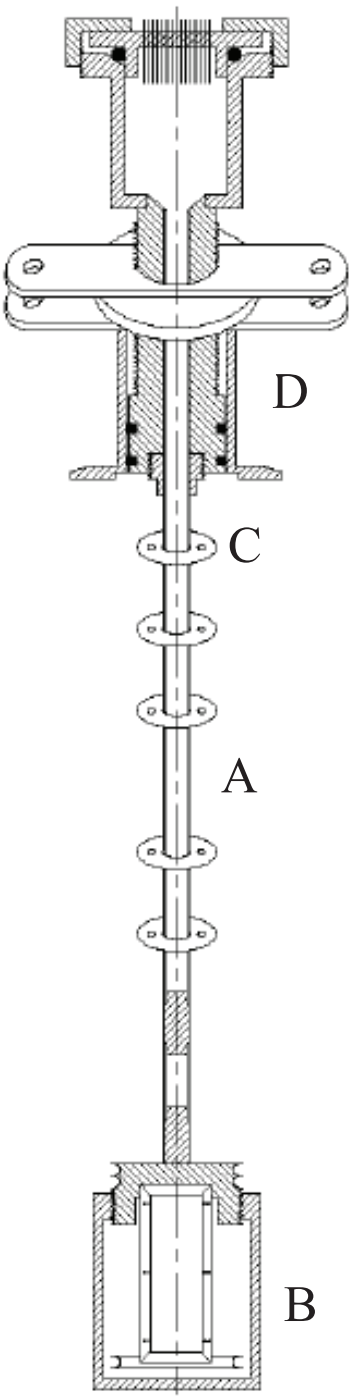

Figure 2.6: A schematic diagram of the insert for the transport and magneto-transport measurement.

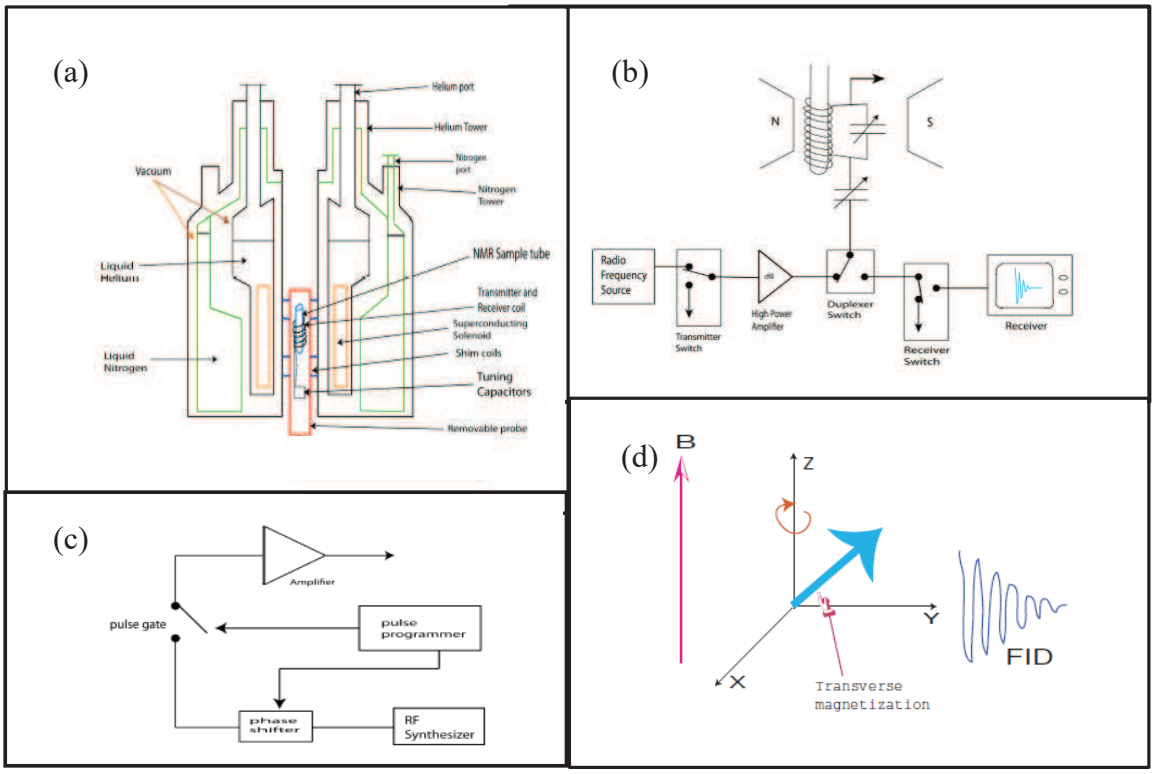

Figure 2.7: Figure represents (a) Cross-section of NMR magnet (b) Schematic diagram of Nuclear Magnetic resonance spectrometer (c) Block diagram of the transmitter (d) The FID of an NMR signal.

off, (4) a transmitter and detector coil containing the sample, (5) a switch or gate in front of the receiver for protection, and (6) a receiver. A bock diagram of NMR spectrometer is shown in Figure 2.7.

Measurement procedure

- Free induction decay

  The NMR spectrometer is basically a device capable of: (i) magnetizing the nuclear spins with a large applied magnetic field, (ii) rotating the spin polarizations by rf pulses to produce transverse nuclear magnetization, and, (iii) detecting the small oscillating electric currents induced by the precessing transverse spin magnetization. Magnetic moment of a sample is fluctuating with time by the influence of local

fluctuating magnetic field, which arises due to the fact that the nuclear spin is in its immediate thermal environment. This fluctuating magnetic field breaks the isotropic distribution of spin polarization, and a resultant magnetic moment arises along the direction of the external magnetic field. In this situation, a radio frequency field in the form of a pulse of short time duration is applied at a direction perpendicular to the external magnetic field through a electrical wire wound over the sample. There arises a transverse magnetization along the perpendicular direction of the external magnetic field. The transverse magnetization also rotates with time and stays though with a decaying intensity even after the pulse is withdrawn. The rate of decay is determined by the interaction of the nuclear magnetic moments with their surroundings and also the interaction among the nuclear moments themselves. The rotating transverse magnetic moment generates a rotating magnetic field, and therefore an oscillating electric current is induced in the same coil. It is possible to detect this small oscillating current by using a sensitive rf detector. The oscillating electric current induced by the precessing nuclear transverse magnetization is called the NMR signal or *free-induction decay* (FID).

CHAPTER 3

Study of Magnetic and magnetocaloric properties of vanadium substituted layered intermetallic compounds $RE(Co_{1-x}V_x)_2Si_2$ (RE = Pr and Nd; 0 $\leq x \leq$ 0.35)

3.1 Introduction

Magnetic properties of $RECo_2Si_2$ compounds have been extensively studied [40, 51, 95, 96]. Both $PrCo_2Si_2$ and $NdCo_2Si_2$ are antiferromagnetic. Neutron diffraction studies [57] on single crystal of $PrCo_2Si_2$ shows magnetic moments only on rare-earth ions in a square-wave structure with propagation vectors (0,0,l), (0,0,0.074) and (0,0,0.223) appear in the sequence of $T \leq 9$ K (T_1), 9 K $\leq T \leq$ 17 K (T_2) and 17 K $\leq T \leq$ 30 K (T_N), respectively.

$NdCo_2Si_2$ also have a similar magnetic structure [52] in which the propagation vectors (0,0,l), (0,0,0.07) and (0,0,0.21) appear in the sequence of $T \leq 15$ K (T_1), 15 K $\leq T \leq$ 24 K (T_2) and 24 K $\leq T \leq$ 32 K (T_N), respectively. Therefore, at lowest temperatures, both compounds exhibit a collinear antiferromagnetic (AFM) ordering of alternate up and down moments along *c*-axis. However, it is important to note that in planes perpendicular to *c*-axis, the moments are ferromagnetically aligned. The temperatures 30 K and 32 K are denoted as the AFM ordering temperatures, T_N, for $PrCo_2Si_2$ and $NdCo_2Si_2$, respectively.

RET_2X_2 compounds have a tendency of magnetic instability arising out of an interplay of on-site and inter-site magnetic fluctuations [97]. Significant modifications in their magnetic properties have been obtained by the use of externally applied pressure or substitution at either *RE* or T sites [71, 73, 74, 98]. So far, all the substitutions involved combinations of only those *RE* and T elements that are known to form *RE*T_2X_2 compounds of $ThCr_2Si_2$ type structure. We have investigated modifications in the magnetic properties of *RE*Co_2Si_2 (*RE* = Pr,Nd) compounds upon substitution of cobalt with vanadium which is not known to be among the elements forming $ThCr_2Si_2$ type pure compounds. The substitutions have resulted in the appearance of ferromagnetism at temperatures $\sim$ 30 K. This is the first instance of antiferromagnetic *RE*Co_2Si_2 compounds becoming ferromagnetic upon incorporation of a non-magnetic transition element. Also, for the first time in *RE*T_2X_2 systems, the substituted compounds yield a significant exchange bias field, which, together with their magnetoresistance, present strong evidence for these compounds behaving as natural multilayers.

3.2 Sample preparation and X-ray diffraction studies

Polycrystal samples of *RE*($Co_{1-x}V_x$)$_2Si_2$ (*RE* = Pr, Nd; x = 0, 0.05, 0.1, 0.15, 0.2, 0.25, 0.3 and 0.35) were prepared by arc melting high-purity elements in purified argon

atmosphere. For better homogeneity, the ingots were turned over and re-melted six times resulting in the end a weight loss of less than 1 %. The samples were subsequently annealed at 900° C for 7 days. X-ray powder diffraction (XRD) studies at room temperature were performed with a Rigaku TTRAX-III x-ray diffractometer, and the lattice parameters were obtained by Rietveld refinement of the data using Fullprof program. Figure 3.1 shows x-ray diffraction patterns and Rietveld refinements of some of the prepared samples. The XRD studies showed the samples to be single phase for low doping of vanadium. However, for higher vanadium doping there were lines due to un-reacted elemental Pr, Nd and Si that constituted $\sim 3\%$ of XRD peak intensities. No extra lines due to elemental V were obtained, and apart from the intended *122* phase, no other known binary or ternary minority intermetallic phases involving these elements could be detected. Compared with the parent compounds, vanadium substituted samples show a broadening of x-ray diffraction lines with increasing vanadium content indicating substitution induced micro-strain in the lattice. Scanning electron microscopic (SEM) images (Figure 3.2) show uniform textures of the prepared samples consisting of interconnected micron-size flake-like substance with some voids. Energy dispersive x-ray spectroscopy (EDS) analysis shows the relative atomic percentages of vanadium substitution matching with the desired values within the error limit. For the parent compounds, the lattice parameters agree quite well with the published data [23].

Vanadium has a molar volume larger than that of cobalt. In substituted compounds, with increase in V, the lattice parameter a shows small increase, but c increases markedly. The change in the lattice parameters as a function of V concentration is a strong indication of Co being replaced by V. Figure 3.3 shows lattice parameters and unit cell volumes of all $RE(Co_{1-x}V_x)_2Si_2$ samples.

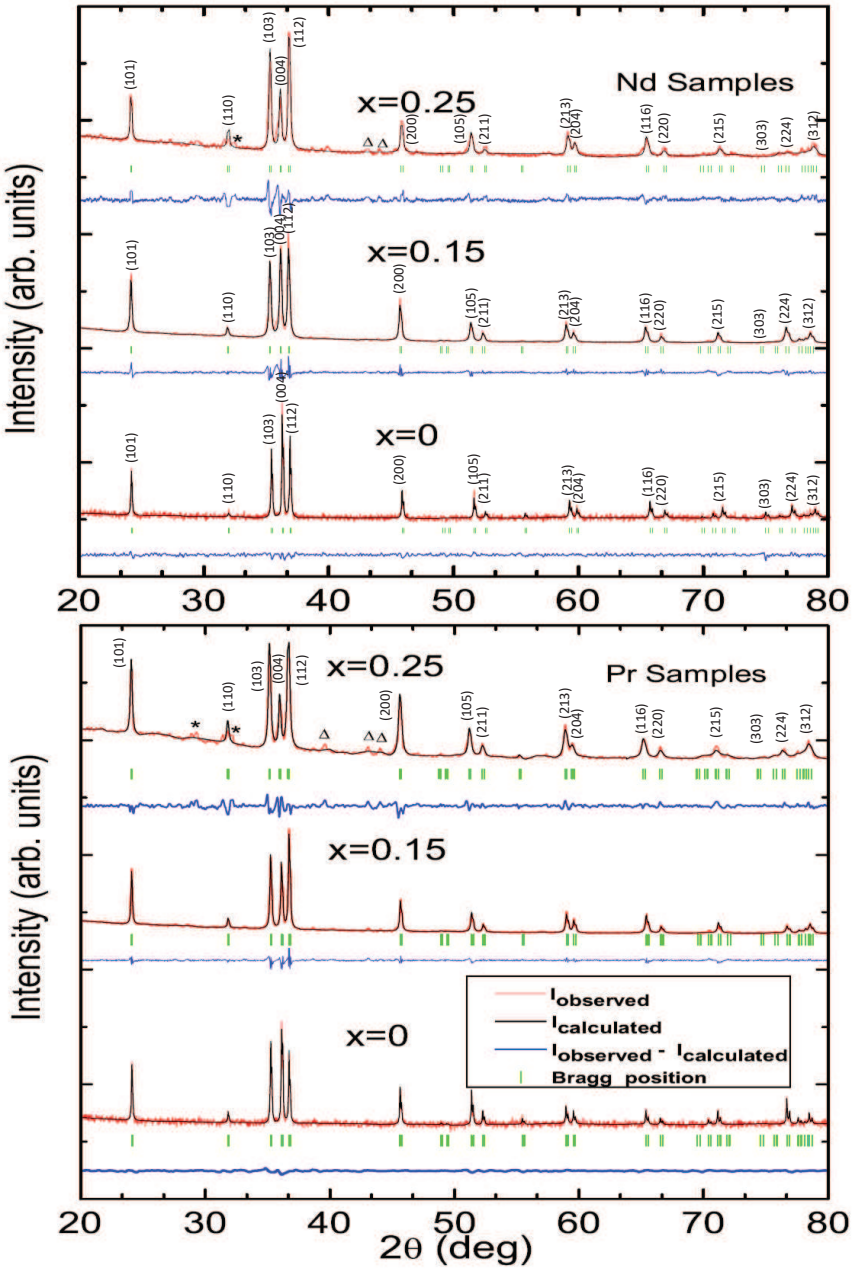

Figure 3.1: Powder x-ray diffraction patterns of Pr($Co_{1-x}V_x$)$_2Si_2$ (Bottom panel; x = 0, 0.15 and 0.25) and Nd($Co_{1-x}V_x$)$_2Si_2$ (Top panel; x = 0, 0.15 and 0.25) at 300 K with Rietveld fitting. $\star$ and $\triangle$ denote un-reacted rare-earth and Si, respectively. Miller indices corresponding to the diffraction peaks have been shown for Nd samples and one of the Pr samples as a representative of the other series.

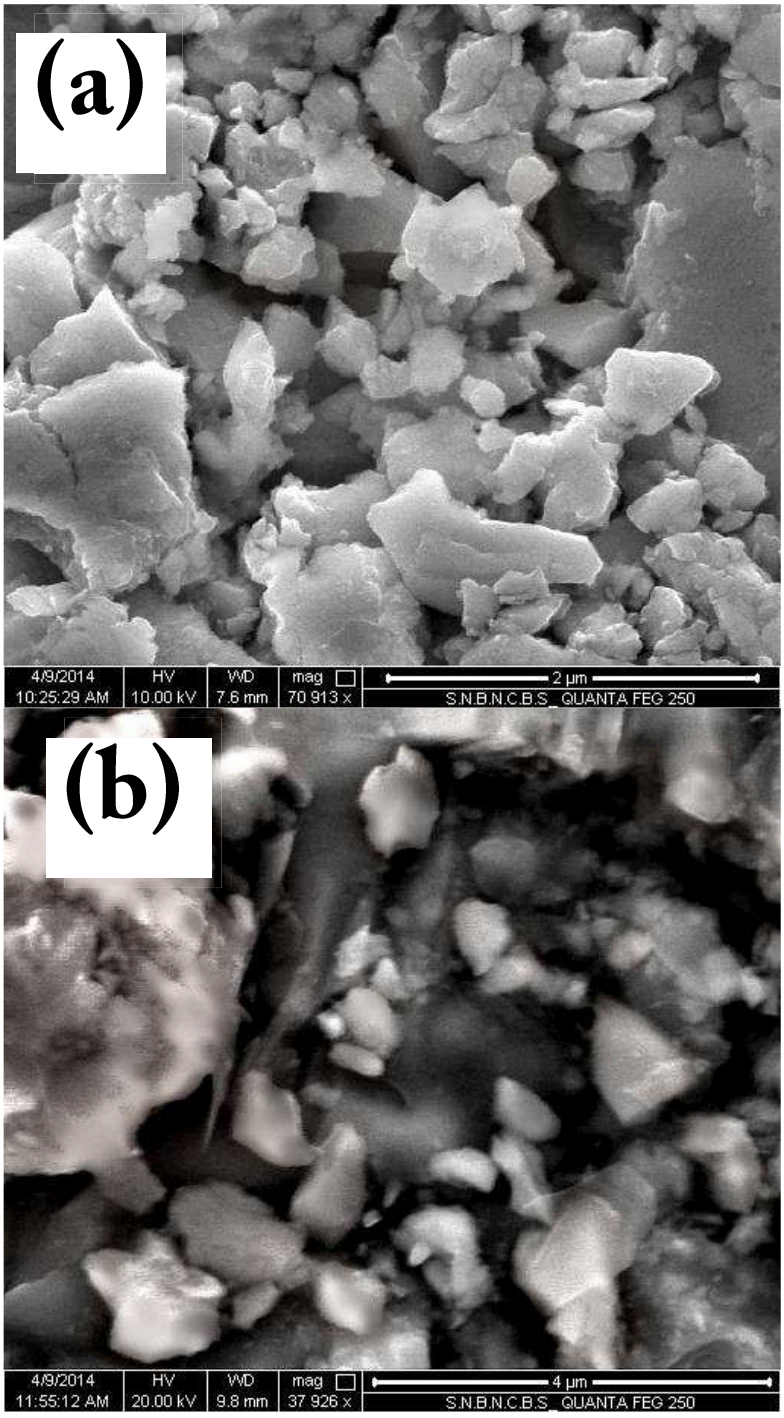

Figure 3.2: FESEM images of $Nd(Co_{1-x}V_x)_2Si_2$; (a) top panel; $x = 0.05$, and, (b) bottom panel; $x = 0.35$.

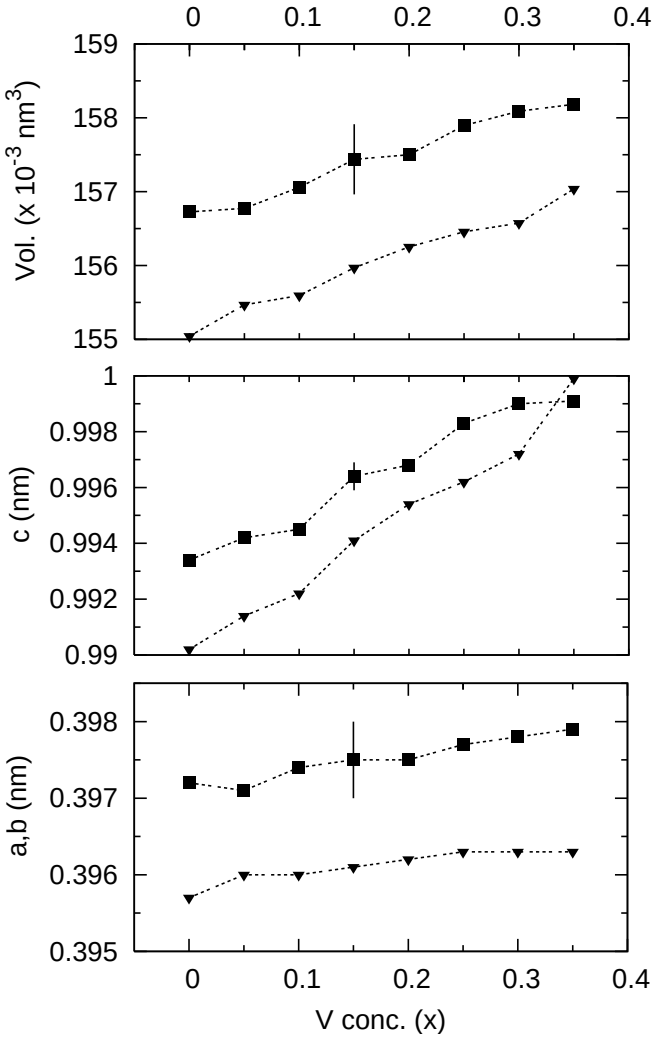

Figure 3.3: Lattice parameters (*a*, *b* and *c*) and unit cell volumes in *RE*($Co_{1-x}V_x$)$_2Si_2$ (RE = Pr(■), Nd(▼); $0 \leq x \leq 0.35$) obtained from Rietveld refinement of XRD data. The bars denote maximum limits of error in similar data in a panel.

3.3 Experimental Results and discussions

3.3.1 Magnetization measurements

Magnetic measurements in the temperature range 4-300 K were made with both Physical Properties Measurement System (PPMS) and Superconducting Quantum Interference Device Vibrating Sample Magnetometer (SQUID-VSM) of Quantum Design. The temperature dependence of molar magnetic susceptibility, χ_M, in $Pr(Co_{1-x}V_x)_2Si_2$ ($0.1 \leq x \leq 0.35$) at 0.5 T in between 4-250 K is shown in Figure 3.4(a). For the parent compound, *i.e.*, $PrCo_2Si_2$ ($x = 0$) and $Pr(Co_{1-0.05}V_{0.05})_2Si_2$, χ_M have small values and are shown separately in inset of Figure 3.4(a). The three reported transitions in the parent compound [56] have been obtained as different peaks in χ_M versus temperature at positions T_1 = 9 K, T_2 = 17 K and T_N = 32 K. Above 32 K, χ_M follows Curie-Weiss (CW) behavior. For V substituted samples, with increase in V content, χ_M increases more and more rapidly as temperature is decreased below 60 K. For x values of 0.05 and 0.10, an AFM transition is observed as a broad peak in χ_M at around 26 K which is followed by a minimum at 11 K. For $x \geq 0.15$, χ_M does not show the peak. Instead, it reaches a broad plateau at $\sim$ 30 K, and then it tends to increase further as temperature goes below $\sim$ 12 K. The latter behavior is clearly observed in the sample with $x \geq 0.30$. In high temperature side, $50 \leq T \leq 300$ K, χ_M in samples with $x \geq 0.15$ follow ferrimagnetic behavior which is given by [99],

$$\chi_M = \chi_0 + [(T-\theta)/C + \xi/(T-\theta_1)]^{-1} \tag{3.1}$$

where, θ_1 and ξ are proportional to $\eta_i\eta_j C(\eta_i - \eta_j)$ and $\eta_i\eta_j C$ (η_i and η_j are the fractional occupancies of the two magnetic sublattice sites in ferrimagnetism, C being the

Curie constant), respectively. The magnetic ordering temperature (θ_1) corresponds to the point where the hyperbola of equation 3.1 crosses the temperature axis. Figure 3.4(b) shows the experimental data of temperature dependence of inverse molar susceptibility and their simulation using equation 3.1 for all samples Pr($Co_{1-x}V_x$)$_2Si_2$ ($0.15 \leq x \leq 0.35$) and $PrCo_2Si_2$. Table 3.1 shows the values of various parameters in equation 3.1 as obtained from the simulation. For the parent compound (x = 0), C yields an effective magnetic moment, p_{eff}, of 3.86 Bohr magneton per formula unit (μ_B/f.u.), which is close to the theoretical p_{eff} of Pr^{3+}. For the V substituted samples, p_{eff} is reduced, and the ferrimagnetic ordering temperature (θ_1) is in the range 40-45 K, which is much higher than T_N of the parent compound. The temperature parameter θ which can be identified with the paramagnetic Curie temperature increases continuously with increase in V content of the samples.

Study of magnetic field (H) dependence of magnetization (M) shows that below $\sim$ 30 K, M in Pr($Co_{1-x}V_x$)$_2Si_2$ for x $\geq$ 0.15 have a tendency of saturation at $H \geq 2$ T, and they exhibit hysteresis loops. Figure 3.4(c) shows M versus H from 0 to 7 T for these samples measured at 4 K. For the parent compound (x = 0), M versus H plot is linear and shows step-like increase in magnetization near 2 and 5 T as reported [56]. For samples of $x \geq$ 0.15, magnetization increases with increasing V content, and their M versus H data have been compared with the following equation,

$$M(H) = \chi_1 H + M_S \tan^{-1} \chi_2 H \tag{3.2}$$

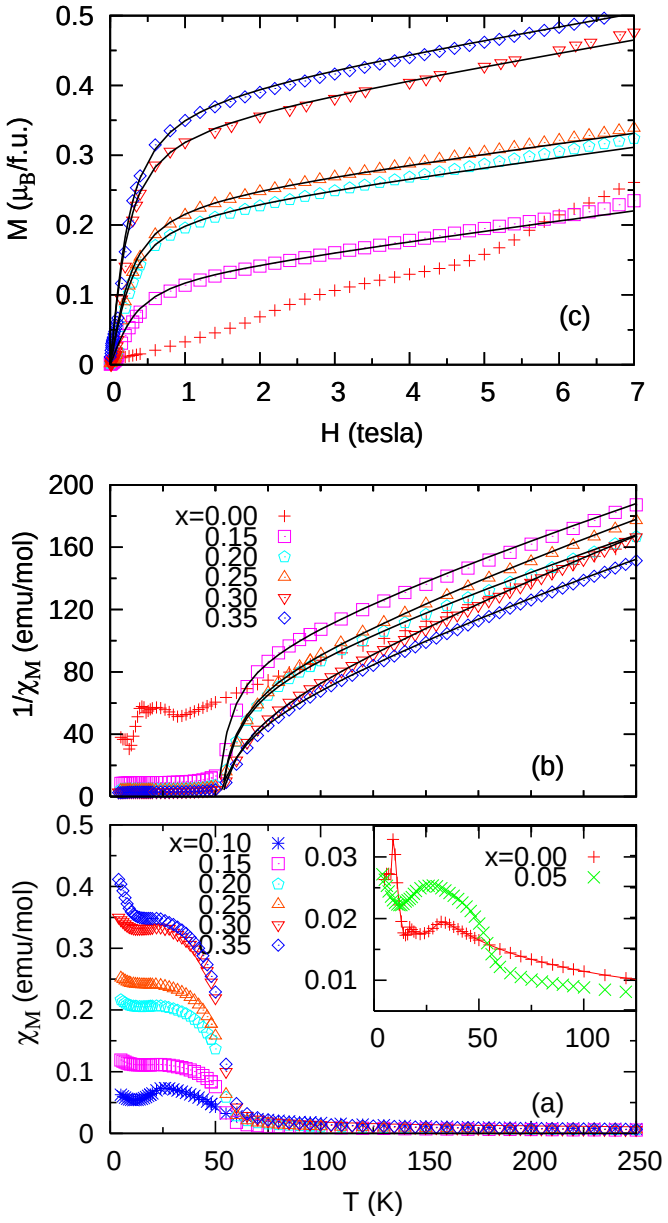

Figure 3.4: Plots of magnetic measurements in $Pr(Co_{1-x}V_x)_2Si_2$ ($0 \leq x \leq 0.35$); (a) temperature dependence of molar susceptibility χ_M, inset shows plots for the samples with $x = 0$ and 0.05 which have small values of χ_M, (b) temperature dependence of $1/\chi_M$ and the fitting with equation 3.1 as line plots, and, (c) magnetic field (H) dependence of Magnetization (M) at 4 K and the fitting with equation 3.2 as line plots. In (b) and (c), the symbols have the same correspondence with samples as in (a).

Table 3.1: Paramagnetic Curie constant(θ), effective number of Bohr magnetons (p_{eff}), constant (ξ), magnetic ordering temperature (θ_1), and saturation magnetization (M_S) obtained from the fitting of magnetization data, $1/\chi_M$ vs. temperature and M vs. H at 4 K, with equation 3.1 and 3.2, respectively, in $Pr(Co_{1-x}V_x)_2Si_2$ ($0 \leq x \leq 0.35$)

x	θ (K)	p_{eff}	ξ mol.K/emu	θ_1 (K)	M_S (μ_B/f.u.)
0	-66(2)	3.86(1)	–	–	–
0.15	-90(2)	3.41(1)	-600(5)	45(2)	0.080(2)
0.20	-60(2)	3.46(1)	-600(5)	45(2)	0.139(2)
0.25	-50(2)	3.29(1)	-600(5)	45(2)	0.152(2)
0.30	-22(2)	3.35(1)	-600(5)	42(2)	0.220(2)
0.35	-20(2)	3.43(1)	-600(5)	40(2)	0.245(2)

Figure 3.4(c) shows good fit of experimental data with equation 3.2. The first term in the equation is linear in magnetic field and represents the linear contribution to the magnetization. It remains significantly large in all samples with χ_1 being in the range 0.5-1.0 x 10^{-3} emu/mol. The second term represents magnetic field dependence of magnetization in a ferromagnetic material giving saturation of magnetization at high field. Table 3.1 lists the saturation magnetization, M_S, in terms of Bohr magneton per formula unit (μ_B/f.u.). M_S increases with x, but remains much smaller than the free-ion magnetic moment of Pr^{3+}.

Vanadium substitution in $NdCo_2Si_2$ results in a similar effect as that in $PrCo_2Si_2$. The temperature dependence of χ_M in $NdCo_2Si_2$ and $Nd(Co_{1-x}V_x)_2Si_2$ ($0.15 \leq x \leq 0.35$) at 0.5 T in between 4-300 K is shown in Figure 3.5(a). $NdCo_2Si_2$ shows the three transitions at T_1 = 13 K, T_2 = 24 K and T_N = 34 K, and above 34 K χ_M follows CW behavior. In V containing samples, deviation from CW behavior is observed below 60 K. Below this temperature, χ_M increases markedly with decrease in temperature and increase in vanadium concentration x. Not shown in the figure are the data for samples with x = 0.05 and 0.10, for which χ_M show a broad peak at about 28 K, followed by a broad minimum at about 12 K. In higher V containing samples, as temperature decreases, χ_M goes on increasing, though not

Table 3.2: Similar parameters as in Table 3.1 obtained from the fitting of magnetization data, $1/\chi_M$ vs. temperature and M vs. H at 4 K, with equations 3.1 and 3.2, respectively, in $Nd(Co_{1-x}V_x)_2Si_2$ ($0 \leq x \leq 0.35$)

x	θ (K)	p_{eff}	ξ mol.K/emu	θ_1 (K)	M_S (μ_B/f.u.)
0	-37(2)	4.00(1)	–	–	–
0.15	-40(2)	3.88(1)	-220(5)	41(2)	0.108(2)
0.20	-28(2)	3.89(1)	-220(5)	41(2)	0.148(2)
0.25	-27(2)	3.85(1)	-220(5)	40(2)	0.180(2)
0.30	-22(2)	3.87(1)	-220(5)	40(2)	0.265(2)
0.35	-7(2)	3.61(1)	-300(5)	38(2)	0.310(2)

monotonously. There are plateaus in magnetization near 28 K and again below about 8 K. Figure 3.5(b) shows temperature dependence of $1/\chi_M$ and its fit to equation 3.1 for all the samples. The fitting parameters are given in Table 3.2. The high temperature magnetization behavior is almost paramagnetic, and the p_{eff} values very nearly correspond to free Nd^{3+} ions. The ferrimagnetic ordering temperature (θ_1) is in the range 38-41 K, higher than T_N of the parent compound. θ increases markedly with increase in V content and tends to become positive.

Figure3.5(c) shows the plots of M versus H at 4 K and 0-7 T for all the $Nd(Co_{1-x}V_x)_2Si_2$ (x = 0, 0.15, 0.20, 0.25, 0.30 and 0.35) samples and their fitting with equation 3.2. For V containing samples, the plots clearly show the effect of saturation of magnetization at a field of about 2 T, though the slope of the plots beyond 2 T remains almost same as that of the M versus H plot of the parent compound. Although these samples behave as ferromagnets, there remain a linear component which does not saturates with magnetic field and also, which is as strong as that would arise from $4f$ moments in the parent compound. This observation and also the fact that M_S is much smaller than p_{eff}, clearly indicate that $4f$ moments may not be responsible for the observed ferromagnetic-like behavior in V substituted samples.

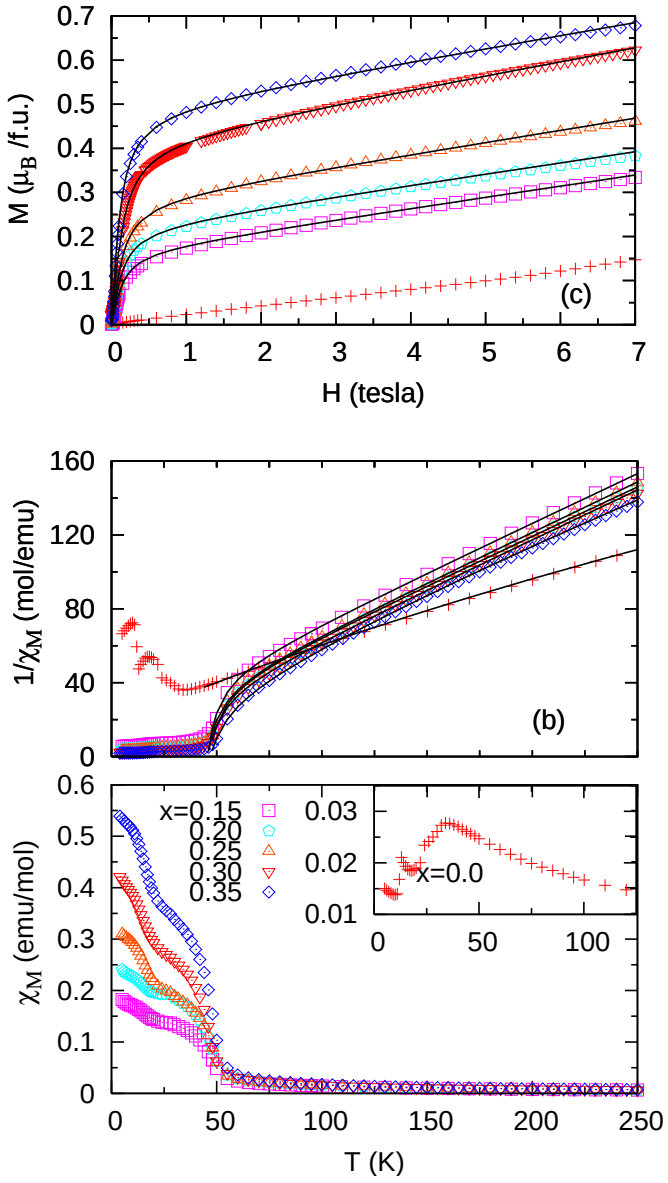

Figure 3.5: Plots of magnetic measurements in Nd($Co_{1-x}V_x$)$_2Si_2$ ($0 \leq x \leq 0.35$); (a) temperature dependence of molar susceptibility χ_M, inset shows data for the parent compound, (b) temperature dependence of $1/\chi_M$ and the fitting with equation 3.1 as line plots, and, (c) magnetic field (H) dependence of Magnetization (M) at 4 K and the fitting with equation 3.2 as line plots. In (b) and (c), the symbols have the same correspondence with samples as in (a). The vertical dashed line in (a) indicates the temperature of ferromagnetic ordering (see text).

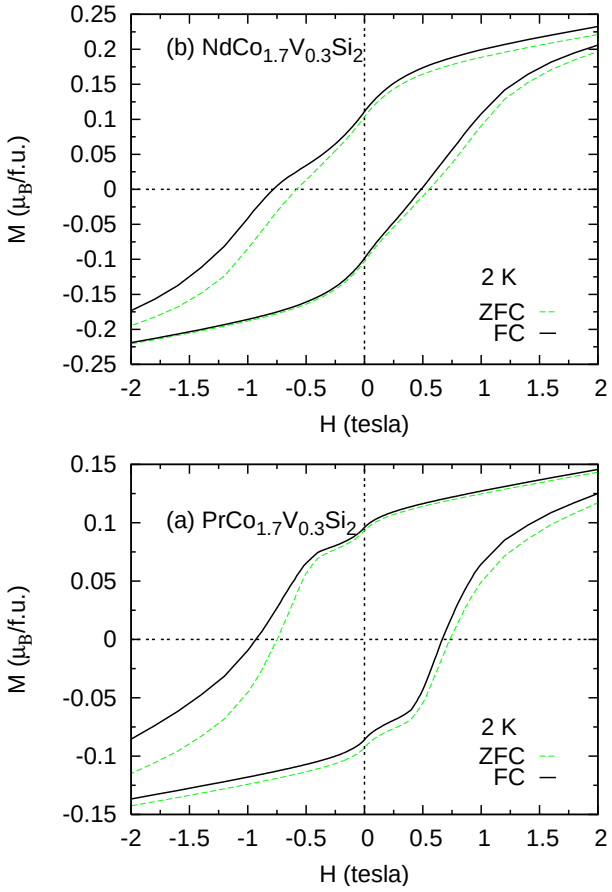

Figure 3.6: Hysteresis loops at 2 K in zero-field cooled (ZFC) and field cooled (FC) conditions in $Pr(Co_{0.85}V_{0.15})_2Si_2$ (bottom panel) and $Nd(Co_{0.85}V_{0.15})_2Si_2$ (top panel). Data are shown for magnetic fields (H) $-2 \leq H \leq 2$ T whereas experiments were performed at $-7 \leq H \leq 7$ T.

The magnetic hysteresis of V doped samples were studied first by cooling down the samples from room temperature to a temperature set in the range $2 \leq T \leq 30$ K at zero external magnetic field. In this so-called zero-field cooled (ZFC) condition, the hysteresis loop in between $-7 \leq H \leq 7$ T was symmetric about the zero on the field axis, and coercive field (H_C) was obtained. With the sample in 7 T magnetic field, it was warmed to 300 K and then cooled down to the same temperature. In this field-cooled (FC) condition, the

hysteresis loop was asymmetric and both the ascending and descending curves of $M-H$ loop were shifted from their ZFC positions in the negative magnetic field direction. The average of the shifts measured on both sides of the H-axis is defined as the exchange bias field (H_{EB}). Figures 3.6(a) and 3.6(b) show parts of hysteresis loops at -2 $\leq H \leq$ 2 T at 2 K in ZFC-FC conditions in $PrCo_{1.7}V_{0.3}Si_2$ and $NdCo_{1.7}V_{0.3}Si_2$, respectively. Figures 3.7(a) and 3.7(b) shows the temperature dependence in between 2-30 K of H_C and H_{EB} for all the Pr($Co_{1-x}V_x$)$_2Si_2$ and Nd($Co_{1-x}V_x$)$_2Si_2$ samples with x $\geq$ 0.15. An appreciable coercivity is obtained in all the samples. Though there are variations in H_C from sample to sample, it does not vary systematically with the vanadium content. Above $\sim$ 30 K, H_C values are very small. In between 2 to 8 K for Pr($Co_{1-x}V_x$)$_2Si_2$ and 2 to 12 K for Nd($Co_{1-x}V_x$)$_2Si_2$, H_C decreases fast with temperature, whereas, above these temperatures H_C is small and decrease slowly. Inset 1 of Figures 3.7(a) and 3.7(b) shows that H_{EB} values are small in between 30-10 K, but increases sharply below this temperature and reaches $\sim$ 16 % of H_C at 2 K. For samples $PrCo_{1.3}V_{0.7}Si_2$ and $NdCo_{1.3}V_{0.7}Si_2$ data have been taken at close interval in the range of temperature 2-30 K, and the logarithm of H_C when plotted against temperature shows two well-defined linear segments below and above $\sim$ 10 K as shown in inset (2) of Figures 3.7(a) and 3.7(b). These observations and the resistivity measurements described in the next section indicate that the ferromagnetic phase below $\sim$ 10 K is different from the ferromagnetic phase above this temperature.

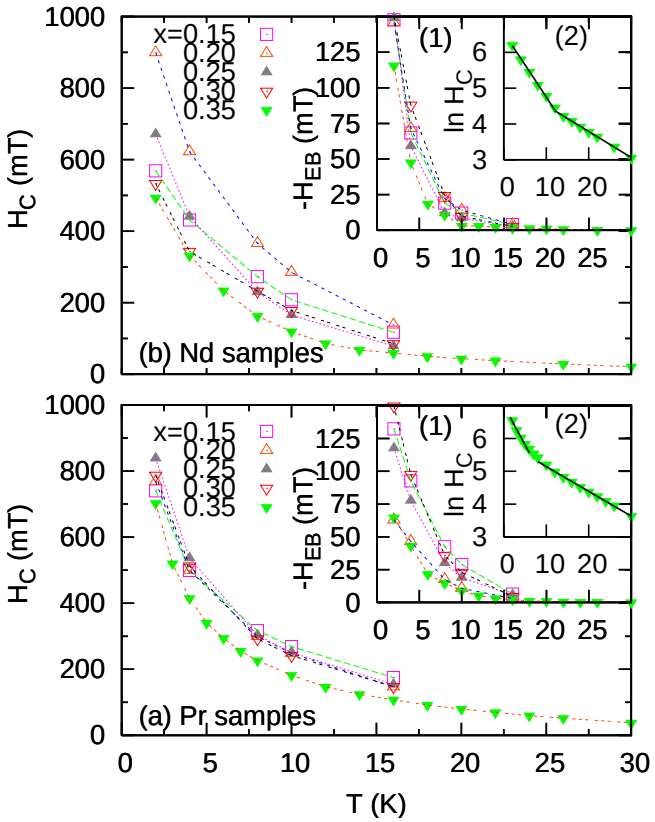

Figure 3.7: (a) Temperature dependence of coercive field (H_C)in (a) $Pr(Co_{1-x}V_x)_2Si_2$ (x = 0.15, 0.20, 0.25, 0.30 and 0.35, and (b) $Nd(Co_{1-x}V_x)_2Si_2$ (x = 0.15, 0.20, 0.25, 0.30 and 0.35). Inset 1; temperature dependence of exchange bias field (H_{EB}) for the same samples. Inset 2; for $Pr,Nd(Co_{0.65}V_{0.35})_2Si_2$ the plot of lnH_C vs. temperature having two linear segments. The lines are guide to the eye.

3.3.2 Transport property measurements

Temperature (T) dependence of resistivity (ρ) measured as ρ_T/ρ_{300}, were obtained at zero magnetic field and in the magnetic field of 9 T. Figure 3.8 shows the data for the parent compounds $PrCo_2Si_2$ (Figure 3.8(a)) and $NdCo_2Si_2$ (Figure 3.8(c)), and V

substituted samples $Pr(Co_{0.75}V_{0.25})_2Si_2$ (Figure 3.8(b)) and $Nd(Co_{0.65}V_{0.35})_2Si_2$ (Figure 3.8(d)), which are representative of other V substituted Pr and Nd samples, respectively. The various transitions are clearly indicated specially in zero-field resistivity behavior, as marked by arrows in Figure 3.8. In both the parent compounds, the AFM transition at $T_N \sim$ 30 K is reflected as a rapid change in the slope of ρ_T/ρ_{300} near that temperature both in zero field and in 9 T magnetic field. An overall positive magnetoresistance is observed below T_N. In V doped samples, a similar change in the slope of ρ_T/ρ_{300} appear near 50 K for Pr samples and 45 K for Nd samples. These positions are just above the temperatures of ferrimagnetic transitions described in Section 3.3.1. In contrast to the parent samples, a negative magnetoresistance is obtained below these temperatures and down to $\sim$ 10 K. Interestingly, below $\sim$ 9 K, there is a sharp drop in zero field resistivity in all V doped samples, indicating occurrence of another magnetic transition. On application of a magnetic field of 9 T, the drop in resistivity occurs at a lower temperature. Consequently, a positive magnetoresistance is obtained in all V doped samples in between 2-9 K.

3.3.3 Specific heat measurements

The specific heat, $C_P(T)$, at zero external magnetic field were measured for the parent compounds and some of the vanadium substituted compounds, *e.g.*, $Pr(Co_{1-x}V_x)_2Si_2$ (x = 0, 0.20 and 0.35), and $Nd(Co_{1-x}V_x)_2Si_2$ (x = 0, 0.20 and 0.35), and also for isostructural $LaCo_2Si_2$ from 3-300 K. Figure 3.9 shows the data for the temperature range $2 \leq T \leq 80$ K. In parent compounds, the T_N and T_2 transitions are clearly indicated by λ-like peaks at the respective temperatures. At the lowest temperature T_1 transition (commensurate-incommensurate), there is a barely detectable hump which is not shown in these figures. All the V doped samples show two prominent peaks. The higher temperature peaks are at 52 K for $PrCo_{1.6}V_{0.4}Si_2$ and $PrCo_{1.3}V_{0.7}Si_2$, and at 46 K for $NdCo_{1.6}V_{0.4}Si_2$ and $NdCo_{1.3}V_{0.7}Si_2$. These temperature positions are a little higher compared to those of the

ferrimagnetic transitions obtained in magnetic measurements.

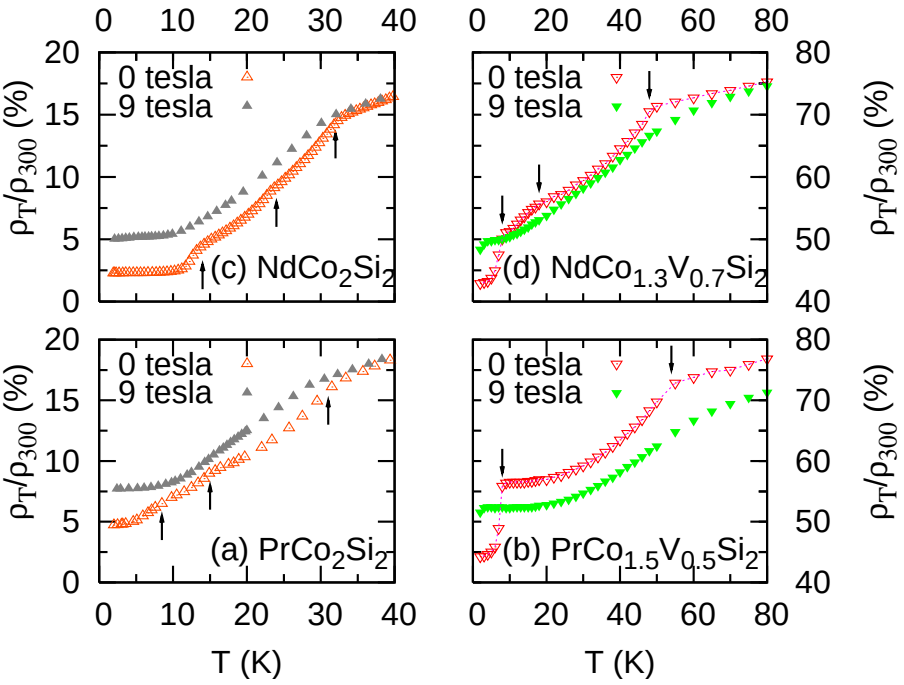

Figure 3.8: Plots of resistivity ρ_T/ρ_{300} versus temperature in conditions of zero external magnetic field and in the magnetic field of 9 T for (a) $PrCo_2Si_2$, (b) $Pr(Co_{0.75}V_{0.25})_2Si_2$, (c) $NdCo_2Si_2$, and, (d) $Nd(Co_{0.65}V_{0.35})_2Si_2$. The arrows show positions of phase transitions as reflected in zero field resistivity data, which, in (b) and (d) are joined by broken lines as a guide to the eye.

The lower temperature peaks, at 23 K for V doped Pr compounds and at 27 K for V doped Nd compounds, are at a slightly lower position compared to that of the onset of ferromagnetism indicated in magnetic studies. From experimental data of $C_P(T)$, the magnetic specific heat $C_m(T)$ was separated out by subtracting the lattice contributions, which was obtained from the data of nonmagnetic $LaCo_2Si_2$. Hence, the magnetic entropies, S_m, have been calculated by integrating $(C_m/T)dT$, and are also shown in Figure 3.9. It has been observed that S_m levels off at $\sim$ 120 K in Pr compounds, and at $\sim$ 100 K

in Nd compounds giving an idea of their overall crystal field splitting energies. The Debye temperatures as obtained from the fitting of the data using equation 1.14 are 427 K, 440 K and 510 K respectively for the samples Nd($Co_{1-x}V_x$)$_2Si_2$ (x = 0, 0.20 and 0.35).

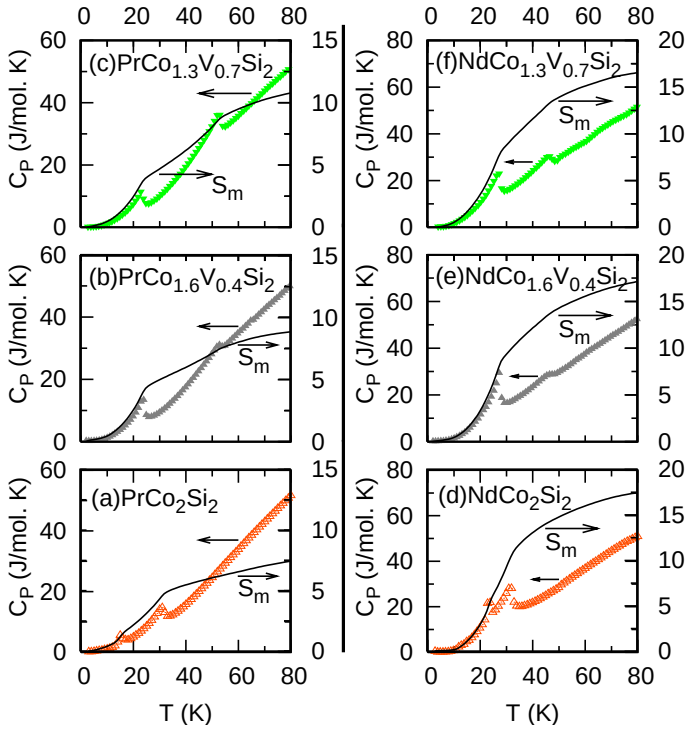

Figure 3.9: Heat capacity (C_P, left y-axis) as discrete data points, and calculated magnetic entropy (S_m, right y-axis) as continuous lines in (a) $PrCo_2Si_2$, (b) Pr($Co_{0.8}V_{0.2}$)$_2Si_2$, (c) Pr($Co_{0.65}V_{0.35}$)$_2Si_2$, (d) $NdCo_2Si_2$, (e) Nd($Co_{0.8}V_{0.2}$)$_2Si_2$, and, (f) Nd($Co_{0.65}V_{0.35}$)$_2Si_2$. Left and right y-axes have the same units.

Table 3.3 compares the values of experimental S_m at 120 K. As for the parent compounds, $PrCo_2Si_2$ attains only 46% of the theoretical S_m expected for Pr^{3+} ions, whereas, for $NdCo_2Si_2$, S_m is 94% of the theoretically expected value for Nd^{3+} ions. Such a large difference in experimental S_m could be found also in $PrCo_2Ge_2$ and $NdCo_2Ge_2$ [100]. Specific heat measurements indicate a rather complicated effect of crystal electric field on magnetic moments in these compounds. Even then in Pr($Co_{1-x}V_x$)$_2Si_2$, S_m increases consistently with V doping which is possibly an indication of an overall increase in the

Table 3.3: Magnetic entropy S_m at 120 K in $Pr(Co_{1-x}V_x)_2Si_2$ and $Nd(Co_{1-x}V_x)_2Si_2$ (x = 0, 0.20 and 0.35)

Sample	S_m J/mol. K	Sample	S_m J/mol. K
$PrCo_2Si_2$	8.5±0.5	$NdCo_2Si_2$	18.0±0.5
$PrCo_{1.6}V_{0.4}Si_2$	9.6±0.5	$NdCo_{1.6}V_{0.4}Si_2$	18.2±0.5
$PrCo_{1.3}V_{0.7}Si_2$	11.8±0.5	$NdCo_{1.3}V_{0.7}Si_2$	17.5±0.5

number of magnetic ions that are involved in the magnetic ordering. In Nd compounds in which crystal field seems to have a comparatively small effect, S_m at the ordering temperature of 27 K reach values close to $Rln3$ indicating that the ordering moment comes from a pseudo-triplet ground state.

3.3.4 Magnetocaloric effect study of vanadium substituted intermetallic $NdCo_2Si_2$ compounds

To understand the nature of the magnetic ground state study of magnetocaloric effects is one of the most sensitive tool. In this chapter, as a representative example, the magnetocaloric properties of vanadium doped intermetallic $NdCo_2Si_2$ compounds were discussed to probe the modification of the ground state due to the vanadium substitution. The results are correlated with the magnetic properties as discussed before. The dc magnetization study have been performed in the presence of H = 5 kOe external magnetic field. Magnetization as a function of temperature for the all compounds are already discussed in the magnetization measurement subsection of this chapter. For the parent compound $NdCo_2Si_2$, three distinct transitions are clearly visible. Such temperature induced transition in this compound also exactly matches with the earlier reported results [52]. On the other hand in case of the vanadium doped samples the magnetization values abruptly increases in the low temperature region.

To calculate the magnetocaloric entropy changes at different constant external magnetic field, we have collected the magnetic isotherms data at different temperatures. To measure the magnetization as a function of external magnetic field, the sample was cooled down from the room temperature (T = 300 K) in the absence of any external magnetic field (ZFC) to the specified temperature and the data were recorded. This same procedure was followed for all the measurements to remove the previous history of the measurements if present. The magnetic isotherms for all the compounds at some specified temperature is shown in Figure 3.10.

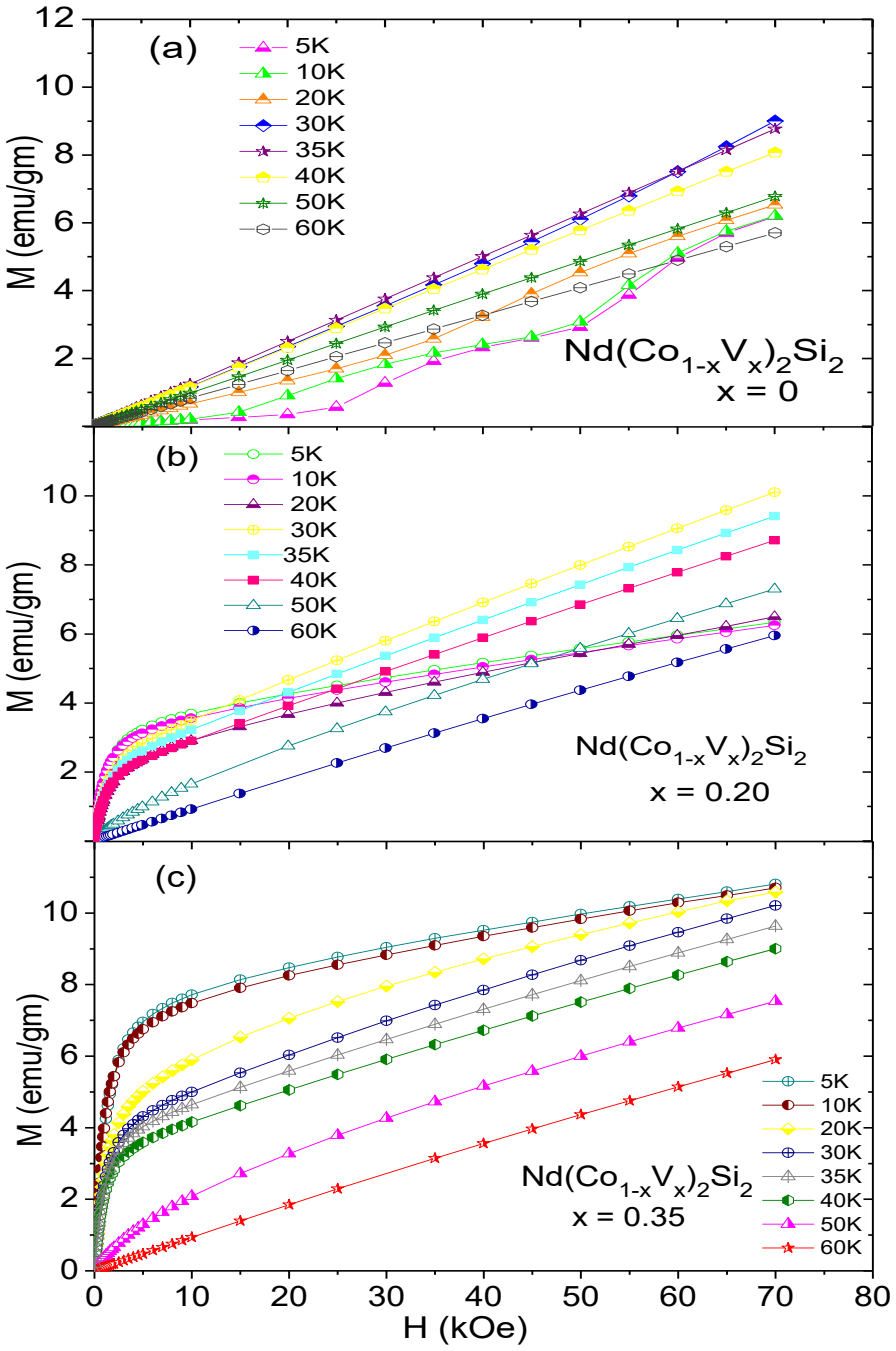

Figure 3.10: Magnetization as a function of external magnetic field for (a) $NdCo_2Si_2$, (b) $Nd(Co_{0.80}V_{0.20})_2Si_2$ and (c) $Nd(Co_{0.65}V_{0.35})_2Si_2$ compounds at different temperatures.

As discussed earlier, the magnetization values due to the vanadium doping substantially increases especially at the low temperature region. Additionally it should also be

mentioned that ferromagnetic like signature appears in vanadium doped sample in contrast to the parent $NdCo_2Si_2$ compound (below 30 K). Such variation of the magnetization (at low temperature) in doped sample further implies that the modification of the ground state of the compound. Regarding the $M(H)$ isotherms (Figures 3.10(a), (b) and (c)) it should be mentioned that for parent compound the magnetization increases with the temperature which is usually observed in case of a conventional antiferromagnetic compound, whereas in case of the doped compound (x = 0.20), the magnetization increases up to 30 K then decreases with temperature. For further doping x = 0.35, ferromagnetic like magnetic isotherms have been observed.

To elucidate the reflection of the doping in magnetocaloric properties, we have calculated the magnetic entropy changes for all the compounds by using Maxwell's thermodynamic relation According to the Maxwell's thermodynamic relation magnetocaloric entropy change (ΔS_M) is given by

$$\Delta S_M = \int_0^H (\partial M/\partial T) dH \tag{3.3}$$

The isothermal entropy changes as a function of temperature for the all compounds is shown in Figure 3.11. Regarding this issue it is worth mentioning that the nature of the magnetocaloric responses as a function of temperature as well as the numerical value changes with the doping concentration of vanadium. In case of the parent layered structure compound $NdCo_2Si_2$, the antiferromagnetic interaction is predominant resulting in the inverse magnetocaloric effect as expected. Whereas in case of the vanadium substituted materials the antiferromagnetic interaction become weaker especially for x = 0.20. The suppression of the strength of the antiferromagnetic ordering with the vanadium doping already reported in Section 3.3.1. Particularly for the doping x = 0.20 compound the magnetic randomness is expected to increase due to the ferrimagnetic type magnetic state below $\sim$ 40 K, resulting in large inverse magnetocaloric entropy changes in the presence

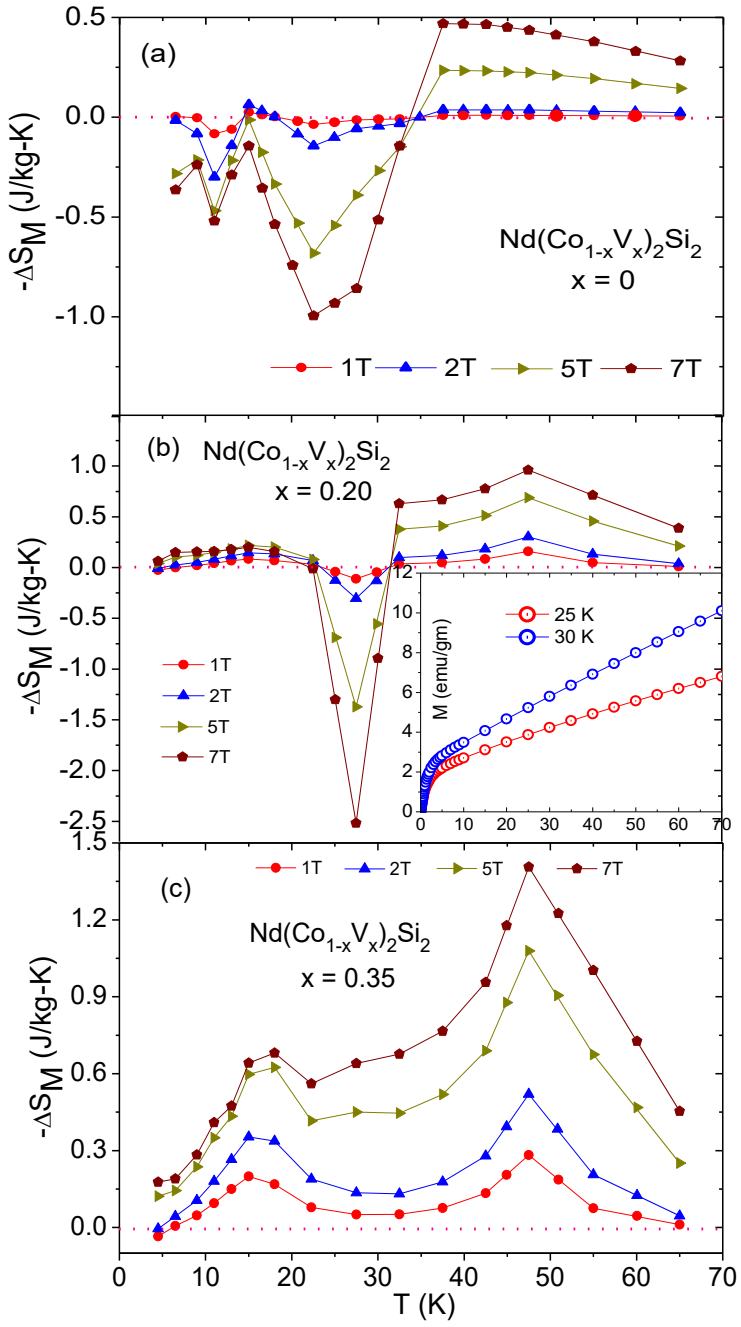

Figure 3.11: Isothermal entropy changes as a function of temperature at different external magnetic field for $Nd(Co_{1-x}V_x)_2Si_2$ (x = 0, 0.20, 0.35) compound. Inset of (b) is the $M(H)$ isotherms of the $Nd(Co_{1-x}V_x)_2Si_2$ (x = 0.20) compound at 25 K and 30 K temperature, indicates the increasing magnetization with increasing temperature resulting large inverse magnetocaloric entropy changes.

of 70 kOe external magnetic field compared to its parent compound. Further substitution of vanadium (x = 0.35) results in ferromagnetic like phase predominant at low temperature resulting in the conventional large magnetocaloric effect.

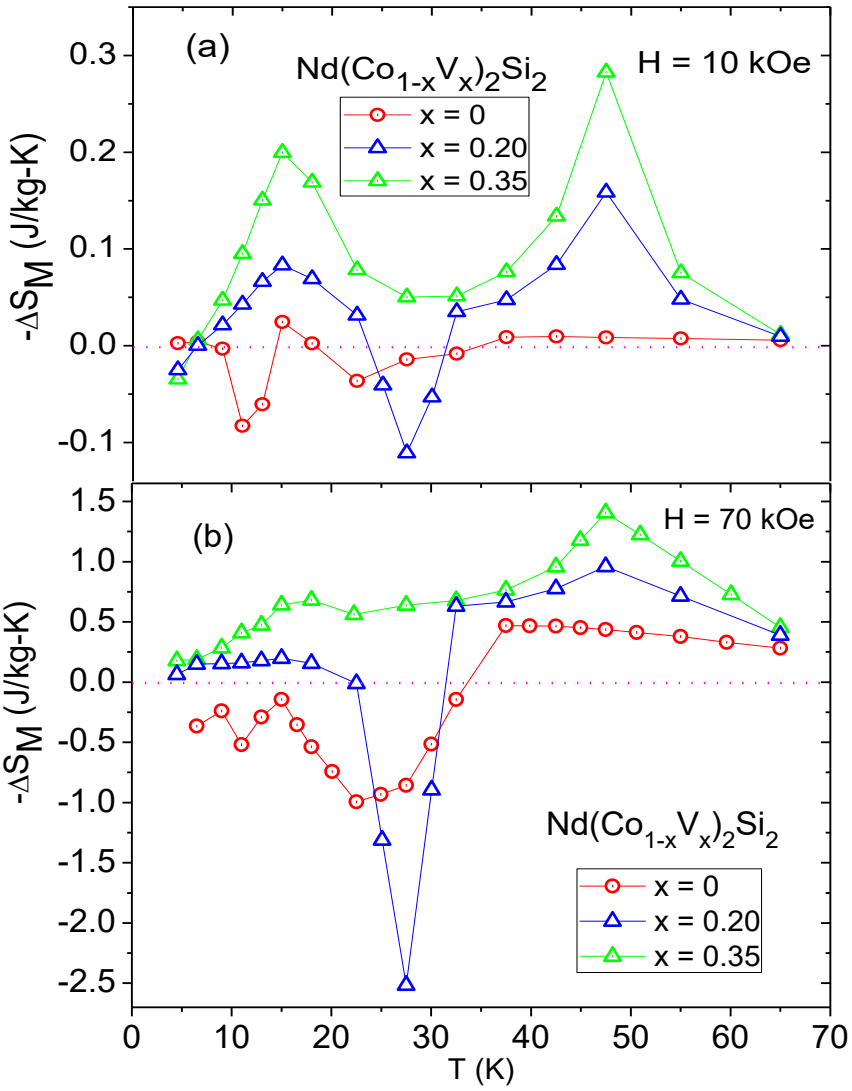

Figure 3.12: Comparison of magnetocaloric entropy changes as a function of temperature in (a) H = 10 kOe and (b) H = 70 kOe external magnetic field for Nd($Co_{1-x}V_x$)$_2Si_2$ (x = 0, 0.2, 0.35) compound.

The comparison of the enhancement of the magnetocaloric effect due to the vanadium substitution is shown in Figure 3.12. The enhancement of the magnetic entropy changes was observed not only at high magnetic field (70 kOe) but also at lower field values (10 kOe). In

contrast to the parent compound, for lower doping level, $x = 0.20$ the inverse magnetocaloric effect increases due to the increase of the magnetic randomness below 40 K. On the other hand for the doping concentration, $x = 0.35$, the magnetic ground state becomes almost ferromagnetic (below 30 K) indicated in $M(H)$ isotherms (Shown in Figure 3.10) resulting in the large magnetic entropy changes in the presence of external magnetic field.

3.4 Conclusions

The XRD results have shown that partial substitution of Co by V in $PrCo_2Si_2$ and $NdCo_2Si_2$ results in lattice expansion which is more pronounced along c axis than in ab plane. These compounds have a layered structure with one type of atom in each layer, and in V substituted compounds, the atoms are stacked in a sequence Pr(Nd)-Si-Co/V-Si-Pr(Nd). Presumably, there should be a dominant antiferromagnetic interaction involving only Pr(Nd) moments along c axis, as in parent compounds. However, the magnetic, specific heat and resistivity measurements indicate a magnetic transition, which, in spite of the lattice expansion, takes place at a temperature of 40-45 K, much higher than the Neel temperature ($\sim$ 30 K) of the parent compounds. This clearly indicates a possibility of occurrence of magnetism in the intervening Co/V layers facilitating the interaction between successive Pr(Nd) layers. Indeed, the analysis of the data indicates ferrimagnetism, and hence, the presence of more than one type of magnetic ions. The increased value of exponent in the temperature dependence of resistivity just below the ferrimagnetic transitions and the increased values of S_{mag} also indicate the participation of more magnetic ions in the magnetic ordering of V doped samples compared to that in parent compounds.

In parent compounds, the rare-earth ions are already in 3^+ state. As discussed earlier, the magnetization of substituted samples at low temperatures has a strong paramagnetic

component (χ_1 in equation 3.2) and a rather small value of saturation magnetization. These are strong indications that rare-earth $4f$ moments contribute only to paramagnetism even at low temperatures, and that the ferrimagnetic behavior at high temperatures and weak ferromagnetism at low temperatures arise from partial localization of $3d$ electrons. There is no localized moment on Co atoms in parent compounds. Either the Co-$3d$ levels are completely filled up by p-electrons from Si atoms, or there is $3d$ band which is close to the Fermi level and therefore completely filled [51]. Substitution of cobalt by vanadium which has fewer $3d$ electrons than cobalt, should affect the $3d$ electron character in these compounds. Moreover, a negative chemical pressure resulting from lattice expansion may also lead to the localization of the $3d$ electrons. However, even though there is electron localization, vanadium substitution actually lowers the value of p_{eff} (Tables 3.1 and 3.2), which might be a result of lattice distortion and an increased effect of crystalline electric field.

The change of sign of magnetoresistance from being positive in parent compounds to being negative upon vanadium substitution is a definite indication of a change in the magnetic interactions, which, in this case, is the dominance of ferromagnetic interactions over antiferromagnetic interactions in V substituted compounds. The peak in specific heat at $\sim$ 30 K coincides with the onset of saturation of magnetization at a comparatively small magnetic field of $\sim$ 2 T and appearance of a coercive field which has a temperature dependence that of a ferromagnetic material (Figures 3.7(a) and 3.7(b), inset (2)). There also appears a small exchange bias field at these temperatures. These are indications that V doped samples undergo a ferromagnetic ordering coexisting with antiferromagnetism, which might be assumed to be a consequence of the existence of both AFM and FM interactions [52, 57].

Only a fraction of Co atoms depending upon vanadium content may have localized moments. Alternatively, if we assume that the ferromagnetic behavior is due to the

magnetism of only vanadium, then at 4 K the saturation magnetic moments (Tables 3.1 and 3.2) are $0.31\mu_B \pm 0.05$ per V atom in Pr samples and $0.40\mu_B \pm 0.04$ per V atom in Nd samples. These values are comparable to the magnetic moments appearing on vanadium when it is present in dilute quantities in alloys and thin films [101, 102, 103]. At low temperatures, the localized 3*d* moments on Co and/or V might order ferromagnetically in *ab* plane, similar to the ordering of Mn ions in isostructural $PrMn_2Ge_2$ and $NdMn_2Ge_2$ [27].

The zero field transition at $\sim$ 8 K in V doped compounds is quite different from the commensurate-incommensurate transition at similar temperatures in parent compounds. In case of latter, there is only a small change in the slope of resistivity at the transition temperature, *e.g.*, at 9 K in the zero-field data of $PrCo_2Si_2$ (Figure 3.8(a)) and at 14 K in $NdCo_2Si_2$ (Figure 3.8(c)); whereas, in V doped samples, following the transition at $\sim$ 8 K, the resistivity drops by $\sim$ 10% within a few kelvin. The transitions in V doped samples are different also from the field induced magnetic transitions in parent compounds [56], *e.g.*, in $PrCo_2Si_2$, in which at temperatures below 10 K, two such transitions at 1.3 and 3.6 T are indicated by steps in *M* versus *H* curve (Figure 3.4(c)). The transitions in the parent compounds did not drastically affect their resistivity and magnetoresistance which has a maximum value of only $\sim$ 2% (Figure 3.8(a)and Figure 3.8(c)). The magnetic transitions below 8 K in V doped samples probably results from a reorientation of either rare earth or 3*d* magnetic moments, affecting interactions at the FM-AFM interface in such a way that there is a sharp rise in exchange bias and rapid decrease in resistivity.

The transition at $\sim$ 8 K leads also to a positive magnetoresistance below this temperature. The magnetoresistance has a maximum value of $\sim$ 8% at 4 K and 9 T. Isostructural ferromagnetic compound $LaMn_2Ge_2$ has shown a positive magnetoresistance [104]. In this compound, the magnetic Mn ions have a conical arrangement along *c* axis, and therefore, coexisting with ferromagnetism there is an antiferromagnetic magnetic moment

component in *ab* plane. Isostructural $SmMn_2Ge_2$, a re-entrant ferromagnet, also shows a magnetoresistance of $4 - 8\%$ [105]. It would be interesting to know how V doping alters the magnetic structure of $RECo_2Si_2$ compounds. However, in addition to positive magnetoresistance, the V substituted compounds have also yielded a significant exchange bias field which might be due to the existence of $3d$ and $4f$ magnetic moments in different atomic layers. The present study therefore strengthens the notion of natural multilayers attributed to these compounds [104, 105].

Some of the experimentally obtained parameters appear not to change systematically with the vanadium content. As said before, p_{eff} and S_{mag} could be directly affected by the modification of crystal electric field (CEF) induced by V doping and lattice expansion, whereas, H_C and H_{EB} could be influenced by other factors, *e.g.*, magneto-crystalline anisotropy. The determination of CEF parameters is complex and outside the scope of this paper. An indirect idea of CEF modification could be made from the study of ^{59}Co nuclear magnetic resonance (NMR) spectrum which combines the effects of nuclear Zeeman and quadrupole interactions [106], the latter being due to the crystal electric field gradient (EFG) at the nucleus. Such study was not possible in either of Pr and Nd compounds due to excessive magnetic broadening of the NMR spectra. However, in isostructural $Ce(Co_{1-x}V_x)_2Si_2$ (x = 0, 0.15 and 0.25), ^{59}Co NMR spectra have been obtained and they show evidence of significant modification of EFG and its asymmetry (η) with increase in x as discussed in details in Chapter 5.

For the first time, vanadium, an element not known to form $ThCr_2Si_2$ type pure compounds, have been used for partial substitution of cobalt in antiferromagnetic compounds $PrCo_2Si_2$ and $NdCo_2Si_2$ causing lattice expansion and significant modification of magnetic properties. With lowering of temperature, vanadium doped compounds become ferrimagnetic at $\sim$ 40 K, and then ferromagnetic below $\sim$ 30 K. The observations of a significant exchange-bias field and magnetoresistance indicate the coexistence of FM and

AFM interactions probably occurring in different atomic layers consisting exclusively of rare-earth or 3*d* atoms. Further studies using microscopic techniques, such as, inelastic neutron scattering and nuclear magnetic resonance would be helpful to identify the local moments and magnetic structures of the substituted compounds. On the other hand, there are many other rare-earth ternary silicides of $ThCr_2Si_2$ or related [107, 108] structure types $TbFeSi_2$ and CeFeSi, and it would be interesting to perform similar studies on those compounds. The magnetocaloric properties of vanadium doped $Nd(Co_{1-x}V_x)_2Si_2$ (x = 0.2, 0.35) compound have been investigated. Our study clearly indicates that the magnetic ground state and magnetocaloric responses of the parent compound is drastically modified upon substitution of Co by non magnetic vanadium. Though the values of the magnetocaloric entropy changes are small compared to the other intermetallic materials however the present study indicates a route for enhancement of magnetocaloric effect in such class of compounds.

CHAPTER 4

Transport property study of NdT_2Si_2 (T = Co, $Co_{0.65}V_{0.35}$, Ru) intermetallic compounds

4.1 Introduction

Intermetallic compounds of rare earth (*RE*), transition metal (T) provides an interesting area of research due to its diverse nature of electronic and magnetic properties. The discovery of giant magnetoresistance (GMR) in Fe/Cr multilayers [109] have led to the development in the research of magnetic multilayers and magnetoresistance has become one of the frequently studied properties because of its implications as one of the key ingredients in electrically controlled magnetic memory and sensor devices as well as high density read head technology. Generally, in systems exhibiting GMR, the magnetic layers are separated by non-magnetic layers and the indirect exchange interaction between the magnetic layers leads to an antiferromagnetic coupling between the magnetic

layers. This serves as the origin of the large MR in these systems. The ternary rare earth silicides/ germanides possess naturally occurring layered magnetic structure which are qualitatively similar to GMR systems. While the artificial compounds are fascinating from the perspective of applications, the naturally occurring layered compounds serve as an alternative route for solving fundamental issues regarding electronic transport in two dimensional magnetic materials [110]. The magnetoresistance in such compounds have been the focus of extensive research through several decades [111, 112, 113, 114, 115].

In the first section of this chapter we describe the magneto-transport behavior of $NdCo_2Si_2$, which forms in $ThCr_2Si_2$ crystal structure that shows layering along the *c*-axis in the following sequence ... Nd —Si —Co —Si —Nd.. This intermetallic compound is antiferromagnetic below $\sim$ 32 K due to the ordering of localized magnetic moments occurring only in the rare earth ions as described earlier in Chapter 3. $NdCo_2Si_2$ exhibits a complex magnetic structure in which the propagation vectors (0,0,1), (0,0,0.07) and (0,0,0.21) appear in the sequence of $T \leq 15$ K (T_1), 15 K $\leq T \leq$ 24 K (T_2) and 24 K $\leq T \leq$ 32 K (T_N), respectively [52]. A brief account of the transport property of this compound along with its vanadium substituted compounds has been provided in Chapter 3.

It has been described in Section 3.3.1 that V substitution in $RECo_2Si_2$ have resulted in the appearance of ferromagnetism from the original antiferromagnetic state of the parent compound. This is the first instance of antiferromagnetic $RECo_2Si_2$ compounds becoming ferromagnetic upon incorporation of a non-magnetic transition element. For the doped compounds, it has been observed that the magneto-resistance (MR) is negative up to $\sim$ 10 K representative of a ferromagnetic state while below $\sim$ 10 K, the compound exhibits an anomalous positive MR.

In order to understand the magnetoresistance behavior of these compounds, we continued with the study of another isostructural rare earth silicide $NdRu_2Si_2$. Even though there has been studies on the $NdRu_2Si_2$ detecting multiple magnetic transitions [65, 66],

there has been no conclusive study on the comparison between MR and MCE studies of the compound. Detailed information about the magnetic state of a compound can be obtained from a comparison of MR and MCE properties. In the last section of this chapter, we study these phenomena extensively hoping to shed new lights on the properties of $NdRu_2Si_2$. Recently, a lot of focus has been directed towards the understanding of the complex magnetic states existing in these type of systems. In addition, there has also been several reports on large magneto-resistance in these compounds, *e.g.*, FeRh, GdSiGe, MnAs, $SmMn_2Ge_2$ [113]etc. The mechanism varies depending on the specifics in different systems. The value of the MR in these materials are considerably large and thus can be considered to be a candidate material for large MR besides the well-known compounds like perovskite manganites showing CMR or the artificial multilayers showing GMR. The naturally layered structure of these compounds makes them suitable material for investigation and tuning of spin-dependent MR similar to GMR.

In the last section of this chapter we report on the magneto-resistance and magnetic properties of the compound $NdRu_2Si_2$. We have observed for the first time, the existence of an anomalous property in this compound which is evidenced to arise from the complex magnetic states in the system. In addition, the magnetocaloric property of the system is also investigated to provide more insights into the complex nature of magnetic interactions.

4.2 Experimental details

Polycrystalline samples of $NdCo_2Si_2$, $Nd(Co_{0.65}V_{0.35})_2Si_2$ and $NdRu_2Si_2$ were prepared by arc melting high-purity elements in purified argon atmosphere. For better homogeneity, the ingots were turned over and re-melted six times resulting in the end a weight loss of less than 1 %. The samples were subsequently annealed at 900° C for 7 days. The $NdRu_2Si_2$ sample was quenched in liquid nitrogen. The single phase nature of the

sample was checked by x-ray diffraction in a Rigaku TTRAX diffractometer using Cu-Kα radiation. The magnetization measurements were carried out in SQUID VSM (Quantum Design). The specific heat measurement in zero field was done in Quantum design PPMS. The electrical resistance measurements were carried out following the conventional four probe method in the presence and absence of magnetic field. Magneto-transport properties were studied using conventional four probe longitudinal geometry.

4.3 Large positive magnetoresistance in $NdCo_2Si_2$

In order to get a better insight into the transport property of this layered compound, temperature dependence of electrical resistivity (ρ) and magnetoresistance (MR) measurements were carried out as described in the current section.

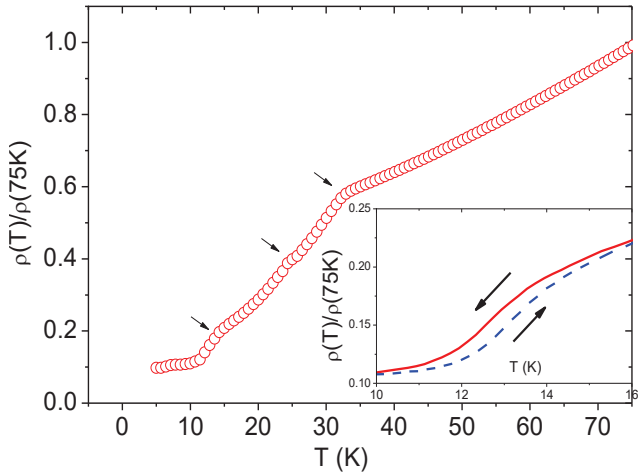

Figure 4.1: Plots for the compound $NdCo_2Si_2$; temperature dependence of resistivity in zero field. Inset shows the zero field resistivity versus temperature plot in heating and cooling cycle.

Magneto-transport properties were studied using conventional four probe longitudi-

nal geometry. For MR measurements, the sample was first cooled from room temperature down to a temperature set in the range 3-150 K under zero external field (ZFC) condition and then the data as a function of temperature were collected during the warming cycle, both in absence of magnetic field as well as in magnetic fields of 1, 3, 5, and 8 T. The values of MR were calculated using the conventional definition [MR (%) = $\Delta\rho/\rho_0$ (%)=((R(H) - R(0))/R(0)) $\times$ 100] in longitudinal configuration. The ρ vs. T data, as shown in Figure 4.1 and 4.2(a), are normalized to its value at 75 K. At high temperatures, $T > 60$ K, the zero field resistivity (Figure 4.1) exhibits simple metallic behavior. The changes in the slope of ρ vs. T data at $\sim$ 14, 24 and 32 K reflect the respective magnetic transitions that are indicated in χ_M vs. T data shown in Chapter 3. The high temperature resistivity data were fitted using the equation [116],

$$\rho(T) = B + CT - DT^3 \tag{4.1}$$

Figure 4.2(c) shows the fit of Equation 4.1 in the high temperature regime with the experimental data. A good fit of the resistivity data suggests that the resistivity at high temperatures is determined by the $s-d$ scattering [116]. The estimated values of B, C and D are $2.5 \times 10^6 \Omega$cm, $7.27 \times 10^{-7} \Omega$cm/ K and $1.09 \times 10^{-12} \Omega$cm/K^3, respectively. Furthermore, the zero field resistivity shows thermal hysteresis as shown in the inset of Figure 4.1, indicating first order nature of the transition at $T \sim 14$ K [117]. The application of a magnetic field modifies the resistivity behavior, as can be seen in Figure 4.2(a), and also results in the suppression of the transitions at $T_1 \sim 14$ K and $T_2 \sim 24$ K which were observed clearly in the zero field resistivity data. The only magnetic transition which can be observed at 8 T is that at $T \sim 32$ K. Though the zero-field and in-field (8 T) resistivity values around 32 K are quite close, the deviation between the two resistivity values increases with decrease of temperature, yielding a positive MR that reaches a value of $\sim 123\%$ at ~ 5 K.

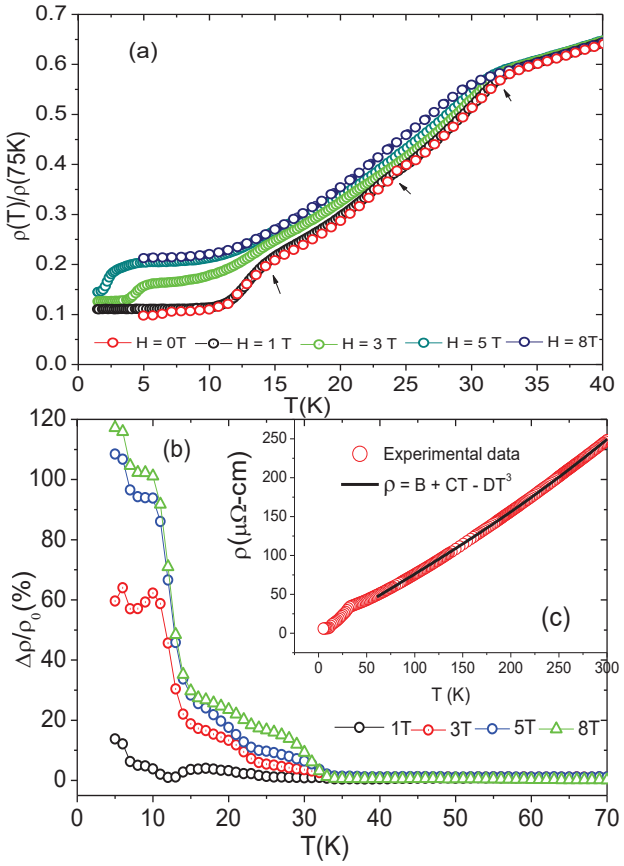

Figure 4.2: (a) Temperature dependence of electrical resistivity at different fields in $NdCo_2Si_2$; (b) Temperature dependence of magnetoresistance (MR) at different fields. The inset (c) shows fit to the high temperature resistivity data.

Figure 4.2(b) shows the variation of MR as a function of temperature (T) for various applied magnetic fields. With the reduction of T, MR starts to increase and shows prominent step-like jumps at $T \sim 32$, 24 and 14 K. A further jump has also been observed at $T \sim 10$ K. The increase of MR due to the application of magnetic field within the temperature range of $T \sim$ 24-32 K arises due to the onset of antiferromagnetic ordering. An antiferromagnetic compound can be considered to be composed of two sublattices with opposite magnetization directions. The application of a magnetic field decreases the spin fluctuation of the sublattice whose magnetization is aligned along the field while increases

the fluctuation for the antiparallel one. The competition between these two opposing effects results in a positive MR as has been observed here. The increase of MR with the increase of applied magnetic field is due to the increased spin fluctuation for the sublattice magnetization opposite to the applied magnetic field.

The incommensurate magnetic structure of this compound below T $\sim$ 24 K demands a more closer inspection of MR behavior in this range. However, the effect of spin fluctuation alone does not explain the resistivity features below $T \sim 24$ K. Previous reports on isostructural compound shows similar changes as has been observed in our case [118], although the change in slope in our work is comparatively less prominent. The resistivity data exhibits a change in slope about 24 K and indicates a change in the magnetic structure of the compound below 24 K into an incommensurate structure and furthermore there is possibility of opening up of superzone energy gaps on or near the Fermi surface. The zero field resistivity as shown in Figure 4.1 around 24 K might be related to the onset of the gap effect. Even though the reduction is not drastic, however, we cannot rule out the possibility of the existence of superzone energy gap in our sample. In accordance with the previous reports on isostructural compounds [118], thus the magneto-transport behavior in the temperature range of below 24 K is expected to arise due to a complex interplay of the incommensurate magnetic structure and superzone energy gap effect. With the application of magnetic field, the energy gap may vanish or move away from the Fermi surface resulting in an increase of the charge carriers and thus causing decrease of resistivity. However, there is an incommensurate-to-commensurate transition below $\sim$ 14 K, and the decrease in resistivity below this temperature is most probably due to the disappearance of superzone energy gap.

The isotherms (5, 10, 20, 30, and 50 K) of MR as a function of magnetic field are shown in Figure 4.3. The arrows in Figure 4.3 mark the magnetic fields at which there were steps in magnetization *vs*. magnetic field data obtained at 4.2 K by Ivanov et al. [119]. The

sharp jumps in magnetization were attributed to the transition between different magnetic phases. A butterfly-shaped MR loop has been noted while cycling the field in the field dependence of magnetoresistance at 5 and 10 K. This hysteresis loop

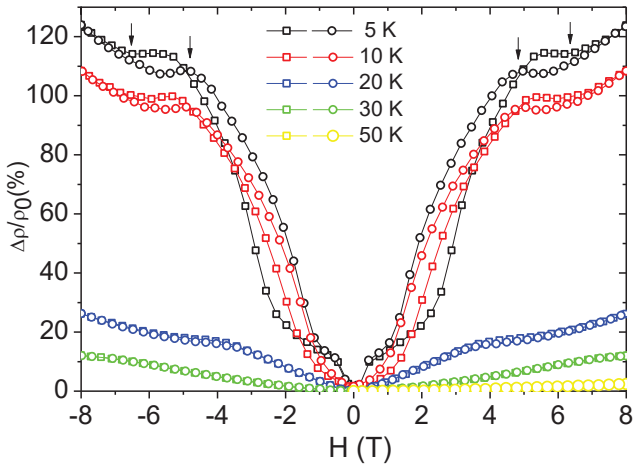

Figure 4.3: Field dependence of MR at different temperatures in $NdCo_2Si_2$. Open square symbols represent the warming cycle, whereas the open round symbols represent the cooling cycle data. The line is a guide to the eye.

vanishes at higher temperatures. At about $\sim$ 30 K, $\Delta\rho/\rho_0$ is positive and small compared to the low temperature values ($\sim$ 12%). For small magnetic field it follows H^2 dependence; which results from a competition between the two sublattices of an antiferromagnet under the application of magnetic field, as has been described earlier. The positive H^2 dependence is expected for a simple antiferromagnet in absence of gap effect [120, 121]. This signature indicates that at $\sim$ 30 K, the major contribution to magnetoresistance is due to the spin-dependent scattering, whereas the change in carrier number with application of magnetic field is negligible. We observed a high value of MR of about 108 % at the highest field at 10 K. Further reduction of temperature down to $\sim$ 5 K results in a gigantic increase of magnetoresistance to $\sim$ 123%. Usually large positive MR behavior is understood in terms of Lorentz contribution to resistivity. In pure

metals and single crystals, a large positive MR (a few hundred per cent) is observed if the condition $\omega_C\tau >> 1$ (where ω_C and τ are the cyclotron frequency and conduction electron relaxation time, respectively) is satisfied [122]. The above condition holds good for many pure elemental metals at low temperatures (where τ is large which implies that the resistivity is very small, of the order of $10^{-3}\mu\Omega$ cm) and in high magnetic fields. In case of polycrystalline Cu a large positive MR has been reported at low temperature of $\sim$ 4 K ($\sim$ 100% in a field of 5 T)[122]. However, it is to be noted that in the above case the observed resistivity is quite small $\sim$ 20 nanoΩ cm at 4 K. $NdCo_2Si_2$ presents a relatively high resistivity ($\sim \mu\Omega$ cm at 5 K), and the large MR appears to be too high to be explained only in terms of Lorentz force effect.

A large positive MR has also been reported in in the ferromagnetic state of isostructural multilayer compounds $SmMn_2Ge_2$ and $LaMn_2Ge_2$ [113, 114]. The scattering of the conduction electrons by the nonmagnetic layers and the presence of field induced pseudo-gaps in some portions of the Fermi surface were assumed to be the reasons behind the positive MR. A similar prediction can also be made for the present compound though it is antiferromagnetic. When the magnetic periodicity does not match with the lattice periodicity in antiferromagnets, an extra set of energy gaps appear at the magnetic superzone boundaries [123]. This results in new energy gaps in the conduction band other than the *k*-independent splitting observed for ferromagnetic case. Magnetic superzone gap can increase with lowering of temperature as can be seen in comparing between our 5 K and 10 K data (Figure 4.3). Alternatively, the application of field presumably induces more spin fluctuations below $\sim$ 10 K in contrast to the usual influence of magnetic field to suppress spin fluctuations in an otherwise more stable arrangement; as a result of which resistivity increases in the presence of magnetic field.

4.4 Effect of V substitution in the transport property of $NdCo_2Si_2$

Significant modifications in the magnetic properties of RET_2X_2 compounds have been obtained by the use of externally applied pressure or substitution at either *RE* or T sites [71, 73, 74, 98]. In this thesis for the first time we have dealt with substitution of Co by another transition metal V which is not known to form the $ThCr_2Si_2$ structure. As already discussed in the Chapter 3 of this thesis we have observed profound modifications in the magnetic properties as a result of V doping. The substitutions have resulted in the appearance of ferromagnetism at temperatures $\sim$ 30 K. Thus substitution of vanadium in the cobalt site resulted in changes in the magnetic state of the antiferromagnetic parent compound. Our motivation in this section is to study whether this change is reflected in the magnetoresistance of the doped compound $Nd(Co_{0.65}V_{0.35})_2Si_2$.

Temperature dependence of electrical resistivity normalized to the value at 75 K in the absence of a field is shown in Figure 4.4. In contrary to the parent compound, no thermal hysteresis is observed in the doped compound as can be observed from the inset of Figure 4.4. Slope change in the resistivity data is observed at $\sim$ 48 and $\sim$ 28 K reflecting the transitions seen in the $M-T$ data. There is a further change in slope below$\sim$ 9 K. In the paramagnetic region, the resistivity varies almost linearly with temperature, indicating that the electron-phonon interaction is dominant. Temperature dependence of resistivity has been studied in the presence of different magnetic fields of 1, 3, 5 and 8 T. The transitions get suppressed in the presence of field as can be observed from Figure 4.5(a). Resistivity behavior for temperatures below 9 K in the presence of field is rather interesting.

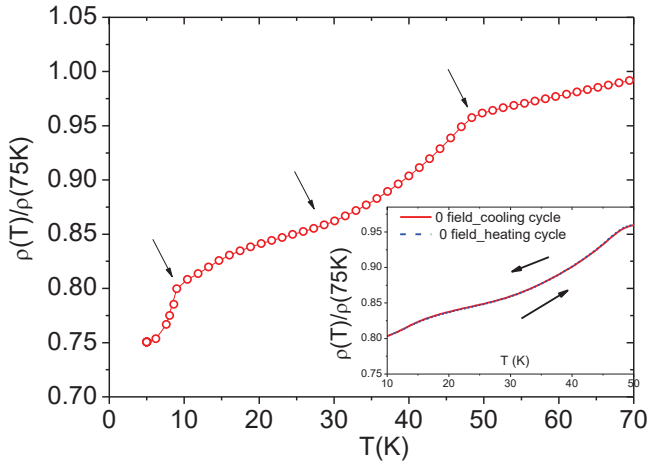

Figure 4.4: Plots for the compound $Nd(Co_{0.65}V_{0.35})_2Si_2$; temperature dependence of resistivity in zero field. Inset shows the zero field resistivity versus temperature plot in heating and cooling cycle.

The temperature dependence of magnetoresistance defined as [MR (%) = $\Delta\rho/\rho_0$ (%)=((R(H) - R(0))/R(0)) $\times$ 100], in fields of 1,3,5 and 8 T is plotted in Figure 4.5(b). MR is significantly negative below about 60 K and stays negative upto a temperature $\sim$ 9 K. The MR data corresponds to the magnetization behavior in the V doped sample where we observed a deviation from CW behavior below 60 K and magnetic susceptibility was observed to increase with decrease in temperature. Though the MR is negative throughout the temperature range investigated for H = 1 T, there is a sharp decrease in the magnitude at about 9 K. As the field is increased to 3 T, the MR exhibits a sign reversal at about 9 K. The negative sign of the MR changes to positive at this temperature and remains positive. The highest value of the positive MR is found to be $\sim$ 5% at 5 K in 8 T magnetic field. The MR data clearly reflect the $M-T$ data by exhibiting a minimum at 48 K corresponding to the ferrimagnetic transition in the sample as discussed in Chapter 3. The highest value of negative MR is found to be $\sim$ 3% at $\sim$ 48 K under 8 T magnetic field.

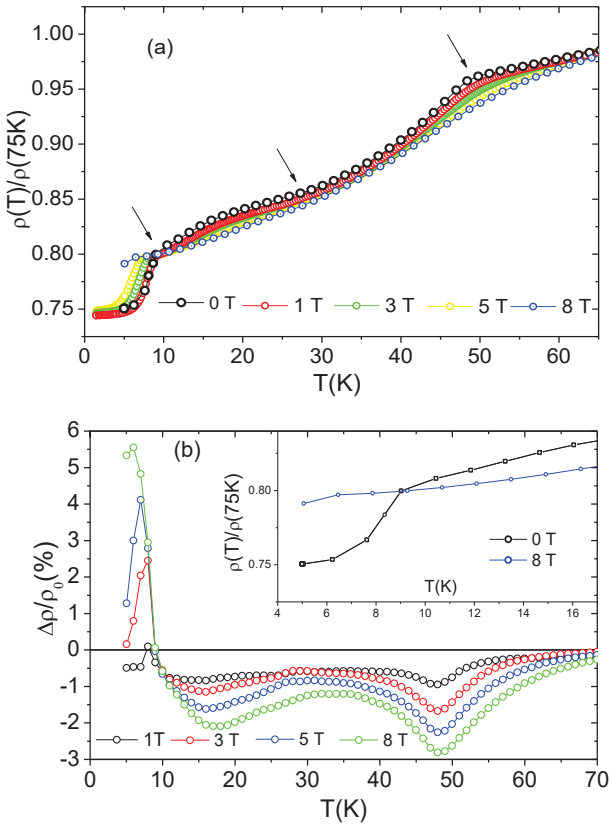

Figure 4.5: a) Temperature dependence of electrical resistivity at different fields in $Nd(Co_{0.65}V_{0.35})_2Si_2$; (b) Temperature dependence of magnetoresistance (MR) at different fields. Inset of (b) shows temperature dependence of resistivity in the low temperature range for zero field and 8 T magnetic field.

It is important to note that when the magnetic field is increased from 1 T to 3 T, it has opposite effects on the MR data at $\sim$ 48 K and below $\sim$ 9 K. The increase in MR (or a decrease in resistivity) at the ferrimagnetic ordering temperature as the field is increased from 1 T to 3 T suggests an increase in the ordering of the ferromagnetic sublattice with increase in field. This signature exists throughout the temperature range. The magnitude of negative MR near about 9 K has decreased very slightly as the field is increased from 1 T to 8 T which indicates the onset of some positive contribution to the MR at this temperature.

MR isotherms measured in the range of -8 T to +8 T at different temperatures are shown in Figure 4.6. One can see that at 5 K, the MR is positive in the entire range except for a narrow low field region, in agreement with the MR vs. T data where it can be seen that near 5 K the low field MR is nominally negative. Moreover, the positive MR continues to increase with field and reaches to about $\sim$ 5.5% at 5 K at 8 T. As the temperature is raised to 10 K, the nature of MR isotherms changes abruptly to exhibit a positive value of MR. The behavior is found to be identical for the positive and the negative field variations. One of the key findings is the drastic modification of the MR properties with V substitution of Co in $Nd(Co_{0.65}V_{0.35})_2Si_2$ as compared to the parent compound $NdCo_2Si_2$. The MR behavior corroborates magnetization behavior indicating that the two share a common origin. However, another important observation is that of the anomalous positive MR in the ferromagnetic state below 9 K in $Nd(Co_{0.65}V_{0.35})_2Si_2$.

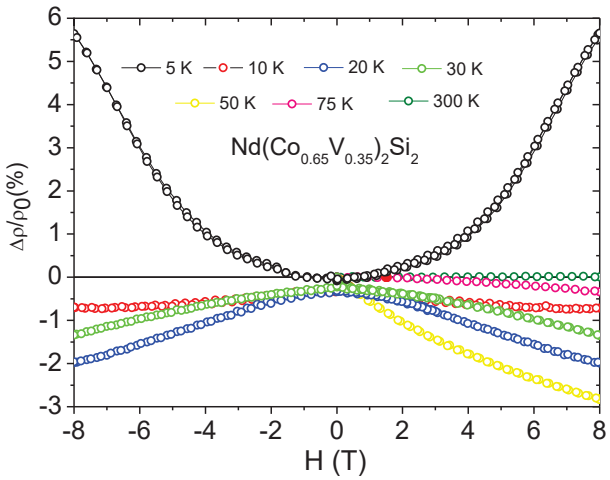

Figure 4.6: Field dependence of MR at different temperatures in $Nd(Co_{0.65}V_{0.35})_2Si_2$. Open square symbols represent the warming cycle, whereas the open round symbols represent the cooling cycle data. The line is a guide to the eye.

4.5 Comparative studies of magnetoresistance and magnetocaloric effect to understand the anomalous magnetoresistance in $NdRu_2Si_2$

The temperature dependence (T) of magnetization (M) of $NdRu_2Si_2$ at 10 Oe, in the field cooled (FC) condition is shown in Figure 4.7(a). In accordance with the previous reports, antiferromagnetic transition at $T_N \sim 24$ K and a low temperature transition at $T_C \sim 10$ K has been observed as shown in Figure 4.7(a).

In order to gain better insight into the magnetic and transport properties the critical field values have been estimated from $Mvs.H$ measurement (Figure 4.7(b)). The critical field (H_C) values required for the various magnetic phase transitions at different temperatures obtained from the magnetic field derivative of magnetization are shown in Figure 4.7(c). These critical field values will be compared with the same obtained from different other measurements in the later part of the manuscript. In this work, we follow the convention where the maxima in the derivative of the magnetization curve is considered as the critical field. The magnetic property at 10 K and 24 K of this sample shows similar results with previous reports and also indirectly indicates the phase purity of the sample under investigation.

4.5.1 Resistivity and magnetoresistance

Figure 4.8(a) shows the temperature dependence of resistivity both in the absence and presence of magnetic fields. The resistivity values have been normalized with respect to that at 150 K. The arrows in Figure 4.8(a) indicate the magnetic phase transition temperatures from paramagnetic to magnetically ordered state obtained from $M(T)$ curves

for the corresponding magnetic fields. With the application of a magnetic field from 1 T to 8 T, the transitions are gradually suppressed. Above the transition temperature, ρ varies almost linearly with temperature exhibiting metallic behavior and it indicates the dominance of electron-phonon interaction.

Figure 4.8(b) shows the temperature dependence of magnetoresistance under various magnetic fields. MR defined as MR (%) = $\Delta\rho/\rho_0(\%)$ = [(R (H)- R (H= 0))/ R(H = 0)] $\times$ 100 (%) is negative in the paramagnetic region down to $\sim$ 24 K for all measured fields. Around the antiferromagnetic ordering temperature, MR data shows a minimum. Application of magnetic field modifies the response of temperature dependence of MR. As is seen from Figure 4.8(a), the magnetic transition at 24 K is suppressed with the application of higher magnetic fields. The value of MR corresponding to the minima is found to be $\sim$ 5% at H = 1 T which increases to $\sim$ 34% at H = 8 T.

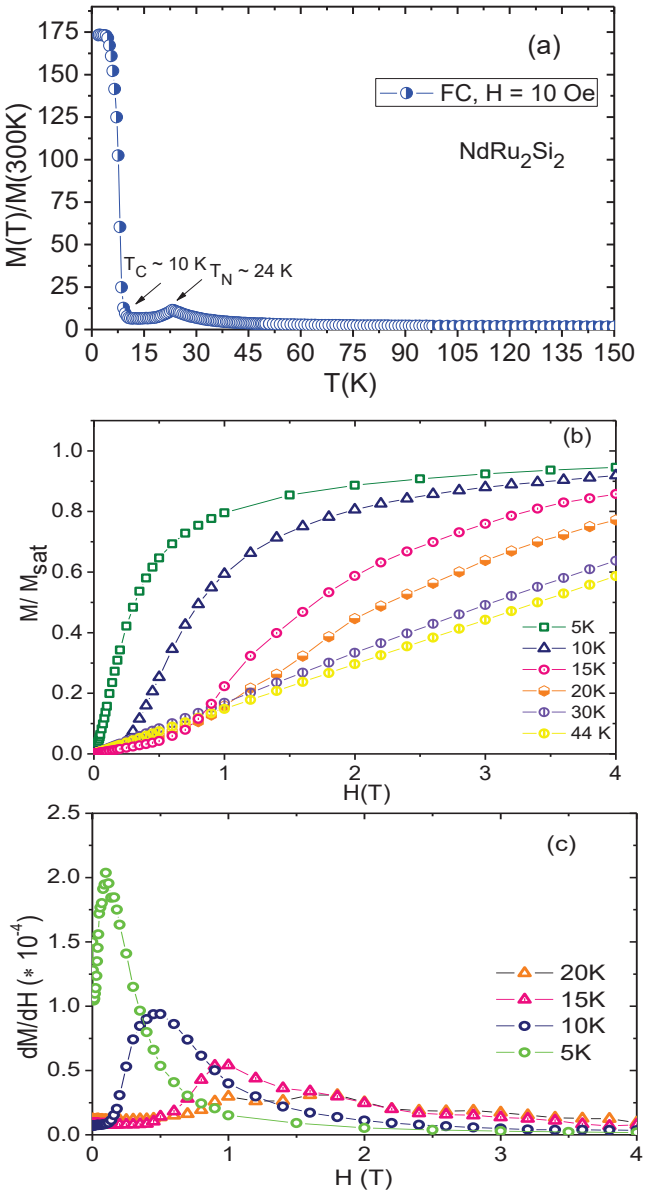

Figure 4.7: For the sample $NdRu_2Si_2$, (a) Temperature dependence of magnetization under a field of 10 Oe; (b) Field dependance of magnetization at different temperatures; (c) Derivative of field dependence of magnetization versus magnetic field.

Below $\sim$ 24 K, there is a change in slope and magnetoresistance becomes positive in the region around 23 to 18 K, for low magnetic field (H = 1 T), below which it again

becomes negative. In this temperature regime, the initial positive sign of $\Delta\rho/\rho_0$ (%) changes to negative values on application of higher fields (from 3 T to 8 T) and remains negative as shown in Figure 4.8(b).

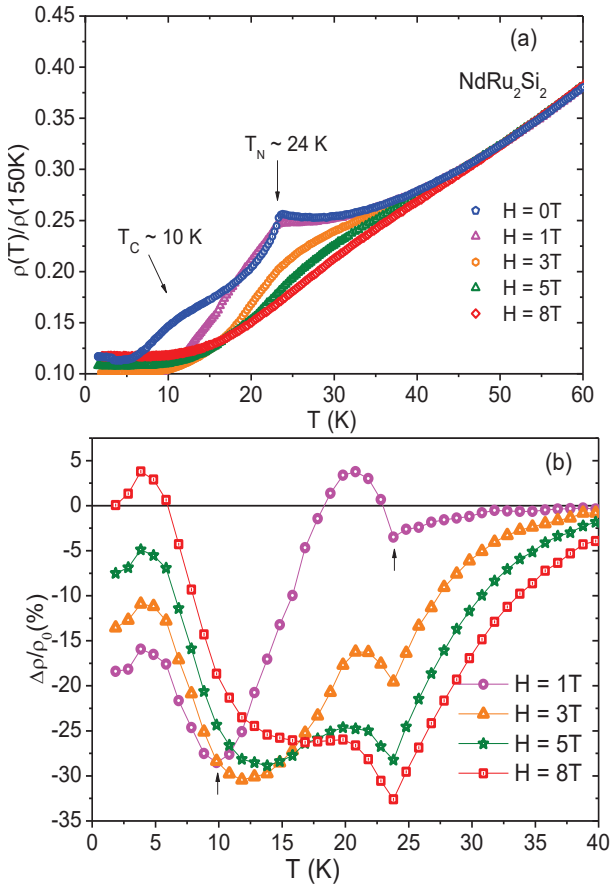

Figure 4.8: The curves (a) Temperature dependence of resistivity in zero field and under 1, 3, 5, 8 T magnetic fields ; (b) Temperature dependence of magnetoresistance (MR)(%)(symbols). The line joining the data points is a guide to the eye.

There is a tendency of further decrease in the magnitude of MR at about $\sim$ 10 K. The MR value corresponding to this minima is $\sim$ 29% at 10 K for a magnetic field of 1 T. Application of increasing magnetic fields of magnitude H = 3, 5 and 8 T causes a shift in the position of the minima. On further lowering of temperature, below $\sim$ 10K, there is a slope change but the value remains negative up to an applied field of 3 T. However, for the

highest observed field (8 T) at $\sim$ 6 K, there is a change of MR from negative to positive with the highest value of positive MR being around 5%. Thus, the magneto-transport properties of the system shows tuneable behavior with application of external applied magnetic field over a wide range of temperature. The sign reversal of MR in low fields as observed in Figure 4.8(b) from negative above T_N to positive just below T_N can be explained on the basis of onset of different magnetic phases. In this compound, in low fields a succession of paramagnetic, 'ferro-like' and sinusoidally modulated phases exist [68]. For low fields, the sample is supposed to go from the paramagnetic to the ferro-like phase at $\sim$ 24 K and then into the sinusoidal phase at $\sim$ 23 K. Neutron diffraction studies performed on $NdRu_2Si_2$ [64, 124] also supports this. As can be observed in our work, under a field of 1 T, the reversal in sign of $\Delta\rho/\rho_0$ (%) occurs at $T \sim T_N - 1$ K in agreement with the crossing of the ferrimagnetic-sinusoidal line in magnetic phase diagram [68]. So, the trend observed in $\Delta\rho/\rho_0$ (%) under 1 T is quite consistent with earlier study [68]. The sudden reversal in the sign of $\Delta\rho/\rho_0$ (%) below T_N may be attributed to the onset of new field-induced magnetic phase in $NdRu_2Si_2$.

The observation of sign reversal in the low temperature regime ($\sim$ 6 K) under the application of 8 T magnetic field is surprising. The compound undergoes a AFM - FM transition at $\sim$ 10 K [63], below which MR becomes positive. This observation again indicates the complex magnetic structures in these compounds.

To further clarify the response of MR vs temperature, field dependence of magneto-resistance (MR) has been studied at different temperatures between +8 T to -8 T as shown in Figure 4.9(a). The sample was zero field cooled from the paramagnetic state to the measurement temperature and the variation of MR vs magnetic field was investigated. Magnetoresistance isotherm at $\sim$ 30 K, i.e., at a temperature higher than T_N, varies quadratically with magnetic field. Magnetic field dependence of MR at T = 20 K shows an initial increase starting from zero field up to 0.8 T with a maximum value of 5%.

Subsequently, it decreases and becomes negative at a field value of 1.4 T. Further increasing of magnetic field results in a steep decrease of MR up to a field of 1.4 T where a maximum value of 24 % is obtained. Above 4 T magnetic field, MR is flattened and saturates to a value of 25 % at 8 T. A reduction in temperature manifests in different response of MR isotherms. At 10 K, MR is negative over the entire field range. MR value reaches a maximum of $\sim$ 30% at around 1 T, and then the value decreases and at the highest measured field reaches to about $\sim$ 17%. Interestingly, field dependence of MR at 5 K shows contrasting results enabling more insights into the positive MR in ferromagnetic phase as has been observed in Figure 4.9(a). A complete reversal of MR from negative to positive is observed at $\sim$ 6.5 T magnetic field with an increase in the value of 5 % at the maximum applied field.

Magnetoresistance in ternary rare earth intermetallic compounds exhibit complex behavior. Below T_N, we observe a rise in MR isotherm which can be explained in terms of the suppression of spin fluctuations. It was shown by Yamada et al. that the combination of decrease in spin fluctuation in the parallel sublattice and its increase in the antiparallel sublattice on application of magnetic field may result in a positive MR [82]. However, as the Zeeman energy due to the applied field overcomes the anisotropy energy, the magnetic structure displays a spin flop transition. The resistivity of an antiferromagnetic compound decreases and MR is small, until the AF configuration is forced to an FM alignment by the application of magnetic field and MR becomes negative. Therefore, when the field is applied to the system in its AF region, it moves in the ferromagnetic state through a metamagnetic transition at some critical field. Such a behavior is observed in our data at $\sim$ 20 K.

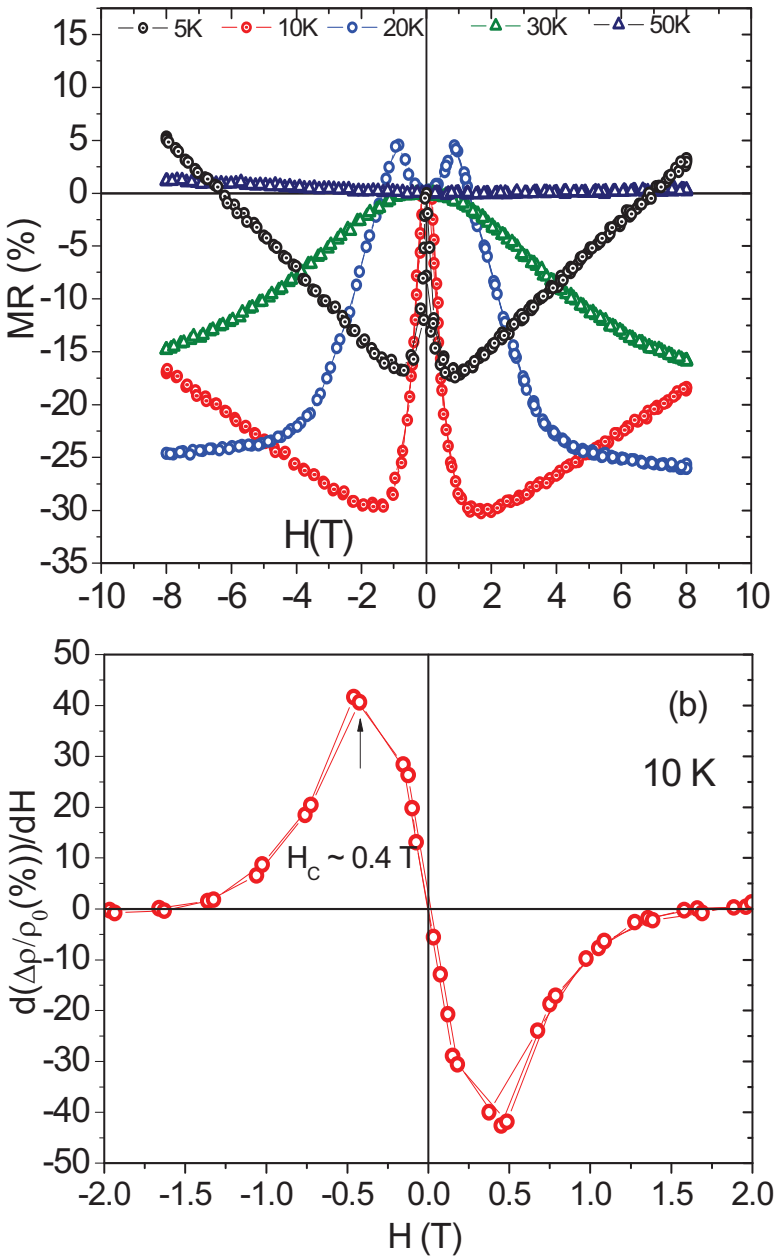

Figure 4.9: Plots of (a) field dependence of magnetoresistance at different temperatures; (b) derivative of field dependence of magnetoresistance at 10 K (open symbols). The line joining the data points is a guide to the eye.

The MR data is consistent with the field dependence of magnetization. One of the

interesting observation in this work is that the MR is positive below $\sim$ 6 K despite of the ferromagnetic ordering at these temperatures since it is normally expected that positive MR arises in antiferromagnetic compounds only [111, 112, 113, 125]. The positive MR can not be explained only in terms of the Lorentz force effect, as discussed earlier. Large low temperature MR is found in materials with large anisotropy due to the domain wall pining. In the present study the magnetic anisotropy does not appear to be the significant reason for this positive MR. The scattering of conduction electrons by the nonmagnetic layers and the presence of field induced pseudo gaps in some portion of the Fermi surface was assumed to be the possible reason for the positive MR in $LaMn_2Ge_2$ [114]. Due to the layered structure of the $NdRu_2Si_2$, a similar kind of explanation could be made for the present compound. In some geometrically confined ferromagnets, a positive isotropic MR which is linear in field was observed by Gerber et al. and was explained by the quantum electron-electron interference effect [126]. The positive GMR observed in the $RE_2Ni_3Si_5$ materials was explained on the basis of their layered structure similar to Dy/Sc superlattices [127]. GMR in Dy/ Sc superlattices has been speculated to arise from the multiple reflections of carriers from the interface before scattering thereby increasing the sensitivity of resistance to momentum loss upon reflection. All these previous results could serve as a possible explanation for the observed variation of MR below the transition temperature as the field is increased from 1 T to 8 T, as exhibited in Figure 4.8(b).

Comparison between the critical field (H_C) values required for magnetic phase transitions at the different temperatures from the magnetic field derivative of magnetization (Figure 4.7(c)) and magnetoresistance data are found to be quite consistent. A representative figure for the field derivative of magnetoresistance data at $\sim$10K is shown in Figure 4.9(b). The critical field value at 10 K from the magnetoresistance study is about 0.4 T which is in agreement with that obtained from magnetization derivative.

4.5.2 Magnetocaloric efect

In this section, we describe investigation of the magneto-thermal properties of $NdRu_2Si_2$ in the same temperature range as in MR studies. According to Banerjee criterion [128], the negative slope of the Arrott plot implies that the system possesses a first order magnetic transition (FOMT), whereas a positive slope corresponds to a second order magnetic phase transition. Therefore, the observed negative slope in log-log $H/Mvs.M^2$ plot (M here stands for the normalized magnetization with respect to the saturation magnetization M_{sat}) (shown in Figure 4.10) in low field below the transition temperature $T_N \sim 24$ K indicates FOMT.

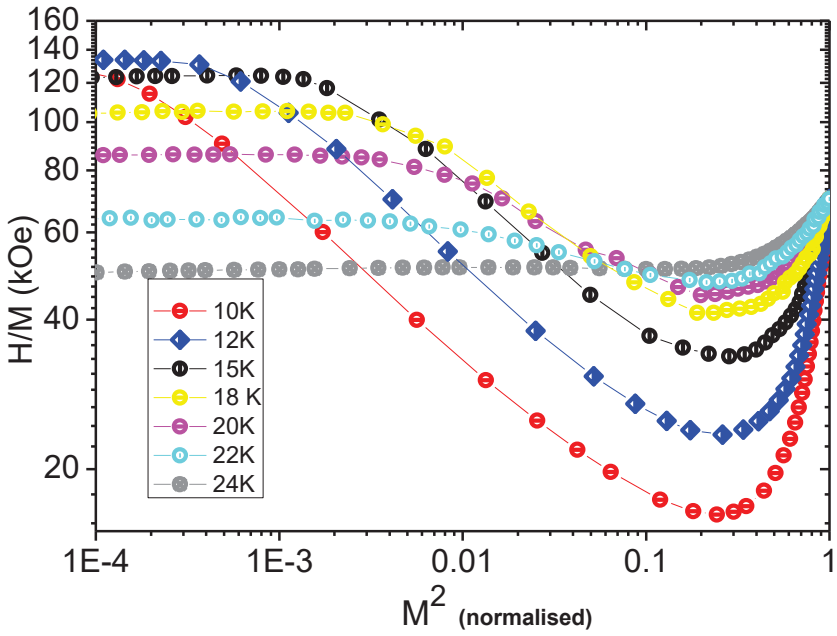

Figure 4.10: The curves represent log-log $H/MvsM^2$ plot of isotherms; Arrott plot.

Below T_N, the system undergoes a transition from AFM to FM state with application of magnetic field. Since it is known that magnetic structure is linked with magneto-transport

and magneto-thermal properties, thus investigation of magnetocaloric effect might reveal additional information about the complex magnetic phases.

Magnetocaloric responses of the compound has been calculated from the magnetic isotherm data employing Maxwell's thermodynamic relation

$$\left(\frac{\Delta S}{\Delta H}\right)_T = \left(\frac{\Delta M}{\Delta T}\right)_H \tag{4.2}$$

The temperature variation of -ΔS_M at different magnetic field up to 7 T, is shown in Figure 4.11.

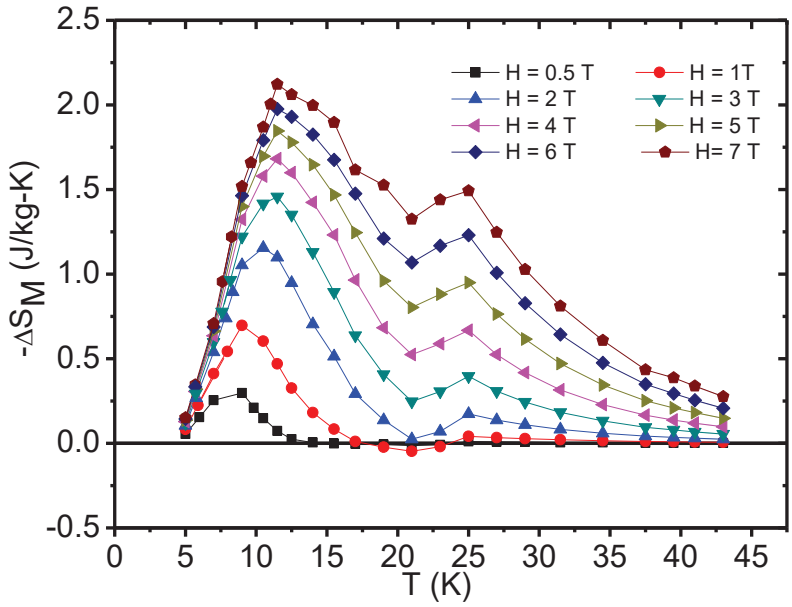

Figure 4.11: Temperature dependence of isothermal magnetic entropy change -ΔS_M in $NdRu_2Si_2$ determined by magnetization measurements. The line joining the data points is a guide to the eye.

The nature of the magnetocaloric entropy change can provide valuable information about the magnetic ground state of the material. In the present case, below T_N, -ΔS_M is negative for H = 0.5-1 T, apparently indicating the dominance of AFM ordering as

negative value of -ΔS_M is observed in the case of AFM ordering due to the disorder of the magnetic sublattice antiparallel to the applied magnetic field. On the contrary, the value of -ΔS_M is positive in the case of FM and paramagnetic state because of magnetically more ordered configuration with the application of external magnetic field. The temperature dependence of -ΔS_M for higher magnetic field change of H = 2 –7 T shows a positive caretlike shape, and -ΔS_M is positive in the entire temperature range under investigation. The cause behind the observed positive -ΔS_M for $H \geq 1$ T in the case of $NdRu_2Si_2$ is associated with the field-induced first order metamagnetic transition from AFM to FM state. At the other ordering temperature, *i.e.*, $\sim$ 10 K, -ΔS_M is positive as is expected for ferromagnetic transition. Thus, there are two well defined peaks observed in the MCE data corroborating the magnetization data. At low fields the peak corresponding to T_N is lower in intensity compared to the one at $\sim$ 10 K. With the increase of field from 1 T to 7 T the intensity of both the peaks increases. The maximum -ΔS_M is found to be $\sim$ 2.5 J/kg K near the ferromagnetic transition temperature. The MCE peak at T_N is quite broad, indicating that the ferromagnetic state (field induced) between T_N and 10 K is not strictly collinear. The anomaly observed in magnetoresistance behavior is not quite prominently reflected in the temperature dependence of magnetic entropy study at different temperatures in this compound. As a continuation of our efforts in probing the anomalous MR behavior in this compound we extended our study to calculate the adiabatic temperature (ΔT_{ad}) and draw a qualitative comparison with the temperature dependence of $\Delta\rho/\rho_0(\%)$, as shown in Figure 4.12(a)and (b). ΔT_{ad} has been calculated from the zero field specific heat data and using equation

$$\Delta T_{ad}(T,H) = -\left(\frac{T}{C_H(T,H)}\right)\Delta S_M(T,H) \tag{4.3}$$

The maximum value of ΔT_{ad} is found to be 4.7 K (in presence of 1 T field)as can be seen in Figure 4.12(b). Magnetoresistance in bulk intermetallic compounds can be

complicated due to the change in conduction electron relaxation time (electron-magnon scattering) as well as the change in conduction electron concentration. With the increase (decrease) of ΔT_{ad}, the magnitude of $\Delta\rho/\rho_0$ (%) is expected to decrease (increase). As a result, if the variation of $\Delta\rho/\rho_0$ (%) is dominated by the change in conduction electron relaxation time due to the change in magnetic moment configuration, then the dependence of - $\Delta\rho/\rho_0$ (%) will be similar to that of ΔT_{ad} [129].

On the other hand, if the variation of $\Delta\rho/\rho_0$ (%) is dominated by the change in carrier concentration, then inspite of the large variation in $\Delta\rho/\rho_0$ (%), the corresponding change in ΔT_{ad} is expected to be small. Thus it may be possible to distinguish between the two above mentioned major contributions to MR. The negative value of $\Delta\rho/\rho_0$ (%) is plotted in Figure 4.12(a) as this is expected to be similar to $\Delta\rho/\rho_0$ (%). For this compound, the temperature dependence of $\Delta\rho/\rho_0$ (%) in the temperature range from 10-40 K is qualitatively similar to ΔT_{ad}. It indicates that the change in resistivity is dominated by the change in relaxation time of the conduction electron in this temperature range. But below $\sim$ 6 K the behavior of the two curves are different. This can be due to the modification of energy gap on application of a magnetic field resulting in a change in the carrier number and resistivity.

4.6 Conclusions

To summarize, we have studied the transport and magnetotransport properties of three intermetallic rare earth silicides viz. $NdCo_2Si_2$, $Nd(Co_{0.65}V_{0.35})_2Si_2$ and $NdRu_2Si_2$. Magnetotransport studies corroborate the magnetization and resistivity studies. The observed magnetoresistance in the layered intermetallic $NdCo_2Si_2$ is significantly large and positive, and can be useful in modeling artificial multilayers in various applications. In addition, the present experimental results have thrown more light on the properties of $NdCo_2Si_2$ and could also trigger such studies in other rare earth intermetallics, particularly those with

layered structure. Effect of vanadium substitution in the Co site has resulted in profound modifications in the transport property of $Nd(Co_{0.65}V_{0.35})_2Si_2$. The magnetoresistance observed is negative up to a temperature of about 10 K below which it becomes positive. The change from such a large positive magnetoresistance observed in the parent compound to a negative value of magnetoresistance in the doped compound exhibits a change in the magnetic structure upon vanadium substitution. The transport property studies clearly reflect the evidence of appearance of ferromagnetism in antiferromagnetic parent compound $NdCo_2Si_2$ upon being doped with vanadium.

The temperature dependence of normalized resistivity in $NdRu_2Si_2$ exhibits two magnetic transitions at $\sim$ 24 K and $\sim$ 10 K. The magneto transport properties in this compound is observed to be tunable with application of external magnetic field. We have observed interesting anomalies in MR behavior in $NdRu_2Si_2$. For high magnetic field, MR is observed to be positive in the low temperature region below $\sim$ 6 K, although the compound is in the ferromagnetic regime.

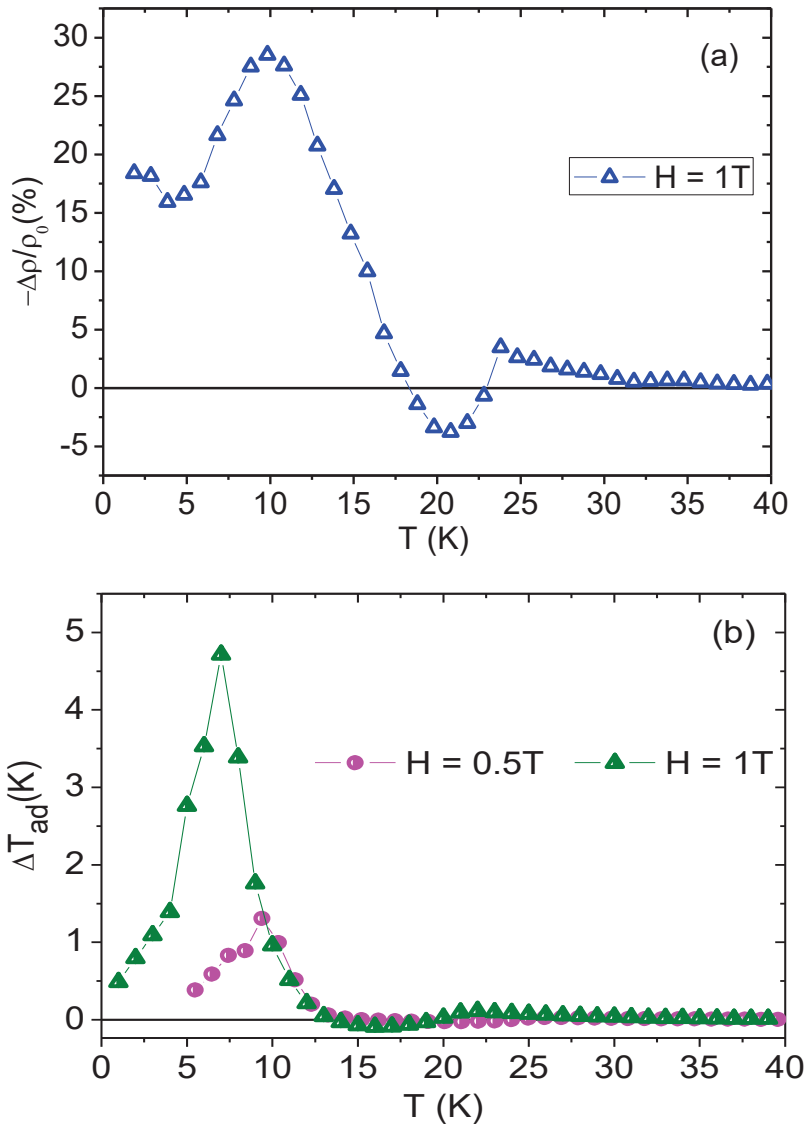

Figure 4.12: The curves represent (a) temperature dependence of the difference of zero field and infield resistivity normalized by zero field resistivity ($-\Delta\rho/\rho_0$ (%)); (b) temperature dependence of adiabatic temperature((ΔT_{ad})). The plots are for compound $NdRu_2Si_2$ in the presence of 0.5 T and 1 T.

Considering the magneto-transport and magnetocaloric study, one of the possible explanations for the anomalous behavior of positive magnetoresistance in the low temperature

(below ferromagnetic ordering) could be due to the presence of field induced pseudogaps in some portions of the Fermi surface. Both the spin-dependent scattering effects arising from the competing ferromagnetic and antiferromagnetic interactions and the typical layered structure of these compounds are found to play a crucial role in the magneto-transport property of this system. This class of Ru alloys is of importance considering they can serve as model systems for artificial multilayers. Detailed investigation of all these alloys, proves to be an interesting scenario in magneto-transport and magnetocaloric study and will serve as a novel route to pursue the field of magnetism in multilayers.

CHAPTER 5

Study of vanadium substitution at cobalt site in $CeCo_2Si_2$

5.1 Introduction

In the major part of this thesis, we have studied the changes in the magnetic properties upon substitution of non-magnetic cobalt in $RECo_2Si_2$ (RE = Pr, Nd). As discussed in Chapter 3, we have observed significant modifications in the magnetic properties of $PrCo_2Si_2$ and $NdCo_2Si_2$ upon substitution by vanadium at the Co site. Magnetization was observed to increase with increase in vanadium doping for all the doped compounds of $Pr(Co_{1-x}V_x)_2Si_2$ and $Nd(Co_{1-x}V_x)_2Si_2$ ($0 \leq x \leq 0.35$). However, some of the experimentally obtained parameters appear not to change systematically with the vanadium content. As said earlier in Chapter 3, effective moment(p_{eff})and magnetic entropy(S_{mag}) could be directly affected by the modification of crystal electric field (CEF) induced by V doping and lattice expansion, whereas, H_C and H_{EB} could be influenced by other factors, *e.g.*, magneto-crystalline anisotropy. Magnetic properties can get influenced under the

presence of crystalline electric field effect. So, it would be helpful to investigate the CEF efect in these compounds. However, the determination of CEF parameters is complex and outside the scope for these two series of compounds. An indirect idea of CEF modification could be made from the study of ^{59}Co nuclear magnetic resonance (NMR) spectrum which combines the effects of nuclear Zeeman and quadrupole interactions [106], the latter being due to the crystal electric field gradient (EFG) at the nucleus. Such study was not possible in either of Pr and Nd compounds due to excessive magnetic broadening of the NMR spectra. This motivated us to study have another isostructural rare earth series $Ce(Co_{1-x}V_x)_2Si_2$ ($0 \leq x \leq 0.50$). In the $CeCo_2Si_2$ compounds effect of vanadium substitution of cobalt has been investigated. Our investigations exhibited similar kind of changes in magnetization properties due to vanadium doping as observed in the other two previously mentioned series. Furthermore, it was possible for us to perform the nuclear magnetic resonance (NMR) study in the parent compound $CeCo_2Si_2$. Therefore, in isostructural compounds $Ce(Co_{1-x}V_x)_2Si_2$ (x = 0, 0.15 and 0.25), ^{59}Co NMR spectra have been obtained and they show evidence of significant modification of EFG and its asymmetry (η) with increase in x.

Cerium(Ce) based intermetallic compounds with the CeT_2X_2 formula crystallize in the $ThCr_2Si_2$ tetragonal structure and offers a variety of anomalous physical properties. Among the CeT_2X_2 family, the $CeCo_2Si_2$ compound belongs to a typical valence fluctuating system as observed from electrical, magnetic and optical measurements [40, 130, 131]. $CeCo_2Si_2$ shows weak paramagnetism characteristic of Ce ion valency fluctuation [132, 133]. In this chapter, we have investigated the changes in magnetic properties in $CeCo_2Si_2$ compound as a result of substitution of cobalt with another non-magnetic transition element vanadium.

5.2 Sample preparation and X-ray diffraction studies

Polycrystalline samples of $Ce(Co_{1-x}V_x)_2Si_2$ ($0 \leq x \leq 0.50$) were prepared by arc melting high-purity elements in purified argon atmosphere as discussed in Chapter 2. X-ray powder diffraction (XRD) studies at room temperature were performed with a Rigaku TTRAX-III x-ray diffractometer, and the lattice parameters were obtained by Rietveld refinement of the data using Fullprof program. Figure 5.1 shows x-ray diffraction patterns and Rietveld refinements of some of the prepared samples.

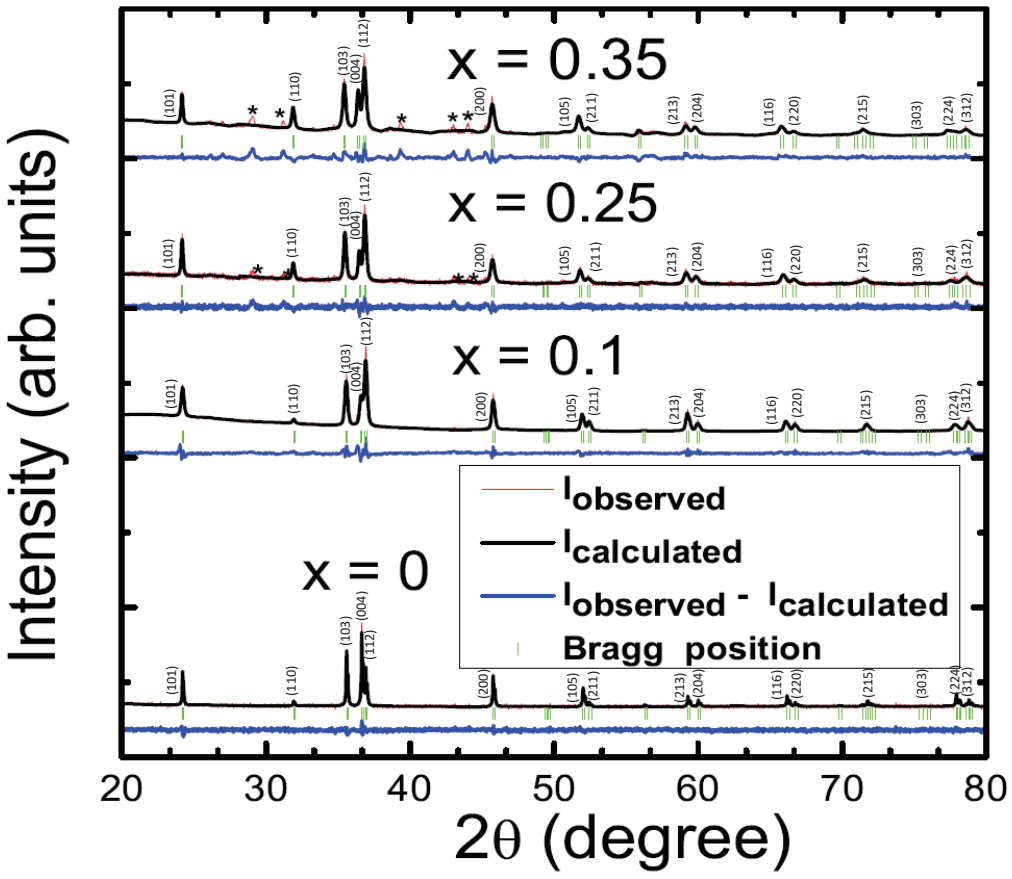

Figure 5.1: Powder x-ray diffraction patterns of $Ce(Co_{1-x}V_x)_2Si_2$ (x = 0, 0.10, 0.25 and 0.35) at 300 K with Rietveld fitting. $\star$ denotes unreacted rare-earth and Si, respectively.

The XRD studies showed the samples to be single phase for low doping of vanadium. However, for higher vanadium doping there were lines due to un-reacted elemental Ce and Si that constituted $\sim 3\%$ of XRD peak intensities. No extra lines due to elemental V were obtained, and apart from the intended *122* phase, no other known binary or ternary minority intermetallic phases involving these elements could be detected. Compared with the parent compounds, vanadium substituted samples show a broadening of x-ray diffraction lines with increasing vanadium content indicating substitution induced micro-strain in the lattice.

For the parent compounds, the lattice parameters agree quite well with the published data [134]. Vanadium has a molar volume larger than that of cobalt. In substituted compounds, with increase in V, the lattice parameter a shows small increase, but c increases markedly. The change in the lattice parameters as a function of V concentration is a strong indication of Co being replaced by V. Figure 5.2 shows lattice parameters and unit cell volumes of all $Ce(Co_{1-x}V_x)_2Si_2$ samples.

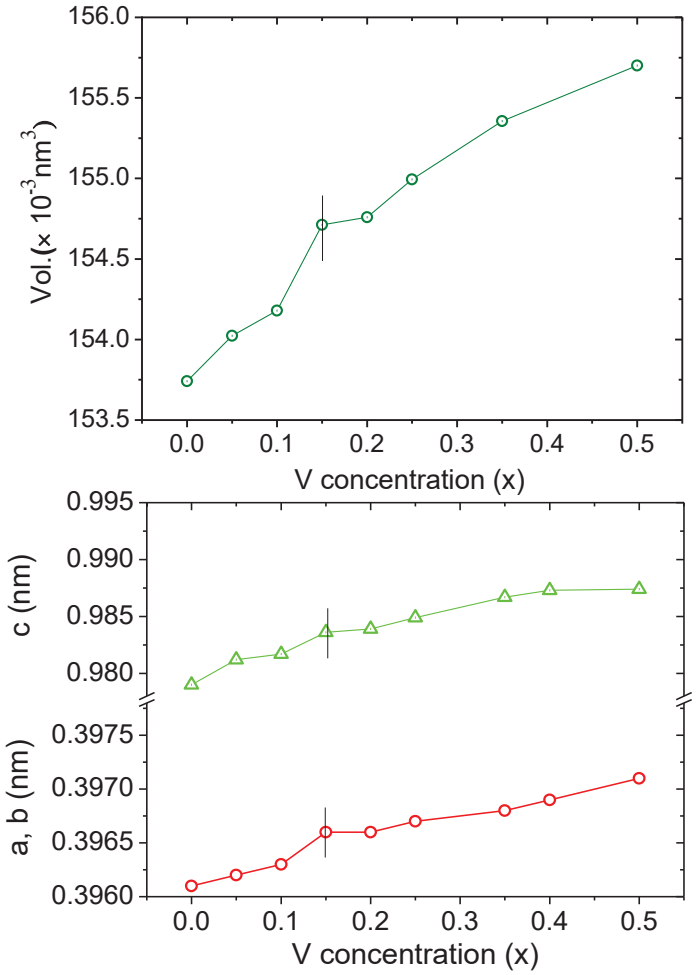

Figure 5.2: Lattice parameters (a, b and c) and unit cell volumes in $Ce(Co_{1-x}V_x)_2Si_2$ ($0 \leq x \leq 0.50$) obtained from Rietveld refinement of XRD data. The bars denote maximum limits of error in similar data in a panel.

5.3 Experimental Results and discussions

5.3.1 Magnetization measurements

Magnetic measurements in the temperature range 4-300 K were made with both PPMS and SQUID-VSM magnetometers of Quantum Design. The temperature dependence

of molar magnetic susceptibility (χ_M) of $Ce(Co_{1-x}V_x)_2Si_2$ ($0<x<0.5$) at 0.5 tesla and temperatures $4-100$ K is shown in Figure 5.3. $CeCo_2Si_2$ is weakly paramagnetic as reported, but in vanadium containing samples χ increases with decrease in temperature. The temperature dependence becomes more and more pronounced with increase in V content. Figure 5.3(a) shows inverse of (χ_M) against temperature and the fit of the data with the equation,

$$\chi_M = \chi_0 + \frac{C}{(T-\theta)} \tag{5.1}$$

where, C = $(NP_{eff}{}^2\mu_B{}^2)/3K_B$. N, μ_B, K_B and θ denote Avogadro's number, Bohr magneton, Boltzmann constant and paramagnetic Curie temperature, respectively. χ_0 corresponds to the temperature independent part of magnetism including the diamagnetic core correction χ_{dia}, the Pauli susceptibility of the electron gas χ_{Pauli}, and the Van Vleck temperature independent paramagnetism. The values of χ_0 as obtained from the fitting, are in the vicinity of 1.1×10^{-3} indicating a large contribution from Van Vleck paramagnetism. Figure 5.3(b) shows p_{eff}, the effective number of Bohr magneton per formula unit, increases almost linearly with increase in vanadium content and reaches a value of 1.67 when vanadium concentration (x) = 0.5, i.e., 50% of cobalt is replaced by vanadium. The result could be explained as follows. Cerium in $CeCo_2Si_2$ is supposed to be in a fluctuating valence state with strong overlap of$4f$ levels and the conduction band. The lattice expansion caused by vanadium substitution results in a negative pressure leading to localization of cerium $4f$ electrons. As vanadium concentration increases, more and more cerium atoms attain the stable Ce^{3+} state resulting in the increase of p_{eff}. But, the x-ray data shows that the lattice expansion in

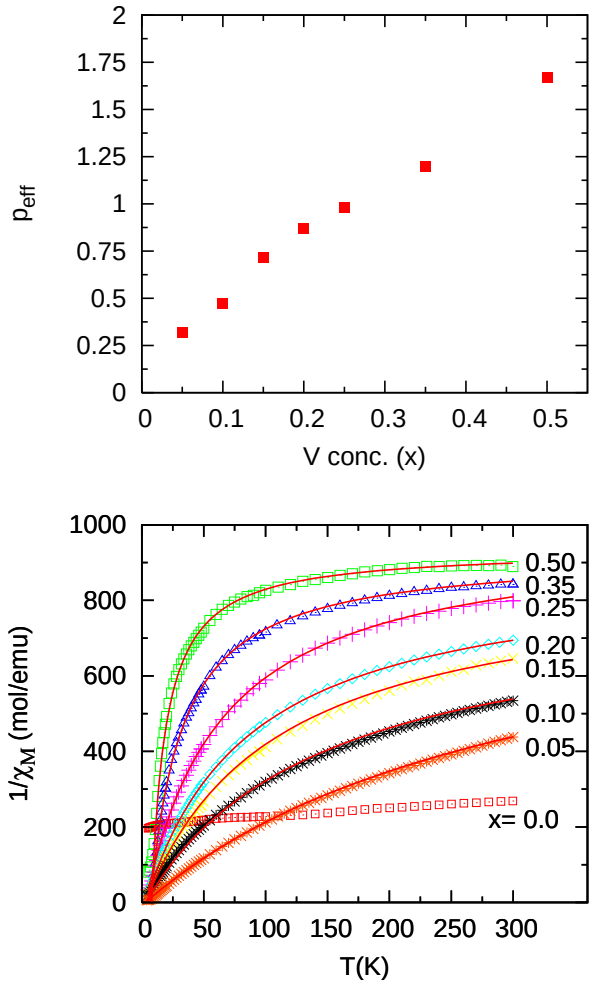

Figure 5.3: Plots of magnetic measurements (a) Temperature(T) dependence of $1/\chi_M$ (at 0.5 tesla) in $Ce(Co_{1-x}V_x)_2Si_2$ ($0 \leq x \leq 0.5$), (b) Plot showing change in p_{eff} value with change in vanadium concentration(x)

$Ce(Co_{1-x}V_x)_2Si_2$ may not have been as large as it should be if there was a conversion from Ce^{4+} to Ce^{3+}. In a series of isostructural rare-earth intermetallics, compounds having trivalent Ce ions have lattice parameters larger than those having trivalent Pr ions. The P_{eff} value of 1.67 would mean that about 65% of cerium ions in $Ce(Co_{0.5}V_{0.5})_2Si_2$ are in Ce^{3+} state. However, in our work, as observed from the XRD data, its lattice parameters and unit cell volume are still much smaller than those of $PrCo_2Si_2$ as can be observed from Section

3.2. Indeed, there is a strong probability that upon vanadium substitution, the magnetic moment may be arising not from cerium ions, but from 3*d* electrons.

5.3.2 Nuclear magnetic resonance study

Figure 5.4 shows the ^{59}Co NMR spectra at 100 K of randomly oriented polycrystalline samples of $Ce(Co_{1-x}V_x)_2Si_2$ (x = 0, 0.15, 0.25). For ^{59}Co, the nuclear spin (I) is 7/2, and the nuclear quadrupolar interaction is expected to yield a central transition and three satellite transitions on each side of the central transition, as seen for the parent compound $CeCo_2Si_2$. Moreover, the central transition shows a clear splitting indicating that the perturbation due to the nuclear quadrupolar interaction is of second order. The magnetic susceptibility of $Ce(Co_{1-x}V_x)_2Si_2$ increases with increase in V content and the intensity of local field fluctuation at ^{59}Co also increases. As a result, the spectra are increasingly broadened and shifted to higher frequency, as seen clearly in the central transitions (inset of Figure 5.4). Furthermore, the broadening also results in the disappearance of the quadrupolar satellites in the spectra of $Ce(Co_{0.85}V_{0.15})_2Si_2$ and $Ce(Co_{0.75}V_{0.25})_2Si_2$.

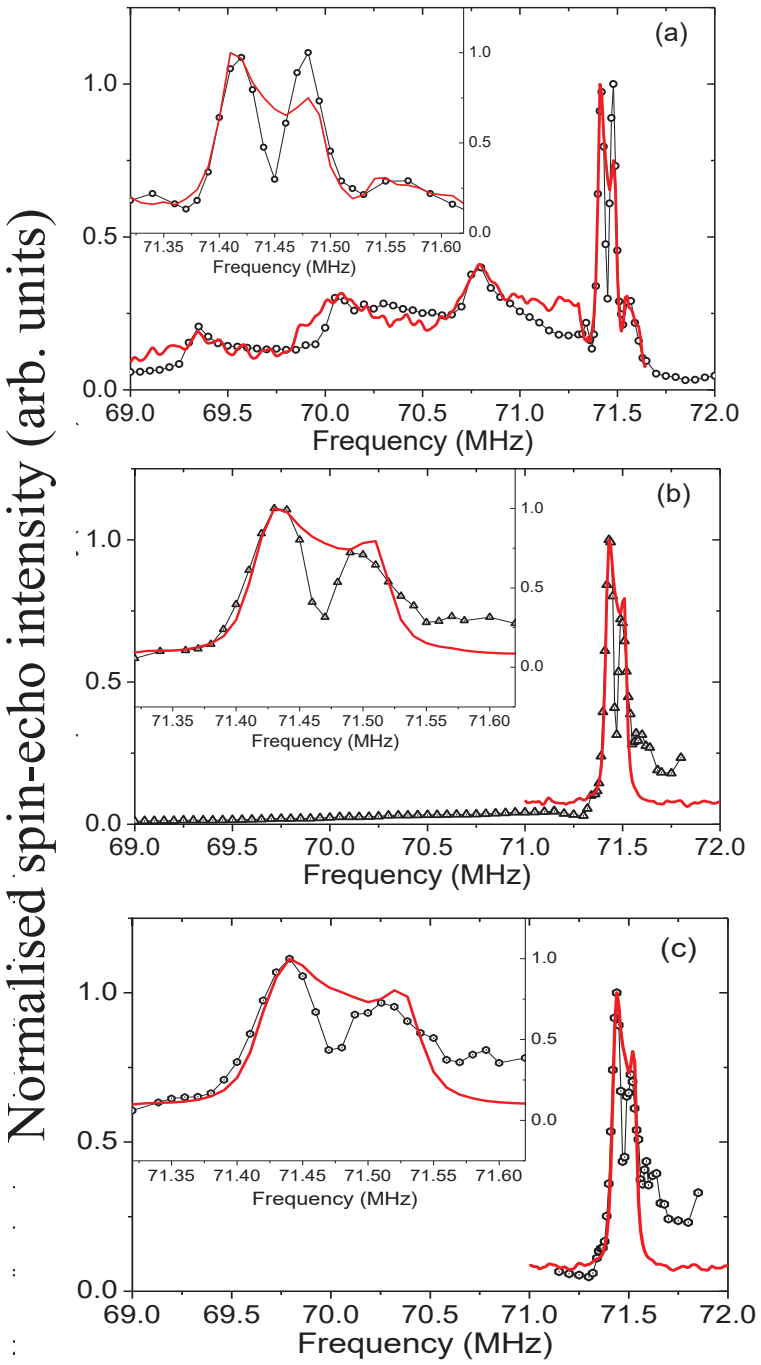

Figure 5.4: Typical ^{59}Co NMR spectra at 100 K and 7 T in random polycrystalline powder of (a) $CeCo_2Si_2$ (b) $Ce(Co_{0.85}V_{0.15})_2Si_2$ and (c) $Ce(Co_{0.75}V_{0.25})_2Si_2$. Inset shows the splitted central transitions for the respective compounds. Open black symbols indicate the experimental data. The red continuous line indicates the theoretically fitted spectrum.

Table 5.1: Various fitting parameters obtained by fitting NMR spectra with equation 1.28 in $Ce(Co_{1-x}V_x)_2Si_2$ (x = 0, 0.15 and 0.25)

Sample	K_{iso}	ν_Q	η
$CeCo_2Si_2$	0.89%	1.5 MHz	0
$Ce(Co_{0.85}V_{0.15})_2Si_2$	0.92%	1.6 MHz	0.17
$Ce(Co_{0.75}V_{0.25})_2Si_2$	0.94%	1.7 MHz	0.19

The spectrum of $CeCo_2Si_2$ and the central transitions of $Ce(Co_{0.85}V_{0.15})_2Si_2$ and $Ce(Co_{0.75}V_{0.25})_2Si_2$ are simulated considering the presence of Knight shift and second order nuclear quadrupolar interaction (equation 1.28), as shown in Figure 5.4. As, we have observed both central transition and satellites in the spectrum of the parent compound, so, for better accuracy we tried to fit both the transitions. Whereas, in case of the doped compounds only central transition could be observed as the satellites are suppressed due to broadening of the spectra, so we have matched the central transition only. The various fitting parameters are as given in Table 5.1

As discussed in the context of magnetic measurements on $Pr(Co_{1-x}V_x)_2Si_2$ and $Nd(Co_{1-x}V_x)_2Si_2$ (Section 3.4), ^{59}Co NMR experiment could not be performed on these compounds because of excessive magnetic broadening of their spectra. However, in case of isostructural $Ce(Co_{1-x}V_x)_2Si_2$, the above results show that V substitution systematically modifies the Knight shift and the EFG parameters, *viz.*, ν_Q and η. The NMR results therefore indicate that in $RECo_2Si_2$ compounds, partial substitution of Co by V modifies the crystalline electric field (CEF), which, in turn, could affect the magnetic properties of these compounds.

5.4 Conclusions

The parent compound $CeCo_2Si_2$ shows weak paramagnetism. The magnetic susceptibility of $Ce(Co_{1-x}V_x)_2Si_2$ increases with increase in V content. The NMR spectra of the doped compounds are increasingly broadened and shifted to higher frequency. The broadening of the spectra also results in the disappearance of the quadrupolar satellites in the spectra of $Ce(Co_{0.85}V_{0.15})_2Si_2$ and $Ce(Co_{0.75}V_{0.25})_2Si_2$. The NMR results therefore indicate that in $RECo_2Si_2$ compounds, partial substitution of Co by V modifies the crystalline electric field which could also affect the magnetic properties of these compounds. Furthermore, the NMR study in this series of compounds also strengthens our claim of single phase nature of the doped compounds. The observed NMR signal is a signature of the intrinsic properties of the samples. Therefore, the present study in this chapter confirms the purity of the doped compounds and indicates the magnetic properties observed in the doped samples are purely intrinsic and not due to formation of any unidentified binary phases of the constituent elements.

CHAPTER 6

Summary and scope of future work

6.1 Summary

A detailed and systematic study to understand the effect of partial substitution of cobalt by vanadium in the magnetic and magnetocaloric properties of antiferromagnetic intermetallic compounds $RECo_2Si_2$ (RE = Pr, Nd) has been carried out. Also the transport properties of the parent and the vanadium substituted compounds have been studied. Furthermore, investigations of transport and magneto-transport properties of isostructural compound $NdRu_2Si_2$ have been carried out. The major findings of this thesis work along with possible scope of future study in this field has been discussed in this chapter.

In these compounds the atoms are arranged in layers perpendicular to c-axis in the sequence RE-Si-Co-Si-RE. The parent compounds are antiferromagnetic with the magnetic moments only on rare-earth ions. In $PrCo_2Si_2$ the magnetic moments are in a square-wave structure with propagation vectors (0,0,l), (0,0,0.074) and (0,0,0.223) appearing in the sequence of $T \leq 9$ K (T_1), 9 K $\leq T \leq 17$ K (T_2) and 17 K $\leq T \leq 30$ K (T_N), respectively. A similar kind of magnetic structure was observed in $NdCo_2Si_2$. As a consequence,

though there is antiferromagnetic interaction along the *c*- axis, the moments are aligned ferromagnetically along the *ab* plane. We have studied the effect of substitution in the non-magnetic Co site with another non-magnetic transition metal vanadium which is not known among elements to form a pure $ThCr_2Si_2$ type structure, and for the first time used for substitution. Vanadium has a molar volume slightly larger than that of cobalt and the substitution results in an increase of the lattice parameter. Several concentrations of V doping have been studied, *viz.*, $RE(Co_{1-x}V_x)_2Si_2$ (*RE* = Pr, Nd), viz., x = 0, 0.05, 0.1, 0.15, 0.2, 0.25, 0.3 and 0.35. The change in the lattice parameters with V doping concentration indicates replacement of Co by V.

The parent compounds are antiferromagnetic below about 30 K due to the ordering of localized magnetic moments that are present only on rare-earth ions, cobalt being non-magnetic in the parent compounds. The present study demonstrates that in these compounds where $3d$ and $4f$ ions occupy different layers in the crystal structure, V substitution and subsequent lattice expansion results in the occurrence of inequivalent magnetic ions and complex interactions that lead to multiple magnetic transitions. At temperatures around 40-50 K, the temperature dependence of magnetization indicates a ferrimagnetic transition which is accompanied by a rapid decrease in the temperature dependence of resistivity. Below temperatures $\sim$ 30 K, the samples begin to show ferromagnetic-like behavior with the appearance of a coercive field and saturation in the magnetization at magnetic fields above $\sim$ 2 T. The heat capacity studies corroborate the magnetization studies. These two magnetic transitions are indicated also by prominent λ-like peaks in specific heat measurements. At around 10 K, a sharp drop in the resistivity indicate another magnetic transition which is followed by a rapid increase in coercive field with decrease in temperature. In both the Pr and Nd doped compounds change in magnetoresistance in observed at around 10 K. In a magnetic field of 9 T, the latter transition shifts to a lower temperature and that leads to a positive magnetoresistance. The onset of ferromagnetism at $\sim$ 30 K is accompanied with an exchange bias field which is observed for the first time

in layered intermetallic compounds. The exchange bias field increases rapidly below the transition at $\sim$ 10 K and reaches $\sim$ 16% of coercive field at 2 K. In the vanadium doped Pr samples exchange bias field measured at the lowest temperature 2 K ranges from about 64 mT - 155 mT, whereas for the vanadium doped Nd samples at 2 K the values of exchange bias field ranges from 115 mT- 152 mT.

In the present study we have observed a large enhancement of magnetocaloric entropy change in vanadium substituted $NdCo_2Si_2$. Our experimental results reveal that the antiferromagnetic transition is gradually suppressed due to the vanadium doping in Co-site and results in a drastic modification of the ground state of the doped compound. In addition to that, predominant ferromagnetism appears for the $Nd(Co_{0.65}V_{0.35})_2Si_2$ compound. The modification of the ground state due to the vanadium substitution in the parent $NdCo_2Si_2$ compound is directly reflected in the magnetocaloric properties. Interestingly, we have observed conventional large magnetocaloric effect for the doped compound instead of the inverse magnetocaloric responses of the parent compound. Our study indicates a route for the enhancement of magnetocaloric effect in such intermetallic compounds.

Transport property measurements corroborates magnetic measurements. At high temperatures, $T > 60$ K, the zero field resistivity exhibits simple metallic behavior. The changes in the slope of ρ vs. T data at $\sim$ 14, 24 and 32 K reflect the respective magnetic transitions that are indicated in χ_M vs. T data shown in Chapter 3. Moreover, thermal hysteresis is observed in the temperature range at around 14 K indicating first order nature of the transition. Magnetoresistance measurements on $NdCo_2Si_2$ reveal large positive MR values of about $\sim$ 123% at $\sim$ 5 K in the presence of 8 T field. Positive magnetoresistance of such large magnitude has not been reported earlier in magnetically ordered polycrystalline compound of the $RECo_2Si_2$ series. It may be associated with the magnetic ordering of the lattice as its value is reduced in the paramagnetic temperature regime. It is worth mentioning that the signature of the field induced pseudo energy gaps on the fermi surface

was obtained. In such layer structure compound the appearance of the energy gap is taken into consideration to explain such an unconventional magnetoresistive behavior at low temperature.

Effect of vanadium substitution in the Co site has resulted in profound modifications in the transport property of $Nd(Co_{0.65}V_{0.35})_2Si_2$. The magnetoresistance observed is negative up to a temperature of about 10 K. Below which it becomes positive. Therefore, this change from such a large positive magnetoresistance observed in the parent compound to a negative value of magnetoresistance in the doped compound exhibits a change in the magnetic structure upon vanadium substitution. In the case of antiferromagnet, with the application of magnetic field along the sublattice magnetization, there exists a competition between the spin fluctuations for the parallel and antiparallel sublattice, which results in a positive magnetoresitance as has been observed for the antiferomagnetic parent compound. However, in $Nd(Co_{0.65}V_{0.35})_2Si_2$ application of magnetic field results in suppression of spin fluctuations and results in negative magnetoresistance as is expected for a ferromagnet. Thus the transport property studies clearly reflect the evidence of appearance of ferromagnetism in antiferromagnetic parent compound $NdCo_2Si_2$ upon being doped with vanadium.

Magnetic, electronic transport and magneto-caloric properties of $NdRu_2Si_2$ have been investigated in detail. Previous investigations on this compound focussed on the investigation of the magnetic and the transport properties near the antiferromagnetic transition. In this work, we report on the low temperature complex magnetic phases of $NdRu_2Si_2$ by comparison of the magnetic, electronic transport and magneto-caloric properties. We have shown that an applied magnetic field greatly modifies the magneto-resistance (MR) properties of the compound at low T ($T \leq 10$ K) from the usual negative MR to an unusual positive MR. A negative slope of Arrott plot indicates first order nature of the transition. In addition, an interesting anomaly between the MR and the

magneto-caloric properties in this compound at $T \leq 10$ K with the application of high magnetic field of $H > 5$ T is also observed. Magneto-caloric investigations at this field and temperature range indicates that the compound is predominantly ferromagnetic while MR results indicates the presence of additional interactions which leads to positive MR in the ferromagnetic phase. Negative MR near T_N shows a modest value of 33% under an applied field of 8 T while lowering of T results in a reversal of MR up to 5%. The results have been explained by considering the appearance of field induced pseudo gaps in the Fermi surface of the compound $NdRu_2Si_2$. Our study indicates that detailed investigations of magnetic, electronic and magneto-caloric properties are important for ternary intermetallic compounds to unravel the complex magnetic and transport properties of these compounds.

In the last part of this work, we have investigated the magnetic properties and ^{59}Co NMR spectra of $Ce(Co_{1-x}V_x)_2Si_2$ ($0 \leq x \leq 0.50$). Vanadium substitution at the Co site in the parent compound $CeCo_2Si_2$ resulted in changes in the magnetic properties. The effective number of Bohr magneton per formula unit, increases almost linearly with increase in vanadium content. Vanadium substitution also modified the NMR spectra of the doped samples. The central transition shows a clear splitting and further indicates that the perturbation due to the nuclear quadrupolar interaction is of second order. The satellite transitions are suppressed for the doped $Ce(Co_{1-x}V_x)_2Si_2$ ($x = 0.15$ and 0.25) compounds. The NMR study shows significant modifications in EFG under vanadium doping.

6.2 Future prospects

In this thesis, we have studied the magnetic, magneto-transport and magnetocaloric properties of some representative compounds. In Chapter 3, we observed that the magnetic properties as well as specific heat and magnetocaloric properties is drastically modified upon substitution of Co by V in $RECo_2Si_2$ compounds. There is also a further scope of

study by substituting Co with other transition metals and observe whether and how the properties get modified. Furthermore, we have carried out the studies in $PrCo_2Si_2$ and $NdCo_2Si_2$ compounds. An extension of this work for other rare earths can throw new light on the modifications in the magnetic structures as a result of substitution in other isostructural compounds.

In Chapter 4, we have highlighted the transport properties of antiferromagnetic compound $NdCo_2Si_2$. It exhibits a giant positive magnetoresistance at low temperature and high field. We have also observed a change in the transport properties upon substitution. This study can be extended for $RECo_2Si_2$ compounds with other rare earths. We have also studied an anomalous magnetoresistance behavior in $NdRu_2Si_2$ at low temperature under high magnetic field. Explanations for this observed behavior has been put forward in this work. It would be quite interesting to investigate the magneto-transport properties of some other isostructural compounds as well as in the vanadium doped compounds of the praseodymium series as these naturally occurring multilayers can serve as models for artificial multilayer systems. Study of magneto-transport properties in this class of compounds can provide us with valuable information.

Chapter 5 throws some insight into the modifications of the magnetic properties in weakly paramagnetic compound $CeCo_2Si_2$ upon being doped with vanadium. The results suggest changes in crystalline electric field in these compounds. Except the magnetic and magneto-transport property studies there is also scope to study NMR, neutron scattering measurements in some of these compounds.

Bibliography

[1] G. E. R. Schulze *Metallphysik*, vol. Berlin: Akademie-Verlag, pp. 1–76, 1967. 12

[2] K. Girgis *Physical Metallurgy:Cahn, R. W., Haasen, P. (Eds.). Amsterdam: North-Holland*, pp. 219–269, 1983. 12

[3] G. Sauthoff, *Intermetallics*. VCH Verlagsgesellschaft, Weinheim (Federal Republic of Germany) VCH Publishers, New York, NY (USA), 1995. 12

[4] de Gennes *J. Phys. Radium.*, vol. 23, p. 510, 1962. 14

[5] Q. Zhang and P. Levy *Phys. Rev. B.*, vol. 34, p. 1884, 1986. 15

[6] D. Noakes and G. Shenoy *Phys. Lett. A.*, vol. 91, p. 35, 1982. 15, 16

[7] E. Sampathkumaran, I. Das, R. Vijayaragjavan, H. Yamamoto, and M. Ishikawa *Solid State Commun.*, vol. 83, p. 609, 1992. 16

[8] N. Russman, H. Hafner, and D. Wohlleben, *Crystalline Electric Field Efects in f-Electron Magnetism*. New York - London: Plenum Press, 1982. 16

[9] P. Morin and D. Schmitt, *Handbook of Ferromagnetic Materials*, vol. 5. Amsterdam: North Holland, 1990. 16, 17

[10] H. Yamauchi, H. Onodera, K. Ohoyama, T. Onimaru, M. Kosaka, M. Ohashi, and Y. Yamaguchi *J. Phys. Soc. Jpn.*, vol. 68, p. 2057, 1999. 17

[11] P. Morin and J. Rouchy *Phys. Rev. B*, vol. 48, p. 256, 1993. 17

[12] H. Yamauchi, H. Onodera, K. Ohoyama, T. Onimaru, M. Kosaka, M. Ohashi, and Y. Yamaguchi *J. Phys. Soc. Jpn.*, vol. 68, p. 2526, 1999. 17

[13] W. Koehler, *Magnetic Properties of Rare Earth Metals*. New York: Plenum Press, 1972. 17

[14] T. Kasuya *T. Prog. Theor. Phys.,(Kyoto)*, vol. 16, p. 45, 1956. 17

[15] M. A. Ruderman and C. Kittel *Phys. Rev.*, vol. 96, p. 99, 1954. 17

[16] M. B. Maple, J. W. Chen, S. E. Lambert, Z. Fisk, J. L. Smith, H. R. Ott, J. S. Brooks, and M. J. Naughton *Phys. Rev. Lett.*, vol. 54, p. 477, 1985. 17

[17] Y. Fujita, K. Endo, M. Terada, and R. Kimura *J. Phys. Chem. Solids*, vol. 33, p. 1443, 1972. 18

[18] K. Andress and E. Alberti *Z. Metallkd.*, vol. 27, p. 12, 1935. 18

[19] Z. Man and M. Sikirica *Acta Crysstallogr.*, vol. 18, p. 594, 1964. 18

[20] B. Eisenmann, N. May, W. Muller, and H. Schafer *Z. Naturforsch. b*, vol. 27, p. 1155, 1972. 18

[21] A. Szytula and J. Leciejewicz *Acta Sci. Litt. Schedae Physicae (Universitas Jagellonica, Fascilus 26)*, 1987a. 19

[22] W. Rieger and E. Parthe *Monatsh. Chem.*, vol. 100, p. 444, 1969. 21

[23] D. Rossi, R. Marazza, and R. Ferro *J. Less-Common Met.*, vol. 58, p. 203, 1978. 21, 61

[24] K. Buschow and D. D. Mooij *Philips J. Res.*, vol. 41, p. 55, 1986. 21

[25] I. Nowik, I. Felner, and M. Seh *J. Magn. Magn. Mater.*, vol. 15-18, p. 1215, 1980. 21

[26] I. Nowik, I. Felner, and M. Seh *Proc. Int. Conf. on Magnetism of Rare Earths and Actinides*, p. 112, 1983. 21

[27] A. Szytula and I. Szott *Solid State Commun.*, vol. 40, p. 199, 1981. 21, 85

[28] A. Szytula and J. Leciejewicz, *Handbook on the Physics and Chemistry of Rare Earths*, vol. 12. Amsterdam: North Holland, 1989. 21

[29] A. Szytula and J. Leciejewicz, *Handbook of Magnetic Materials*, vol. 6. Elsevier, 1991. 21

[30] A. Szytula and J. Leciejewicz, *Handbook of Crystal Structures and Magnetic Porperties of Rare Earth Intermetallics*. CRC Press, Boca Raton, 1994. 21

[31] D. Gignoux and D. Schmitt, *Handbook on the Physics and Chemistry of Rare Earths*, vol. 20. Amsterdam: Elsevier, 1995. 21

[32] E. Bauminger, I. Felner, D. Froindlich, A. Grill, D. Lebenbaum, I. Meyer, I. Nowik, S. Ofer, and M. Schieber *Proc. Int. Conf. on Magnetism*, vol. 5, p. 56, 1974. 21

[33] I. Felner *J. Phys. Chem. Solids.*, vol. 36, p. 1063, 1975. 21

[34] S. Malik, S. Sankar, V. Rao, and R. Obermyer *AIP. Conf. Proc.*, vol. 34, p. 87, 1976. 21

[35] T. T. M. Palstra, A. A. Menovsky, G. J. Nieuwenhuys, and J. A. Mydosh *Phys. Rev. B*, vol. 34, p. 4566, 1986a. 21

[36] J. Yakinthos and P. Ikonomou *Solid State. Commun.*, vol. 34, p. 777, 1980. 21

[37] V. Nguyen, F. Tcheou, J. Rossat-Mignod, and R. Ballestracci *Solid State. Commun.*, vol. 45, p. 209, 1983. 21

[38] C. Routsi and J. Yakinthos *Phys. Status Solidi a*, vol. 68, p. K183, 1981. 21

[39] B. Sales and R. Viswanathan *J. Low Temp.*, vol. 23, p. 449, 1976. 21

[40] T. T. M. Palstra, A. A. Menovsky, G. J. Nieuwenhuys, and J. A. Mydosh *J. Magn. Magn. Mater.*, vol. 54-57, p. 435, 1986. 21, 59, 118

[41] G. W. Hull, J. H. Wernick, T. H. Geballe, J. V. Waszczak, and J. E. Bernardini *Phys. Rev. B*, vol. 24, p. 6715, 1981. 21

[42] V. Murgai, S. Raen, L. C. Gupta, and R. Parks, *Valence Instabilities*. Amsterdam: North Holland, 1982. 21

[43] B. H. Grier, J. M. Lawrence, V. Murgai, and R. D. Parks *Phys. Rev. B*, vol. 29, p. 266, 1984. 21

[44] K. Hiebl and P. Rogl *J. Magn. Magn. Mater.*, vol. 50, p. 39, 1985. 21

[45] R. N. Shelton, H. F. Braun, and E. Musick *Solid State. Commun.*, vol. 52, p. 797, 1984. 21

[46] W. M. McCall, R. S. V. L. Narasimhan, and R. Butera *J. Appl. Phys.*, vol. 44, p. 4724, 1973. 21

[47] M. Kolenda, A. Szytula, and A. Zygmunt, *Crystalline Electric Field Effects in f-electron Magnetism*. New York: Plenum, 1982. 21

[48] C. Ammarguell, M. Escorne, A. Mauger, E. Beaurepaire, M. Ravet, G. Krill, F. Lapierre, P. Haen, and C. Godart *Phys. stat. sol. (b)*, vol. 143, p. 159, 1987. 22

[49] G. Nakamoto, A. Fuse, M. Kurisu, and T. Shigeoka *J. Magn. Magn. Mater.*, vol. 272-276, pp. e75–e76, 2004. 22

[50] M. Koterlyn, I. Shcherba, R. Yasnitskii, and G. Koterlyn *J. Alloys Compd.*, vol. 442, p. 176âĂŞ179, 2007. 22

[51] J. Leciejewicz, M. Kolenda, and A. Szytula *Sol. St. Commun.*, vol. 45, p. 145, 1983. 22, 59, 84

[52] T. Shigeoka, N. Iwata, Y. Hashimoto, Y. Andoh, and H. Fujii *J. de Phys.*, vol. 49, pp. C8–431, 1988. 22, 60, 77, 84, 90

[53] T. Shigeoka, N. Iwata, M. Eguchi, M. Kosaka, and H. Onodera *Physica B*, vol. 211, pp. 121–123, 1995. 22

[54] K. Hattori, C. Chen, M. Sakamoto, T. Shigeoka, and N. Iwata *Physica B*, vol. 252, pp. 76–80, 1998. 22

[55] S. Kawano, T. Hirooka, N. Yamamoto, A. Onodera, Y. Nakai, N. Achiwa, T. Shigeoka, and N. Iwata *J. Phys. Chem. Solids*, vol. 60, pp. 1213–1215, 1999. 22

[56] T. Shigeoka, N. Iwata, H. Fujii, T. Okamoto, and Y. Hashimoto *J. Magn. Magn. Mater.*, vol. 70, p. 239, 1987. 22, 65, 66, 85

[57] T. Shigeoka, H. Fujii, K. Yonenobu, K. Sugiyama, and M. Date *J. Phys. Soc. Japan*, vol. 58(2), pp. 394–397, 1989. 22, 59, 84

[58] T. Shigeoka, N. Iwata, Y. Hashimoto, Y. Andoh, and H. Fujii *Physica B*, vol. 156 157, pp. 741–743, 1989. 22

[59] N. Iwata *J. Magn. Magn. Mater.*, vol. 86, pp. 225–230, 1990. 23

[60] K. Takeda, K. Konishi, H. Deguchi, N. Iwata, and T. Shigeoka *J. Magn. Magn. Mater.*, vol. 104-107, pp. 901–902, 1992. 23

[61] K. Hiebl, C. Horvath, and P. Rogl *J. Magn. Magn. Mater.*, vol. 37, pp. 287–296, 1983. 23

[62] I. Felner and I. Nowik *J. Phys. Chem. Solids*, vol. 46(6), pp. 681–687, 1985. 23

[63] B. Chevalier, J. Etourneau, and P. Hagenmuller *J. Less-Common. Met.*, vol. 111, pp. 161–169, 1985. 24, 106

[64] T. Shigeoka, M. Saeki, N. Iwata, T. Takabatake, and H. Fujii *J. Magn. Magn. Mater.*, vol. 90 91, pp. 557–558, 1990. 24, 106

[65] L. Gondek, A. Szytula, and M. Slaski *Solid State Commun.*, vol. 140, pp. 141–143, 2006. 24, 90

[66] R. Pinto, M. Amado, M. S. Silva, M. Braga, J. Sousa, B. Chevalier, and J. Etourneau *J. Magn. Magn. Mater.*, vol. 104-107, pp. 1235–1236, 1992. 24, 90

[67] J. B. Sousa, M. Amado, R. Pinto, M. S. Silva, and M. Braga *J. Magn. Magn. Mater.*, vol. 111, pp. 239–248, 1992. 24

[68] M. A. Salgueiro, B. Almeida, M. Amado, J. Sousa, B. Chevalier, and J. Etourneau *J. Magn. Magn. Mater.*, vol. 125, pp. 103–109, 1993. 24, 106

[69] P. Kumar, N. K. Singh, K. G. Suresh, and A. K. Nigam *J. Alloys Compd.*, vol. 427, p. 42, 2007. 24

[70] P. Kumar, N. K. Singh, K. G. Suresh, A. K. Nigam, and S. Malik *J. Appl. Phys.*, vol. 101, p. 013908, 2007. 24

[71] S. M. Yusuf, M. Halder, A. Rajarajan, A. Nigam, and S. Banerjee *J. Appl. Phys.*, vol. 111, p. 093914, 2012. 24, 60, 98

[72] M. Halder, A. Bera, A.Kumar, L. Keller, and S. Yusuf *J. Alloys Compd.*, vol. 592, pp. 86–91, 2014. 24

[73] N. Tateiwa, T. D. Matsuda, Y. Haga, and Z. Fisk *Phys. Rev. B*, vol. 89, p. 035127, 2014. 24, 60, 98

[74] E. V. Sampathkumaran, R. S. Chaughule, K. V. Gopalakrishnan, S. K. Malik, and R. Vijayaraghavan *J. Less-Common. Met.*, vol. 92, p. 35, 1983. 24, 60, 98

[75] W. H. Meiklejohn and C. P. Bean *Phys. Rev.*, vol. 102, p. 1413, 1956. 26

[76] W. H. Meiklejohn and C. P. Bean *Phys. Rev.*, vol. 105, p. 904, 1956. 26

[77] E.Gruneisen *Ann. Phys.(Leipzig)*, vol. 16, p. 530, 1933. 31

[78] P. de Gennes and J. Friedel *J. Phys. Chem. Solids*, vol. 4, p. 71, 1958. 31

[79] T. Kasuya *Prog. Theor. Phys.(Kyoto)*, vol. 22, p. 227, 1959. 31

[80] E. Gratz and M. Zuckermann, *Handbook on the Physics and Chemistry of Rare Earths*, vol. 5. Amsterdam: North Holland, 1984. 31

[81] J. Ziman, *Electrons and Phonons*. Oxford: Clarendon Press, 1960. 32

[82] H. Yamada and S. Takada *J. Phys. Soc. Jap.*, vol. 34, p. 51, 1973. 32, 107

[83] H. Yamada and S. Takada *Prog. Theor. Phys.*, vol. 49, p. 1401, 1973. 32

[84] K. Ueda *Solid State Commun.*, vol. 19, p. 965, 1976. 32

[85] K. Ikeda, S.K.Dhar, M. Yoshizawa, and J. K.A. Gschneidner *Solid State Commun.*, vol. 100, p. 292, 1991. 32

[86] A. Tishin, *Handbook of Magnetic Materials*, vol. 12. Elsevier Science, 1999. 33

[87] G. Brown *J. Appl. Phys.*, vol. 47, p. 3673, 1976. 33

[88] E. Warburg *Ann. Phys.*, vol. 13, p. 141, 1881. 33

[89] V. Pecharsky and J. K.A. Gschneidner *J. Magn. Magn. Mater.*, vol. 200, p. 44, 1999. 35, 36

[90] T. Krenke, E. Duman, M. Acet, E. Wassermann, X. Moya, L. Manosa, and A. Planes *Nat. Mat.*, vol. 4, pp. 450–454, 2005. 35

[91] A. Tishin, J. K.A. Gschneidner, and V. Pecharsky *Phys. Rev. B*, vol. 59, p. 503, 1999. 35

[92] S. Yonezawa, T. Kajikawa, and Y. Maeno *Phys. Rev. Lett.*, vol. 110, p. 077003, 2013. 36

[93] T. Samanta and I. Das *Phys. Rev. B*, vol. 74, p. 132405, 2006. 36

[94] T. Samanta, I. Das, and S. Banerjee *Appl. Phys. Lett.*, vol. 91, p. 082511, 2007. 36

[95] L. Vinokurova, V. Ivanov, and A. Szytula *J. Magn. Magn. Mater.*, vol. 99, p. 193, 1991. 59

[96] A. Szytula *J. Alloys Compd.*, vol. 178, p. 1, 1992. 59

[97] V. Sechovsky and L. Havela *J. Alloys Compd.*, vol. 225, p. 444, 1995. 60

[98] R. rawat and I. Das *J. Magn. Magn. Mater.*, vol. 236, p. 285, 2001. 60, 98

[99] J. S. Smart *Am. J. Phys.*, vol. 23, p. 356, 1955. 65

[100] T. Kong, C. E. Cunningham, V. Taufour, S. L. Bud'ko, M. L. C. Buffon, X. Lin, H. Emmons, and P. C. Canfield *J. Magn. Magn. Mater.*, vol. 358-359, p. 212, 2014. 76

[101] I. Mirebeau and G. Parette *J. Appl. Phys.*, vol. 53, p. 1960, 1982. 85

[102] M. Nomura, H. Fujiwara, and Y. Fujiwara *J. Phys. Soc. Japan*, vol. 38, p. 55, 1975. 85

[103] F. Song and G. Bergmann *Phys. Rev. Lett.*, vol. 88, p. 167202, 2002. 85

[104] R. Mallik, E. V. Sampathkumaran, and P. L. Paulose *Appl. Phys. Lett.*, vol. 71, p. 2385, 1997. 85, 86

[105] R. B. vanDrover, E. M. Gyorgy, R. J. Cava, J. J. Krajewsky, R. J. Felder, and W. F. Peck *Phys. Rev.*, vol. B47, p. 6134, 1993. 86

[106] K. Narita, J. Umeda, and H. Kusumoto *J. Chem. Phys.*, vol. 44, p. 2719, 1966. 86, 118

[107] R. Welter, G. Venturini, and B. Malaman *J. Alloys Compd.*, vol. 206, p. 55, 1994. 87

[108] K. Neumann and K. R. A. Ziebeck *J. Magn. Magn. Mater.*, vol. 140-144, p. 967, 1995. 87

[109] M. Baibich, J. Broto, A. Fert, F. N. V. Dau, F. Petroff, P. Etienne, G. Cruezert, A. Friedrich, and J. Chazelas *Phys. Rev. Lett.*, vol. 61, p. 1979, 1988. 89

[110] R. van Dover, E. Gyorgy, R. Cava, J. Krajewski, R. Felder, and W. Peck *Phys. Rev. B.*, vol. 47, p. 6134, 1993. 90

[111] C. Mazumdar, A. K. Nigam, R. Nagarajan, L. C. Gupta, C. Godart, B. D. Padalia, G. Chandra, and R. Vijayaraghavan *Phys. Rev. B.*, vol. 54, p. 6069, 1996. 90, 109

[112] C. Mazumdar, A. K. Nigam, R. Nagarajan, C. Godart, L. C. Gupta, B. D. Padalia, G. Chandra, and R. Vijayaraghavan *Appl. Phys. Lett.*, vol. 68, p. 3647, 1996. 90, 109

[113] E. Sampathkumaran, P. L. Paulose, and R. Mallik *Phys. Rev. B.*, vol. 54, p. R3710, 1996. 90, 91, 97, 109

[114] R. Mallik, E. Sampathkumaran, and P. L. Paulose *Appl. Phys. Lett.*, vol. 71, p. 2385, 1997. 90, 97, 109

[115] R. Nirmala, S. K. Malik, A. Morozkin, Y. Yamamoto, and H. Hori *Europhys. Lett.*, vol. 76(3), pp. 471–476, 2006. 90

[116] K. Suresh and K. R. Rao *J. Alloys Comp.*, vol. 238, p. 90, 1996. 93

[117] R. Rawat, K. Mukherjee, K. Kumar, A. Banerjee, and P. Chaddah *J. Phys. Condens. Matter.*, vol. 19, p. 256211, 2007. 93

[118] R. Rawat and I. Das *J. Mag. Mag. Mat.*, vol. 236, pp. 285–292, 2001. 95

[119] V. Ivanov, L. Vinokurova, and A. Szytula *Acta Physica Polonica A.*, vol. 81, p. 693, 1992. 95

[120] H. Yamada and S. Takada *J. Phys. Soc. Jap.*, vol. 34, p. 51, 1973. 96

[121] H. Yamada and S. Takada *Prog. Theor. Phys.*, vol. 49, p. 1401, 1973. 96

[122] J. L. Olsen and L. Rinderer *Nature(London).*, vol. 173, p. 682, 1954. 97

[123] H. Miwa *Prog. Theor. Phys.*, vol. 29, p. 477, 1963. 97

[124] T. Shigeoka, N. Iwata, T. Kishino, M. Nishi, Y. Oohara, and H. Yoshizawa *Physica B.*, vol. 186-188, pp. 652–654, 1993. 106

[125] A. K. Nigam, S. B. Roy, and G. Chandra *Phys. Rev. B.*, vol. 49, p. 1127, 1994. 109

[126] A. Gerber, I. Kishon, I. Y. Korenblit, O. Riss, A. Segal, M. Karpovski, and B. Raquet *Phys. Rev. Lett.*, vol. 99, p. 027201, 2007. 109

[127] F. Tsui, C. Uher, and C. P. Flynn *Phys. Rev. Lett.*, vol. 72, p. 3084, 1994. 109

[128] S. Banerjee *Phys. Rev. Lett.*, vol. 12, p. 16, 1964. 110

[129] I. Das and R. Rawat *Solid State Commun.*, vol. 115, pp. 207–211, 2000. 113

[130] G. Liang, M. Croft, R. Neifeld, and B. Qi *J. Appl. Phys.*, vol. 61, p. 3183, 1987. 118

[131] E. Sampathkumaran, G. Kalkowski, C. Laubschat, G. Kaindl, M. Domke, G. Schmiester, and G. Wortmann *J. Magn. Magn. Mater.*, vol. 47 and 48, p. 212, 1985. 118

[132] M. McGuire, D. Gout, V. Garlea, A. Sefat, B. Sales, and D. M. Jr. *Phys. Rev. B*, vol. 81, p. 104405, 2010. 118

[133] M. Majumder, K. Ghoshray, A. Ghoshray, B. Bandyopadhyay, B. Pahari, and S. Banerjee *Phys. Rev. B*, vol. 80, p. 212402, 2009. 118

[134] A. Morozkin, Y. Seropegin, A. Gribanov, and J. Barakatova *J. Alloys Comp.*, vol. 256, pp. 175–191, 1997. 120